UNIVERSITY OF LIVERPOOL

An Investigation into the Hydration and Growth of Ice on Metal Surfaces

Thesis of Kallum Mistry

2023

Supervisors

Professor Andrew Hodgson

Dr George Darling

Abstract

Up to now, our picture of what a flat surface looks like has been dominated by the assumption that it is atomically smooth, containing an ordered array of regularly spaced atoms. However, in most real-life cases, metal surfaces will never be entirely flat, they will contain surface defects, such as steps, and more reactive open-faced terraces. Regardless of this, the majority of studies consider such defects to be a part of the background, and therefore little is known about how water interacts at these sites, and whether they play an important role in processes such as water dissociation. In more recent years, close examination of surfaces and their structure using Scanning Tunnelling Microscopy (STM) has shown this to be the case, revealing that the surfaces will inevitably contain some form of surface roughening on the atomic scale, known as defects. Understanding how these defect sites influence the behaviour of water is important for catalysis, and existing technologies that use water as a renewable resource.

In this thesis, we will investigate various metal faces using Temperature Programmed Desorption (TPD), low-current Low Energy Electron Diffraction and Scanning Tunnelling Microscopy to help develop our understanding of how different open and stepped metal surfaces can influence the behaviour of water compared to surfaces that are considered to be flat, or more inert. As well as this, we will discuss the idea of how different step sites, whether ordered or disordered can influence the composition and structure of water on a stepped surface compared to other metal-water systems reported previously.

Thesis content

1.0. Introduction

1.1. Introduction to water and environment 6
1.2. Molecular water 8
1.3. How the chemistry of water underpins its unique properties 9
1.4. Bernal-Fowler-Pauling ice rules 11
1.5. The wetting of solid surfaces 12
1.6. The Bilayer Model 13
1.7. The wetting of water on various transition metal surfaces 15
1.7.1. Intact water 16
1.7.1.1. 1D water 16
1.7.1.2. 2D water 17
1.7.2. Considerations for water dissociation 17
1.7.1.2. Mixed water/OH phase 18
1.8. Overview of thesis 19
1.8.1. Open surfaces 19
1.8.2. Corrugated surfaces 20
1.9. References 21

2.0. Experimental Overview

2.1. Overview of Ultra High Vacuum 26
2.2. Overview of a UHV system pumping 27
2.2.1. Chamber 1 28
2.2.2. Chamber 2 29
2.3. Sample preparation 30
2.3.1. Preparation of a clean metal surface 30
2.4. Surface characterisation 30
2.4.1. Temperature Programmed Desorption 30
2.4.2. Low Energy Electron Diffraction 33
2.4.3. Scanning Tunneling Microscopy 33
2.5. Conclusion 35
2.6. References 35

3.0. An Investigation into the Structure of Intact Water on the Open Ni(110) Surface

3.1. Introduction 36
3.2. Experimental 39
3.3. Results and Discussion 40

3.3.1. Scanning Tunneling Microscopy and DFT of the first water layer 40
3.3.2. Low Energy Electron Diffraction 45
3.3.3. DFT of the second water layer 47
3.4. Conclusion 50
3.5. References 50
4.0. An Investigation into the Influence of Dissociation on the Open Ni(110) Surface
4.1. Introduction 53
4.2. Experimental 56
4.3. Results and Discussion 57
4.3.1. Temperature Programmed Desorption 57
4.3.2. Low Energy Electron Diffraction 59
4.3.3. Scanning Tunneling Microscopy 61
4.4. Conclusion 67
4.5. References 68
5.0. An Investigation into the Structure of Water on the Stepped Cu(110) Surface
5.1. Introduction 71
5.2. Experimental 73
5.3. Results and Discussion 74
5.4. Conclusion 79
5.4. References 79
6.0. An Investigation into the Structure of Water on the Stepped Pt(211) Surface
6.1. Introduction 82
6.2. Experimental 87
6.3. Results and Discussion 88
6.3.1. Discussion of the structure with previous literature 99
6.4. Conclusion 100
6.5. References 101
7.0. An Investigation into the Structure of Water on an Oxygen Pre-covered Cu(511) Surface
7.1. Introduction 104
7.2. Experimental 108
7.3. Results and Discussion 109
7.4. Conclusion 120
7.5. References 121

List of Abbreviations

STM – Scanning Tunnelling Microscopy

H-bond – Hydrogen bond

LEED – Low Energy Electron Diffraction

FTIR – Fourier Transform Infrared Spectroscopy

NEXAFS – Near Edge X-ray Absorption Fine Structure

SEXAFS – Surface Extended X-ray Absorption Fine Structure

NRA – Nuclear Reaction Analysis

ESDIAD – Electron Stimulated Desorption Ion Angular Distribution

RAIRS – Reflection Adsorption Infra-Red Spectroscopy

UPS – Ultraviolet Photoelectric Spectroscopy

TPD – Temperature Programmed Desorption

IRAS – Infrared Reflection Absorption Spectroscopy

MS – Mass Spectrometry

DFT – Density Functional Theory

WFM – Work-Function Measurements

ML – Monolayer

UHV – Ultra-High Vacuum

M – Metal

Z – Zig-zag

P – Pinched

N – Narrow

XPS – X-ray Photoelectron Spectroscopy

Acknowledgements

First and foremost, I would like to thank Professor Andrew Hodgson, as without him giving me the chance to undertake this studentship I would not be here today. In my eyes, you are truly unmatched, and since my undergraduate degree you have inspired me to want to further my career in the field of research. You have been particularly patient with me and it has been an incredible experience, and one I will truly never forget. You have always provided me with the skills I needed to succeed, providing me with encouragement and motivation thought-out my PhD, especially when I needed it the most during Covid. Therefore, you have been an inspiration and a true role model for someone I would like to be, and I will carry forward everything you have taught me in my future career.

I would also like to thank Dr Sam Haq for all your support through Covid helping me on the STM. You have been a very supportive mentor and someone I could reach whenever I needed help and guidance. Thank you for solving all the issues I have had on the STM, and especially for giving me knowledge in UHV systems, as it helped me solve and overcome many issues independently during my PhD.

Dr George Darling, Dr Heike Arnolds and Dr Mathew Dyer, I thank you all for your wise words of wisdom and guidance during my PhD, as I appreciate the help and support you have provided. Dr George Darling and Henry Snowden, thank you for the theoretical calculations that have helped support my research during this PhD, the collaboration has been insightful and has given me a better understanding of the topics I investigated in my thesis.

It has been a pleasure working with everyone in the SSRC and I would especially like to thank Jae, Matty, Marta, Matt, Haitham and Luke for their support in the workplace when times were hard. I will genuinely miss you all and I will not forget all the times in the office when I needed a break and there would be someone to have a friendly chat with. It has been a pleasure working with you all and I wish you all the best in the future.

I particularly would like to thank my mum and dad for always being so compromising and understanding, always pushing me to do well, even when I was down. You both have sacrificed a lot to provide everything I needed to succeed, despite having to work as hard as you both have while I was growing up. You both have shaped and moulded who I am today and I am grateful for everything you have given me.

I would further like to thank my partner Shivani, as I could not have done all this without you. You have always pushed me to be resilient and hardworking, being that positive influence that has always made a bad day better. Thank you for always putting me first and making sure that I was always okay during my PhD, especially through Covid and when I was ill.

Finally, to the reader who is reading this, I would like to thank you for taking the time to read my research. I further hope these the topics give you as much interest and insight into metal-water interactions as they did for me.

Chapter 1
Introduction

1.1. Introduction to water and environment

Water is perhaps the defining species that distinguishes our planet from its apparently barren companions, being ubiquitous in every living system and present either as a trace species or as a major component in almost every process or activity we undertake. Water displays many unusual behavioural and chemical properties that influence the way our environment is shaped and the physical and chemical processes that shape life on earth. Unlike most liquids which become denser as they freeze, water will expand,[1, 2] causing ice to float on water and dramatically enhancing the weathering of solid materials in our environment.[3] This behaviour, and a large proportion of water's unique properties, can be attributed to the polarity of water and the formation of hydrogen bonds between molecules. To fully understand its influence, and to use this abundant resource industrially, one must first understand the behaviour of water, including the solvation of molecules, the dissociation of water and its recombination, along with the way it interacts with solid materials. Therefore, over the past few decades, there have been numerous amounts of studies into the interaction of water with solid surfaces, as they provide an ideal environment.[4-7]

One area that has gained a lot of attention over the years in many research studies is research into anti-corrosion coatings on metallic surfaces, particularly those that involve iron, as it is well-known that water oxidises iron, regardless of its composition.[8, 9] Much of this research has focused on improving the lifetime and cost of materials that incorporate iron, such as beams for bridges, pipes and catalysts.[10-12] Another issue that has received attention is the electrolysis of water for hydrogen fuel cells and clean energy production and storage,[13-16] since the use of finite resources such as fossil fuels, which has increased tremendously over the years, is responsible for global warming. The use of hydrogen provides an alternate energy storage resource that, in principle, does not create any carbon emission or contribute to global warming. Even though both these areas mentioned above have found suitable solutions, currently more research needs to be carried into improving the design of these interfaces to make them more efficient and cost effective. Therefore, a continuing challenge is to understand to a high

standard the role and behaviour that water plays at solid interfaces so that the current processes can be improved.

The foundation of water's ability to solvate ions and ease of proton transfer or charge across an interface is often a result of water being able to form a hydrogen bonded network.[2, 17] This is evident in theoretical models at the electrochemical interface, with reports showing that water and a hydrogen bonded network can alter the barriers associated with reaction of species on the surface, i.e. water modifies the barriers and chemistry that occurs.[18-21] for example, in the reactions that involve a local hydrogen bonded network, such as the water gas shift reaction and various electrolysis reactions.[20, 22, 23] However, water's complexity and disorder make it challenging to identify all the bonding geometries, atom position and binding environments at an interface. Consequently, little is known about the true behaviour of water at an interface, particularly the intermediates involved. This is because the role which intermediates play in a reaction, or the structure formed, is generally inferred from theoretical models, with many experimental techniques giving little to no chemical information to distinguish between H_2O/OH, for example.

In order to solely focus on the interactions at a water/solid interface, ones must use a system that is enclosed to ambient conditions so that other gaseous contaminates cannot interfere. To achieve this, most experimental research studies use Ultra High Vacuum (UHV) systems to limit the contaminants, enabling an ideal environment to study water or reactions involving water and a co-adsorbate. With the removal of many of the unwanted contaminants, one can then gain a molecular understanding at the atomic scale of the binding sites and environment of water within an interfacial layer. This molecular understanding can then be incorporated into models on a macroscopic scale, with the addition of other factors that may influence the behaviour of water, which can help us understand the reactions or surface wetting at an interface.

To gain an understanding of how water will transform its structure into a thick ice film, it is important that we first understand the initial structure that wets a solid surface layer. Over the years many different structural models have been proposed using a combination of experimental and theoretical investigations, however, none of these models closely resemble the structure of bulk ice.[24] This is in part because the growth of ice on these heterogeneous flat interfaces inevitably involves a degree of mismatch between the lattice parameter of the solid surface and ice, I_h. As a result, various studies have focussed on the idea that an open face or

stepped surface may provide a suitable template on which a true 'ice-like' layer will grow.[7, 25-27]

The use of various experimental techniques, such as high-resolution Scanning Tunnelling Microscopy (STM), Low Energy Electron Diffraction (LEED), Temperature Programmed Desorption (TPD) and Density Functional Theory (DFT) can be used as a direct route to articulate how water nucleates, understand the different bonding geometries and binding energies present in the surface wetting layer. This thesis will discuss a combination of open-faced and stepped transition metal surfaces to give a general insight into the wetting at these more reactive faces, with comparisons to their planar counterparts. The discussion will involve how the reactivity of a surface affects the overall hydrogen bond network and the stability of water, which is dependent on dissociation, or whether the influence of step sites or open-faced sites provide favourable binding sites for water.

1.2. Molecular water

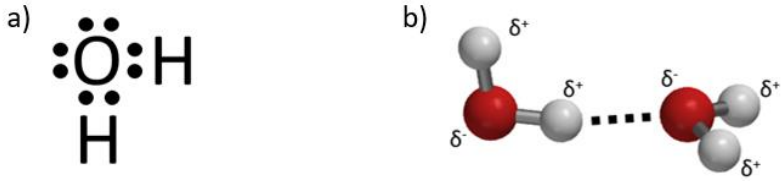

Figure 1. a) Lewis dot structure of water. b) Simulation of a hydrogen bond between two water molecules.

Water has a simple atomic arrangement; its chemical composition consists of one oxygen and two hydrogen atoms. The chemical bonds in this polar molecule is often thought of in terms of a simple Lewis dot structure (fig. 1a), where each hydrogen is chemically bonded to an oxygen, contributing a single electron per hydrogen atom to oxygen's six valence electrons to complete its outer shell. This creates a strong covalent bond between hydrogen and oxygen, which consists of two pairs of electrons being shared.[28, 29] This results in two uncoordinated pairs (or lone pairs) of electrons, which can be used to coordinate to surfaces/other molecules. However, the presence of the lone pairs of electrons creates a repulsive force between the two hydrogens, resulting in a bent shape with C_{2v} symmetry and a bond angle of 104.5°.[2, 30]

Water is a polar molecule, a consequence of the atoms having very different electronegativities.[31] This results in a polar O-H bond, with the hydrogen found to be delta positive and oxygen to be delta negative, and an attractive intermolecular force called a hydrogen bond to be exerted between neighbouring waters (fig. 1b). The hydrogen bond is

created when two water molecules move close to one another, creating an induced dipole moment in the participating hydrogen in one molecule and lone pair on oxygen in the other.[32, 33] A hydrogen bond only exists when specific requirements are met; for example, two molecules with a highly polarised covalent X-H bond (where X = O, N or F).[34, 35] If the polarity is weak in the covalent bond, neighbouring molecules will only exert a weaker intermolecular force, such as a dipole-dipole interaction.[36, 37] Although a hydrogen bond is not as strong as a covalent bond, when a large number of molecules exert the same force a large amount of energy is required to break all the bonds, which is fundamental to waters unique properties, such as high vaporisation energy.[38, 39]

1.3. How the chemistry of water underpins its unique properties

In order to get an elemental perspective of why water exhibits a high surface tension, high heat capacity and low viscosity, one must first understand the interactions between adsorbates and at the surface. The strength of each phenomenon depends significantly on two main factors; the strength of the intermolecular interaction and the size/shape of the molecule. Whether it's dispersion or dipole-dipole interactions, the attractive force (hydrogen bonding in this case) between molecules in a liquid is generally called a cohesive force.[40, 41]

Surface tension is the tendency of molecules to be able to adhere to one another in such a way as to make the surface act like a membrane.[42] The high surface tension in water can be attributed to the strong cohesive interactions that form at the surface, which is a result of water's polarity and its ability to form strong hydrogen bonds with other molecules.[43] In a liquid, the cohesive interactions are felt equally by all molecules, resulting in water molecules being pulled in all different directions. However, this is not the case for a single layer of molecules at an interface, only a lateral and downward pull is experienced, with a negligible intermolecular attraction to any species above the surface. In turn, this creates an overall downward net force on the surface that is counter-balanced by the resistance of the liquid to compression. As a consequence, the surface molecules compress more tightly, to create tension in such a way that isn't present in the bulk of the liquid, resulting in shorter hydrogen bonds and higher surface tension.[44] This contraction of the surface minimises the surface area while maximising the hydrogen bonding that is occurring within the spherical droplet, allowing the system to sit at the lowest energy state possible.[39, 45]

The amount of energy required to raise the temperature of a body of liquid can be directly related to the strength of the intermolecular bonds present within its structural nature.[46] Simply,

heat capacity can be used to compare the amount of energy that is required to raise the temperature of a liquid by 1°C in a fixed amount of liquid, giving one an indication of how strong the bonds are between molecules in a liquid, which can be compared with other liquids.[47, 48] In spite of the fact that water is such a light molecule, it has an exceptionally high heat capacity, which can be attributed to the strong hydrogen bonds that interlink water.[49]

All liquids are in constant random motion, due to the constant kinetic energy of particles within liquids, however, how mobile (or viscous) a liquid is, can depend significantly on a molecule's chemical composition i.e. the strength of the intermolecular force and size of the molecule. For example, larger molecules will interact more with one another via van der Waals interactions than smaller molecules, thus more energy is required to break these bonds, causing the liquid to be less mobile. Subsequently, this is why oils (composed of large chains) tend to have a high viscosity, while smaller molecules, such as water tend to have a low viscosity. Despite the presence of strong hydrogen bonds, its size allows water to be more mobile, thus reducing its viscosity. However, one cannot forget that the temperature of a liquid also plays a significant role, as the higher the temperature, the fewer intermolecular bonds will be present, resulting in a reduction in the viscosity.

To summarise, the strong hydrogen bonding interactions exhibited by water underpin its unique properties. Waters ubiquitous presence, along with its unusual properties described above, make it a particularly interesting molecule to study. Further in this chapter, we will talk about how water interacts with not only other molecules of water, but with other surfaces, such as metals, adopting different structures as the surface condition varies.

1.4. Bernal-Fowler-Pauling ice rules

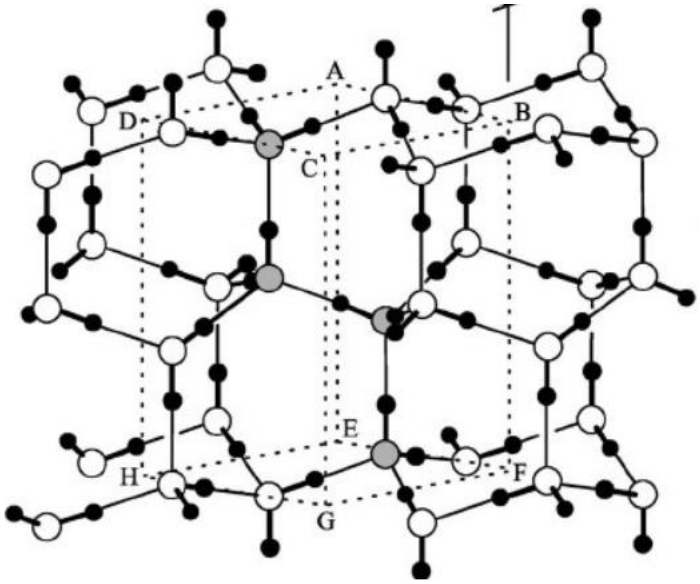

Figure 2. Illustration showing the structure of bulk ice, I_h, with the buckled hexagonal unit cells marked A to H. Adapted from.[50]

The most common naturally occurring structure of crystalline ice is its I_h form, proposed by Linus Pauling in the 1930's. This structure contains C_{3v} point group and T_d symmetry, composing hydrogen bonded hexagonal rings of water, with an O-O bond length of about 2.76 Å at 273 K (fig. 2). Based on insight from this structure, a set of structural models were developed to help provide clarity for the structure and arrangement of water molecules in ice. Introduced by Bernal and Fowler,[51-53] and later amended by Pauling,[54, 55] the set of generalisations rules was created based on experimental and theoretical studies;

1. The internal bond angle of water is about 105° with an O-H bond distance of 0.96 Å.
2. Water's orientation only allows for one bond to form between two adjacent waters along the O-O axis.
3. Each oxygen atom tetrahedrally bonds to four other adjacent water molecules through surrounding hydrogen atoms with respect to the O-O axis.
4. Bulk ice, I_h, can manifest many different conformations, each corresponding to a specific distribution of 'H' atoms with respect to oxygen atoms.

These generalised terms have been widely applied to help interpret the nucleation of water on a solid surface, to see how the structure that represents bulk ice compares to the wetting on a metal surface. Following this, many theoretical and experimental studies have been carried out, forming detailed models for the structure of water on various metal surfaces.

1.5. The wetting of solid surfaces

The properties of water which govern its interaction with a solid surface, can be understood qualitatively from the examination of water's behaviour on a metal surface. Water's ability to adhere to a solid surface can often be interpreted in terms of a Lewis acid-base interaction, with the water acting as the electron donor (Lewis base) and the surface as the electron acceptor (Lewis acid).[56, 57] The interaction between water and a surface is an adhesive force, which can be used to describe the ability of a liquid to adhere to a surface. Therefore, when water comes into contact with a suitable surface, water will wet the surface due to the adhesive forces being stronger than the cohesive, inter-molecular forces. As water moves close to a surface, it can adsorb in two different ways; the first is through the lone pair of electrons, and the second is through its hydrogen. This is a similar interaction to that of a hydrogens bond, creating an induced dipole moment in the solid surface it binds to, resulting in an electron density shift in the participating surface.[5]

Transition metal surfaces provide an ideal environment to study the interactions of water, as water typically absorbs weakly on these metal surfaces, having a binding energy similar to that in bulk ice. A consequence of this weak interaction is that water can only be stabilised by a combination of direct bonding with the metal and with other water through hydrogen bonds.[58] The most strongest interaction involves the oxygen atoms lone pair of electrons, coordinating down towards the metal surface and forming a bond.[59, 60] The second involves a hydrogen atom aligning 'H' down towards the metal surface, resulting in an induced dipole moment in the metal to match that within the water molecule, which in turn, causes a favourable attractive force between the metal electrons and the delta positive hydrogen.[61, 62, 63] During both processes, the electron density within the molecule shifts, causing the non-bonding hydrogen atoms to become more δ^+, favouring the formation of further hydrogen bonds.[30] Water can then extend from each absorption site, forming 1D or 2D islands of water on a surface.[25, 64]

Currently, there is no unified understanding of how water nucleates on a surface to form an ice-like layer. This is due to the fact that it is challenging to unambiguously resolve the precise molecular structure, even for crystalline ice under controlled ultra-high vacuum conditions. With commonly used topological methods having limitations in analysing water, for example low energy electron diffraction cannot provide the precise the hydrogen bond positions or bond geometries, which has resulted in some structures discovered in the past having been

misunderstood e.g. in the bilayer model.[4, 65] Furthermore, upon adsorption to a surface, water can remain intact or dissociate in contact with the surface depending on the surface conditions and temperature. The dissociative process is usually induced by an external factor, such as thermal energy or irradiation, however, one must also consider a variety of surface conditions/factors, such as kinks, steps and co-adsorbates, which can all serve as activated routes to dissociation.[20, 54, 66, 67] However, detecting dissociation is experimentally challenging, due to OH and H_2O sharing many similar spectroscopic/vibrational properties.[4] Although TPD can serve as a useful indicator for the presence of OH, as OH binds to the surface more strongly than H_2O, resulting in water desorbing from a higher temperature (due to recombination of OH),[68] it cannot provide information about the structural arrangement for water. This leaves many questions about the composition and behaviour of water at a metal interface unanswered since the limitations of probing the structures using the techniques mentioned above were not previously widely acknowledged, making much of the early literature suspect or misleading.

1.6. The Bilayer Model

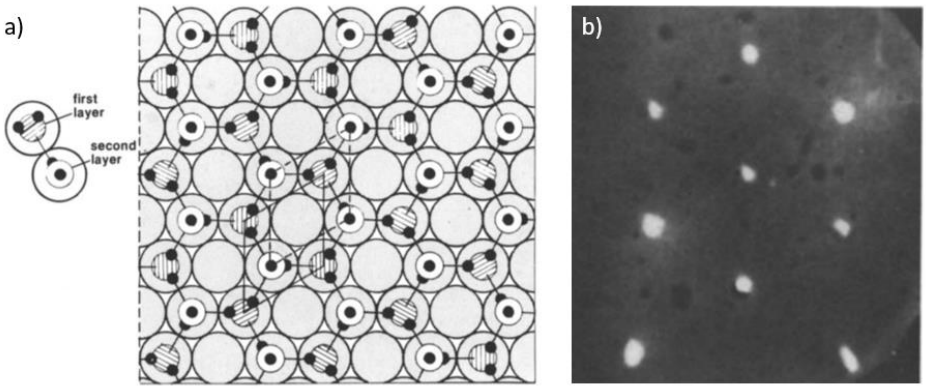

Figure 3. a) Schematic diagram showing a hexagonal bilayer of water molecules. b) LEED images for the adsorption of water on Ru(0001) at 80 K. Adapted from.[65]

The bilayer model was one of the central conceptual ideas that has been used to discuss interfacial water and its binding to a metal surface, aiding many studies with their well-defined structural models of molecularly adsorbed water. The initial development of the bilayer model of water was based on the LEED images taken from the wetting layer on Ru(0001), proposed by Doering and Madey in the 1980's (fig. 3b).[54, 65] The study proposed that the $(\sqrt{3}x\sqrt{3})R30°$ diffraction pattern was formed of a 2D hexagonal network (fig. 3), similar to that of bulk ice, I_h. The term 'bilayer' was used to describe this structure, due to waters sitting at two different distinct heights in their model, with each water forming three different hydrogen bonds to the

nearest neighbouring molecules (fig. 3a). Furthermore, the model consisted of two different types of interactions, with the first being a metal-water interaction and the second involving the hydrogen bonds between waters in hexagonal buckled rings. The first layer of water lies planar, donating electron density through the oxygens lone pair and accepting electron density through its hydrogens. The second layer is composed of H-up water, forming hydrogen bonds to the layer below, which results in the buckled hexagonal arrangement. It is this model that became the 'standard model' for the adsorption of water on all metal surfaces during the next two decades after the 1980's.

Although the BFP rules were considered adequate to describe the bonding of ice, I_h,[55] they were not sufficient for water bound to a surface. Therefore, additional constraints were imposed to better explain water at a metal interface, resulting in the corresponding generalised rules mentioned above being amended to incorporate water adsorption on a surface;

1. Water forms an interaction with a surface through its oxygen's $1b_1$ orbital.
2. The tetrahedral bond configuration is preserved in all water structures, even those that form two dimensional and incomplete layers.
3. In each system, water is required to form a minimum of two bonds per water (either through hydrogen bonds or oxygen lone pair to the metal surface).
4. Each oxygen atom must be constrained to having its free lone pair orbital perpendicular to the surface.

These modified rules above were intended to form a guide to help understand the bonding between water and a metal surface. However, recent technological advances lead to many theoretical studies re-examining the structures reported in previous literature on various surfaces, with findings suggesting that the bilayer model was unlikely to be made of pure water, but water and hydroxyl.[54] One of the first studies that disproved the bilayer model was by Feibelman,[6] who found DFT evidence to suggest that the pure water model was not as stable as a water/OH arrangement, suggesting that the LEED pattern produced was caused by electron induced dissociation. Not only did this create new discussion over the structure of water on Ru(0001), but also on other metal surfaces due to the bilayer model being used as a general model for the adsorption of water for the past two decades previously. Furthermore, this indicated that the wetting of a surface is more complex than what was once thought, with many studies now having to consider models that incorporate both water and hydroxyl, and whether

water dissociates in contact with the surface or induced by external factors e.g. heat or electron induced damage upon using surface techniques.

Since then there has been a significant amount of research into the role of a surface and how it interacts with a wetting layer, to gain an insight into the interactions of water at a metal surface. The vast majority of studies these studies focus on close packed flat metal faces, looking at water's most favourable binding sites with the help of DFT to provide theoretical evidence for the most appropriate site, and structure. However, few of the studies consider the wetting that occurs at steps or defect sites, as in reality a surface is never entirely flat and contains many defect and step sites. This, therefore, leaves it unclear as to whether the wetting on a stepped surface or at defect sites plays an intrinsic role in the adsorption and dissociation of water, as it is important that we consider all aspects of a surface so that we can get a full understanding of the adsorption of water at a surface.

1.7. The wetting of water on various transition metal surfaces

To gain an understanding of the structures that forms on a transition metal surface, we must consider two aspects; the first is the reactivity of the surface, and the second is the arrangement of atoms on the surface. The reactivity of the surface will dictate how strongly water will bind and whether water will dissociate. On the other hand, the arrangement of metal atoms also needs to be considered as water will want to maximise both its water-water and metal-water interactions, while accommodating the metal surface lattice parameter to form a structure that is the most stable. In this section, we will discuss how intact and partially dissociated water does this on various metal surfaces with different surface arrangements, forming structures that have been observed experimentally and theoretically to be the most stable structure.

1.7.1. Intact water

1.7.1.1. 1D water

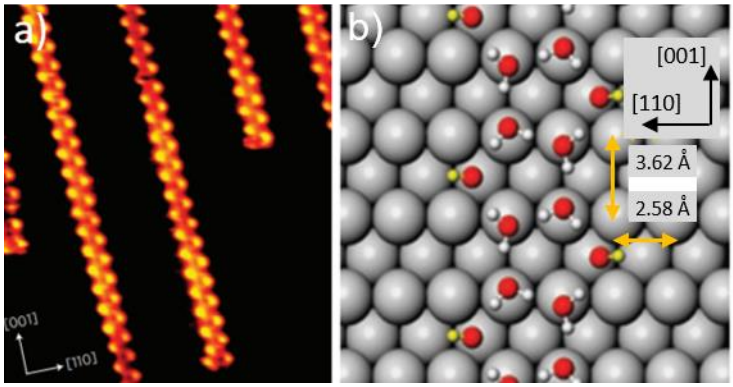

Figure 4. a) STM image of zig-zag chains on Cu(110) taken at 100 K. b) DFT simulation showing the lowest possible energy structure of the zig-zag chains in figure a), showing a face sharing pentamer chains. Adapted from.[69]

Many of the original metal-water adsorption studies use hexagonal templates as the structure for water on a surface, as mentioned above, with extended water structures built from cyclic hexagonal networks. In the case of Cu(110), however, this is not the case, with theoretical calculations and experimental measurements showing that the water structure is formed of face-sharing pentamer chains that grow along the [110] direction. These linear chains maximise the number of flat waters, having four out of its five waters flat at the atop Cu sites with the last pointing H-down in the Cu ridges (fig. 4b). This arrangement results in the waters that lies planar having a lower contrast in STM compared to the waters in the Cu ridge, which creates a zig-zag arrangement in figure 4a. DFT calculations indicated that the pentamer structure is more stable than any of the lowest energy structures on Cu(110), despite containing just 2.67 hydrogen bonds per water. Water achieves its high stability by favouring the strongest water-metal interaction or hydrogen bond interaction, over the number of hydrogen bonds per water.[69]

1.7.1.2. 2D water

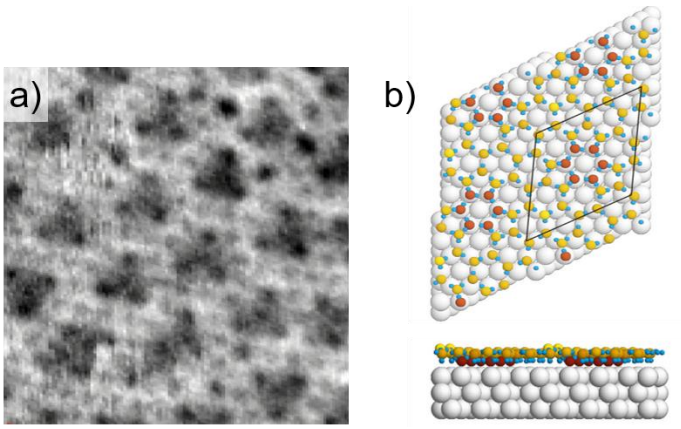

Figure 5. a) STM image of water adsorbed to a Pt(111) surface and heated to 140 K. b) Simulated structure of water on the Pt(111) surface. Adapted from.[6]

While simple 1D zig-zag pentamer chains are observed on Cu(110), more complex 2D structure can be found on Pt(111) with water forming a (√37x√37)R25.3° structure at low coverage (fig. 5).[6, 70] The low coverage (less than a layer of surface water) structure consists of a combination of waters that bind either planar or H-down onto the surface, forming five, six and seven membered rings, with two different sets of hexagonal bonding motifs shown in yellow and dark orange (fig. 5b). Only a small fraction of water in this network adopted the desired hexamer units, creating low-lying tightly bound water rings alternating with high-lying water rings that sit slightly above at a 30-degree rotation. This arrangement is supported by DFT, which shows that it is energetically favourable to have water flat and tightly bound (highlighted in dark orange), with the rest H-bond network (highlighted in yellow) optimising bond geometries (fig. 5a).

1.7.2. Considerations for water dissociation

In studying the adsorption of water, one must also consider whether water dissociates in contact with the surface, as some of the intact water phases may actually be a mix of water/OH, as mentioned above. However, it is challenging to determine the 'true' composition of water's surface structure, as we never know whether dissociative adsorption has occurred and to what extent. This is because experimental techniques, such as low energy electron diffraction and vibration spectroscopy give either little to no chemical information to distinguish between the two species.[71, 72] However, in more recent years the structural characterisation of experimental studies has been guided by STM, which has the capability of accurately probing the precise structural arrangement of water on the surface. Despite the growing number of improvements

in surface diagnostic tools mentioned above, identifying irreversible water adsorption is considerably easier than reversible, since the former is usually accompanied by identifiable dissociative products, such as H_2 or O. Yet, water that irreversibly dissociates on a surface will still reversibly desorb a significant amount of water before any identifiable products form as the surfaces are heated, making the assignment for dissociation more challenging. These issues show that it is important to keep in mind the possibility of dissociation as the subject of adsorption of water is discussed on many of the different stepped and open metal surfaces that may be more reactive than their flatter counterparts.

Having said this, one must also consider the relative stability of an oxide formation and whether it is favourable, e. g. the formation of RhO or Rh_2O_3 from water is an endothermic reaction implying that the reaction is unfavourable.[73, 74] In contrast, some metals are well known for favouring oxidation, such as FeO and Fe_2O_3 via an exothermic reaction.[75, 76] While some reactions can be predicted, some metals behave inconsistently; for example, the oxidation of Re to ReO_3 is endothermic and the formation of ZnO from Zn is exothermic, [77-81] yet water irreversibly decomposes on Re but does not on Zn, suggesting that the dissociation pathway is complex and cannot always be predicted at a metal-water interface.

1.7.2.1 Mixed water/OH phase

Since the fall of the bilayer model, as mentioned above, more studies have been open to the idea that their structural models for the wetting of a solid surface also contain OH, which has resulted in several new water/OH phases being discovered.

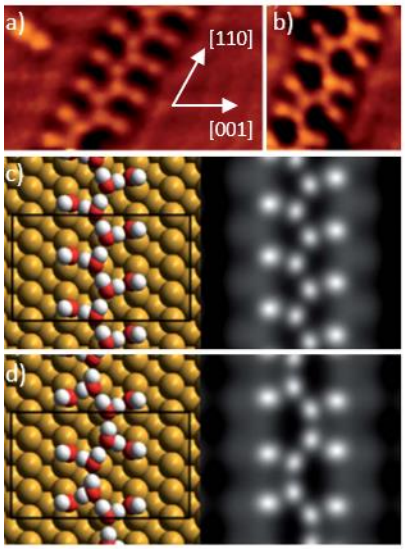

Figure 6. STM images of water/OH linear chains formed at 200 K on Cu(110). a) zigzag structure. b) pinched structure. Calculations for both structures were found using STM for the two most stable chains. c) The "Z" (zigzag) chain structure. d) The "P" (pinched) chain structure. Adapted from.[68]

As water is heated on an oxygen pre-exposed Cu(110) surface, different mixed water/OH phases are formed with different composition of water and hydroxyl. One of the phases is characterised by a 1:1 water/OH phase, as seen in figure 6. This phase can be broken down into two different types of 1D chains, an example is shown in figures 6c and d. The 'Z' zig-zag chain is the majority surface structure, consisting of a flat-water backbone with open branched OH that point slightly out along the Ni bridge sites. Conversely, in the H_2O-OH 'P' chains, water alternates in pairs along the close packed direction with a four times repeat, creating a 'pinch' type structure (fig. 6d). Although both chains have a slightly different arrangement, the core structure along the centre of either chain is the same, with flat-water alternating along either side of the Cu atoms in the close packed direction. Moreover, both chains are also pinned into position by tightly bound OH molecules in the Cu bridge sites, which stabilises the water backbone. Density function theory for the simulated structures above shows the most stable arrangement for water/OH on the Cu(110) surface (fig. 6c and d), revealing an excellent agreement with the STM images in figure 6a and b. All other simulated structures were not comparable, containing binding energies much less stable than those mentioned above.[68]

1.8. Overview of thesis

The majority of studies currently have investigated the interaction of water on a flat terrace, including those mentioned above. However, almost all these studies overlook using a more corrugated surface, reporting structures not at, or near the step edge. Furthermore, none discuss whether the enhanced reactivity of an open surface can change the outcome of the behaviour

of water, forming structures that do not mimic those structures observed on more inert surfaces. This brings the question of how does water interact with a more reactive or highly corrugated surface, compared to a flat surface? In this thesis, we will investigate these anomalies further, in the hope of addressing the differences with planar surfaces and forming an understanding of water's preference for binding, either at the step or on the terrace.

1.8.1. Open surfaces

The discovery of pentamer chains on the Cu(110) surface has prompted new studies to investigate the structure of water on other open-faced surfaces. This is because, before this study appeared, all water studies compared their water structure on a variety of metal surfaces with a hexagonal network. This led to many theoretical calculations predicting the structure and arrangements that could form on other surfaces with smaller lattice parameters, with one study suggesting that the Ni(110) surface would also favour the formation of pentamer chains. Although the Ni lattice parameters matched closely with Cu, the study did not fully consider the enhanced reactivity of Ni with respect to Cu, and whether water even adsorbs intact. While this may be true, the TPD analysis by Callen *et al.* suggests otherwise, with TPD profiles matching closely to those reported on Cu(110). In addition, existing LEED measurements for the structures on Ni(110) surface are almost certainly influenced by electron induced dissociation, as is observed on other reactive surfaces when using conventional LEED systems. The discussion in chapters 3 and 4 debates these ideas, providing clarity for the behaviour of water on this more reactive surface, with analysis of the structure and arrangement of water using various techniques, one of which includes a channel plate amplified LEED system that uses a low dose of electrons to avoid electron induced damage.

1.8.2. Corrugated surfaces

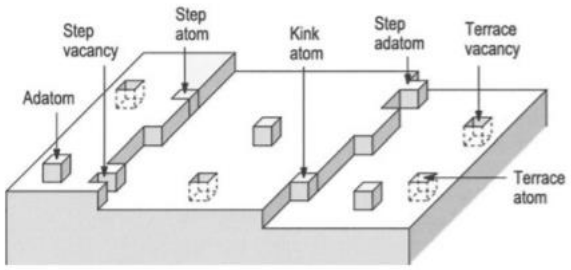

Figure 7. Showing the different types of surface defect sites present on a metal surface. Adapted from.[82]

Up to now, our picture of what a flat surface looks like has been dominated by the assumption that it is atomically smooth, containing an ordered array of regularly spaced atoms. However,

in most real-life cases metal surfaces will never be entirely flat, they will contain many surface defects, such as steps, terraces or gain boundaries. Regardless of this, the majority of studies consider defects to be a part of the background, and therefore little is known about how water interacts at these sites, and whether they play an important role in processes such as water dissociation. In more recent years, close examination of surfaces and their structure using STM has shown this to be the case, revealing that the surfaces will invertibility contain some form of surface roughening on the atomic scale, known as defects. The flat regions known as terraces are surrounded by these defects, such as steps, kinks and point defects (fig. 7). Since the local distribution of the number of defects varies, systems are typically simplified; surfaces containing a low ratio of defects are considered to be flat compared to a system with many defects, such as steps which are considered to be corrugated. Although not representative of all surfaces, this type of simplification resolves many of the issues with the classification of the type of surface used. In light of the above, stepped surfaces have gained more attention in the past decade with the hope of understanding water's complex interaction with different stepped surfaces. Therefore, in this thesis, we will discuss the idea of how different step sites, whether ordered or disordered can influence composition and structure on a stepped surface compared to other metal-water systems reported previously.

1.9. References

1. A. P. Gaiduk, F. Gygi and G. Galli, *The Journal of Physical Chemistry Letters*, 2015, **6**, 2902-2908.
2. E. Brini, C. J. Fennell, M. Fernandez-Serra, B. Hribar-Lee, M. Lukšič and K. A. Dill, *Chemical Reviews*, 2017, **117**, 12385-12414.
3. J. Wade, B. Dyck, R. M. Palin, J. D. P. Moore and A. J. Smye, *Nature*, 2017, **552**, 391.
4. S. Haq, C. Clay, G. R. Darling, G. Zimbitas and A. Hodgson, *Physical Review B*, 2006, **73**, 115414.
5. J. Carrasco, A. Hodgson and A. Michaelides, *Nature Materials*, 2012, **11**, 667-674.
6. S. Nie, P. J. Feibelman, N. C. Bartelt and K. Thürmer, *Physical Review Letters*, 2010, **105**, 026102.
7. K. Mistry, N. Gerrard and A. Hodgson, *The Journal of Physical Chemistry C*, 2023, **127**, 4741-4748.
8. S. Bashir, M. Mustafa, S. W. Safvi, N. A. Farhad and M. A. Rizvi, *Chiang Mai Journal of Science*, 2018, **45**, 1087-1098.

9. N. Kasai, Y. Kaku, S. Okazaki and K. Hirai, *Journal of Materials Engineering and Performance*, 2016, **25**, 4680-4685.
10. B. S. Zhang, S. Liu, S. J. Zhang, Y. Cao, H. L. Wang, C. Y. Han and J. Sun, *Small*, 2022, **18**.
11. D. W. Yang, L. B. Song, C. F. Wang, Z. L. Xiao and Tms, San Francisco, CA, 2009.
12. K. C. Lo and H. Y. Lai, *Coatings*, 2022, **12**.
13. A. S. Aliyev, R. G. Guseynova, U. M. Gurbanova, D. M. Babanly, V. N. Fateev, I. V. Pushkareva and D. B. Tagiyev, *Chemical Problems*, 2018, DOI: 10.32737/2221-8688-2018-3-283-306, 283-306.
14. K. Ito, H. Li and Y. M. Hao, in *Hydrogen Energy Engineering: A Japanese Perspective*, eds. K. Sasaki, H. W. Li, A. Hayashi, J. Yamabe, T. Ogura and S. M. Lyth, 2016, DOI: 10.1007/978-4-431-56042-5_9, pp. 137-142.
15. D. M. F. Santos, C. A. C. Sequeira and J. L. Figueiredo, *Quimica Nova*, 2013, **36**, 1176-1193.
16. N. A. Kelly, in *Advances in Hydrogen Production, Storage and Distribution*, eds. A. Basile and A. Iulianelli, 2014, DOI: 10.1533/9780857097736.2.159, pp. 159-185.
17. B. Zolotov, A. Gan, B. D. Fainberg and D. Huppert, *Journal of Luminescence*, 1997, **72-4**, 842-844.
18. W. T. Cahyanto, S. Zulaehah, W. Widanarto, F. Abdullatif, M. Effendi and H. Kasai, *ACS Omega*, 2021, **6**, 10770-10775.
19. J.-X. Zhu, J.-B. Le, M. T. M. Koper, K. Doblhoff-Dier and J. Cheng, *The Journal of Physical Chemistry C*, 2021, **125**, 21571-21579.
20. H. Prats, P. Gamallo, R. Sayós and F. Illas, *Physical chemistry chemical physics : PCCP*, 2016, **18**.
21. J. P. Clay, J. P. Greeley, F. H. Ribeiro, W. Nicholas Delgass and W. F. Schneider, *Journal of Catalysis*, 2014, **320**, 106-117.
22. Y. Sui and X. Ji, *Chemical Reviews*, 2021, **121**, 6654-6695.
23. X. Li, L. Zhao, J. Yu, X. Liu, X. Zhang, H. Liu and W. Zhou, *Nano-Micro Letters*, 2020, **12**, 131.
24. C. Lin, N. Avidor, G. Corem, O. Godsi, G. Alexandrowicz, G. R. Darling and A. Hodgson, *Physical Review Letters*, 2018, **120**, 076101.
25. C. Lin, G. Corem, O. Godsi, G. Alexandrowicz, G. R. Darling and A. Hodgson, *Journal of the American Chemical Society*, 2018, **140**, 15804-15811.

26. N. Gerrard, K. Mistry, G. R. Darling and A. Hodgson, *The Journal of Physical Chemistry C*, 2020, **124**, 23815-23822.
27. N. Gerrard, K. Mistry, G. R. Darling and A. Hodgson, *The Journal of Physical Chemistry Letters*, 2020, **11**, 2121-2126.
28. Y. Shi, H. Scheiber and R. Z. Khaliullin, *The Journal of Physical Chemistry A*, 2018, **122**, 7482-7490.
29. T. K. Ghanty, V. N. Staroverov, P. R. Koren and E. R. Davidson, *Journal of the American Chemical Society*, 2000, **122**, 1210-1214.
30. A. Hodgson and S. Haq, *Surface Science Reports*, 2009, **64**, 381-451.
31. R. J. Ouellette and J. D. Rawn, in *Principles of Organic Chemistry*, eds. R. J. Ouellette and J. D. Rawn, Elsevier, Boston, 2015, pp. 1-32.
32. D. Herschlag and M. M. Pinney, *Biochemistry*, 2018, **57**, 3338-3352.
33. in *Understanding Hydrogen Bonds: Theoretical and Experimental Views*, The Royal Society of Chemistry, 2021, DOI: 10.1039/9781839160400-00001, pp. 1-40.
34. B. Wang, P. Hou, Y. Cai, Z. Guo, D. Han, Y. Gao and L. Zhao, *ACS Omega*, 2020, **5**, 31724-31729.
35. J. E. Del Bene, I. Alkorta and J. Elguero, *The Journal of Physical Chemistry A*, 2018, **122**, 2587-2597.
36. M. Shibata and T. S. Kuntzleman, *Journal of Chemical Education*, 2009, **86**, 1469.
37. I. D. Madura, K. Czerwińska, M. Jakubczyk, A. Pawełko, A. Adamczyk-Woźniak and A. Sporzyński, *Crystal Growth & Design*, 2013, **13**, 5344-5352.
38. K. A. T. Silverstein, A. D. J. Haymet and K. A. Dill, *Journal of the American Chemical Society*, 2000, **122**, 8037-8041.
39. N. Musolino and B. L. Trout, *The Journal of Chemical Physics*, 2013, **138**, 134707.
40. N. L. Gershfeld, in *Molecular Association in Biological and Related Systems*, AMERICAN CHEMICAL SOCIETY, 1968, vol. 84, ch. 11, pp. 115-130.
41. T. P. Silverstein, *Journal of Chemical Education*, 2004, **81**, 35.
42. M. J. Qazi, S. J. Schlegel, E. H. G. Backus, M. Bonn, D. Bonn and N. Shahidzadeh, *Langmuir*, 2020, **36**, 7956-7964.
43. Y. Zhang, X. Ji and X. Lu, in *Novel Materials for Carbon Dioxide Mitigation Technology*, eds. F. Shi and B. Morreale, Elsevier, Amsterdam, 2015, 87-116.
44. J. Lyklema and I. Volume, *Solid-Liquid Interfaces*, *Academic Press*, 1995.
45. I. M. Hauner, A. Deblais, J. K. Beattie, H. Kellay and D. Bonn, *The Journal of Physical Chemistry Letters*, 2017, **8**, 1599-1603.

46. D. C. Ginnings and G. T. Furukawa, *Journal of the American Chemical Society*, 1953, **75**, 522-527.
47. P. G. Brewer and E. T. Peltzer, *Geophysical Research Letters*, 2019, **46**, 13227-13233.
48. J. G. Speight, in *Gasification for Synthetic Fuel Production*, eds. R. Luque and J. G. Speight, Woodhead Publishing, 2015, pp. 175-198.
49. C. T. A. Chen, *Journal of Chemical & Engineering Data*, 1987, **32**, 469-472.
50. I. Ryzhkin and V. Petrenko, *Physical Review*, 2001, **65**.
51. J. D. Bernal and R. H. Fowler, *The Journal of Chemical Physics*, 1933, **1**, 515-548.
52. V. Buch, P. Sandler and J. Sadlej, *The Journal of Physical Chemistry B*, 1998, **102**, 8641-8653.
53. J. L. Aragones, L. G. MacDowell and C. Vega, *The Journal of Physical Chemistry A*, 2011, **115**, 5745-5758.
54. P. A. Thiel and T. E. Madey, *Surface Science Reports*, 1987, **7**, 211-385.
55. L. Pauling, *Journal of the American Chemical Society*, 1935, **57**, 2680-2684.
56. W. B. Jensen, *Chemical Reviews*, 1978, **78**, 1-22.
57. L. Houqian, D. Guo, N. Ulumuddin, N. R. Jaegers, J. Sun, B. Peng, J.S. McEwen, J. H and Y. Wang, *American Chemical Society*, 2021, **1**, 1471-1487.
58. J. N. Stern, M. Seidl-Nigsch and T. Loerting, *Proceedings of the National Academy of Sciences*, 2019, **116**, 9191-9196.
59. C. Lin, G. Corem, O. Godsi, G. Alexandrowicz, G. R. Darling and A. Hodgson, *American Chemical Society*, 2018, **140**, 15804-15811.
60. J. Carrasco, A. Hodgson and A. Michaelides, *Nature Materials.*, 2012, **11**, 667.
61. G. B. Fisher and J. L. Gland, *Surface Science*, 1980, **94**, 446-455.
62. R. Ludwig, *Angewandte Chemie-International Edition*, 2003, **42**, 3458-3460.
63. M. L. Bocquet and N. Lorente, *Chemical Physics*, 2009, **130**.
64. J. Carrasco, A. Michaelides, M. Forster, S. Haq, R. Raval and A. Hodgson, *Nature Materials*, 2009, **8**, 427.
65. D. L. Doering and T. E. Madey, *Surface Science*, 1982, **123**, 305-337.
66. Z. Pang, S. Duerrbeck, C. Kha, E. Bertel, G. A. Somorjai and M. Salmeron, *The Journal of Physical Chemistry C*, 2016, **120**, 9218-9222.
67. R. Peköz and D. Donadio, *The Journal of Physical Chemistry C*, 2017, **121**, 16783-16791.

68. M. Forster, R. Raval, J. Carrasco, A. Michaelides and A. Hodgson, *Chemical Science*, 2012, **3**, 93-102.
69. J. Carrasco, A. Michaelides, M. Forster, S. Haq, R. Raval and A. Hodgson, *Nature Materials*, 2009, **8**, 427-431.
70. S. Maier and M. Salmeron, *Accounts of Chemical Research*, 2015, **48**, 2783-2790.
71. M. E. Gallagher, S. Haq, A. Omer and A. Hodgson, *Surface Science*, 2007, **601**, 268-273.
72. C. Clay and A. Hodgson, *Current Opinion in Solid State and Materials Science*, 2005, **9**, 11-18.
73. A. Šarić, S. Popovic and R. Trojko, *Journal of Alloys and Compounds - J ALLOYS COMPOUNDS*, 2001, **320**, 140-148.
74. K. Jacob, T. Uda, T. Okabe and Y. Waseda, *High Temperature Materials and Processes*, 2000, **19**, 11-16.
75. B. Phillips and A. Muan, *The Journal of Physical Chemistry*, 1960, **64**, 1451-1453.
76. D. G. Wood, M. B. Brown and S. A. Jones, *International Journal of Pharmaceutics*, 2011, **404**, 42-48.
77. D. Weibel, Z. R. Jovanovic, E. Gálvez and A. Steinfeld, *Chemistry of Materials*, 2014, **26**, 6486-6495.
78. B. Polyakov, E. Butanovs, A. Ogurcovs, S. Vlassov, M. Zubkins, I. Jonane, A. Cintins, A. Kalinko, A. Kuzmin and J. Purans, *Crystal Growth & Design*, 2020, **20**, 6147-6156.
79. P. B. Armentrout, *The Journal of Chemical Physics*, 2013, **139**, 084305.
80. M. Greiner, T. Rocha, B. Johnson, A. Klyushin, A. Knop-Gericke and R. Schloegl, *Zeitschrift für Physikalische Chemie*, 2014, **228**, 521-541.
81. L. J. Venstrom, J. H. Davidson and Asme, Phoenix, AZ, 2010.
82. K. Oura, M. Katayama, A. V. Zotov, V. G. Lifshits and A. A. Saranin, in *Surface Science: An Introduction*, eds. K. Oura, M. Katayama, A. V. Zotov, V. G. Lifshits and A. A. Saranin, Springer Berlin Heidelberg, Berlin, Heidelberg, 2003, DOI: 10.1007/978-3-662-05179-5_10, pp. 229-260.

Chapter 2

Experimental Overview

2.1. Overview of Ultra High Vacuum

In order to gain an atomic understanding of the behaviour and interactions of water on a metal surface and the resulting structures formed, water adsorption is studied under UHV.

These systems significantly reduce the potential issues associated with studying solid surfaces, with the most important fundamental problem being, how does one keep a surface which is susceptible to contaminates, clean and well defined? A UHV system reduces the rate at which containments collide with the surface by reducing the ambient pressure below 10^{-10} torr, which helps maintain a clean surface for as long as possible. This is explained in the example below;

We can demonstrate the importance of using a UHV pressure, if we compare 2 different pressures 10^{-6} and 10^{-10} torr (1 torr = 1.333×10^{-2} bar) at 300 K. The rate of contamination will depend upon the rate at which gaseous molecules will collide with the solid surface, using kinetic considerations this can be approximated.

$$Z = \frac{p}{\sqrt{(2\pi mkT)}} cm^{-2}s^{-1}$$

p = ambient pressure (N cm^{-2}), m = molecular mass (kg $molecule^{-1}$), T = absolute temperature (K), k = Boltzmann constant, Z = rate of surface bombardment.[1]

One must not forget to consider the sticking probability S(θ) of the gaseous molecules which will collide with the surface, as not all molecules will necessarily 'stick' to the surface.[2] The higher the sticking probability the greater the contamination of the surface, as less of the contaminants will deflect off the surface without adsorbing. However, let's consider that all molecules 'stick' (S(θ) = 1) in this instance, using CO as an example, we can estimate the flux using the equation below.

$$Z = \frac{(1.333 \times 10^{-2} \times 10^{-6})}{\sqrt{(2 \times \pi \times \frac{28}{1000 \times 6.02 \times 10^{23}} \times (1.38 \times 10^{-23}) \times 300)}} cm^{-2}s^{-1}$$

$$Z = 3.82 \times 10^{14} cm^{-2}s^{-1}$$

If we assume the atomic density is 10^{15} cm^{-2}.[1]

$$Z = \frac{3.82 \times 10^{14} cm^{-2} s^{-1}}{10^{15} cm^{-2}\ per\ monolayer} = 0.382\ monolayer\ s^{-1}$$

Following the above, the time taken to absorb approximately 1 layer at 10^{-6} Torr will be 2.6 s (1/0.382). Now if we do the same using a pressure of 10^{-10} torr, time per layer increases from 2.6 s to 7 hours and 27 minutes, which is a significant increase in time. This shows that the ambient pressure will have a significant impact on the surface quality when trying to maintain a clean surface. However, the presence of these undesirable contaminants which adsorb to the sample surface and the walls of the chamber is a consequence of spending a period of time at atmospheric pressure. Contaminants and residual gases (e.g. CO) that are present in atmospheric conditions can adsorb to the surface through either two ways, chemisorption or physisorption depending on the nature of the adsorbate.[3, 4] The term used for when species is held to the surface primarily by dispersion, or Van Der Waals interaction, is physisorption.[5, 6] In contrast, chemisorption, involves the formation of a stronger chemical bond (e.g. a covalent bond) between the surface layer and the adsorbate species.[7] Therefore, reducing the number of contaminants which can adsorb via each of the adsorption mechanisms described above is important, so that only the intended adsorbates are present on the surface during analysis and not the products of side reactions (e.g. $O + H_2O \rightarrow 2OH$).[8]

2.2. Overview of a UHV system pumping

To get up to a UHV pressure one must first remove any unwanted water vapour pressure in the chamber, this is achieved by baking the entire chamber to over 100°C for 96 hours, which allows the vapour to be pumped away using rotary, diffusion and turbo-molecular pumps. Once the entire chamber is baked, UHV pressures can be regained with the aid of a Titanium sublimation pump (TSP), which removes any residual gaseous species by sputtering Ti particles around the walls of the chamber via a high current Ti filament. Although the pumps are effective, the base pressure in the chamber is then limited by the presence of hydrogen which diffuses out of the stainless steel.

2.2.1. Chamber 1

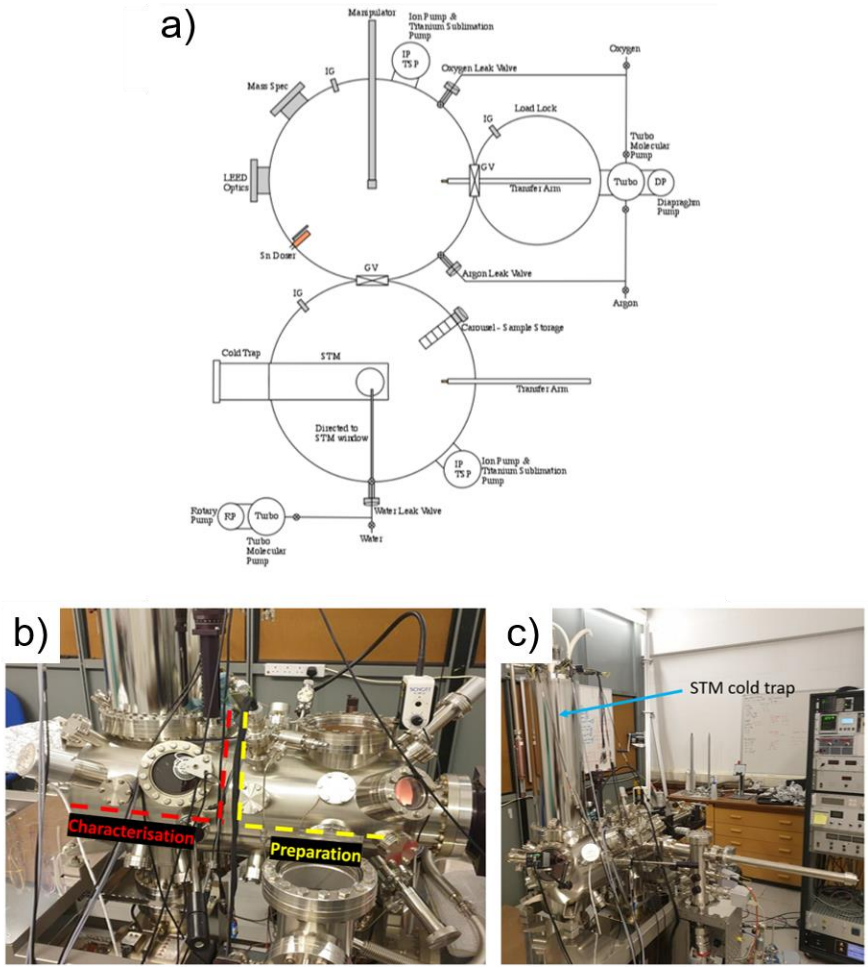

Figure 1. a) Schematic overview of the CreatTec Ultra High Vacuum low temperature instrument. b-c) The CreatTec Ultra High Vacuum instrument is used for STM sample preparation and surface analysis.

The STM chamber above is composed of two chambers that are separated by a gate valve (fig. 1), one is for characterisation and the other is for sample preparation (fig.1b). The samples can be transferred to either side of the chamber using the manipulators that translate a sample in the x, y and z directions, and rotate about θ. This UHV system is equipped with an ion pump and a TSP, which allows for an oil-free pumping system in both chambers. There is an additional separate turbo molecular pump backed by a diaphragm roughing pump in the load lock to allow samples to be loaded into the main chamber without compromising UHV pressures. Moreover, a cold trap is situated in the characterisation chamber at the top of the STM housing unit which is used to further aid the removal of residual gaseous adsorbate, resulting in a base pressure as low as 10^{-11} Torr on either side of the chamber. The STM housing unit is fitted with an outer jacket that acts as a shield to reduce boil-off and an inner jacket which holds the cryogenic liquid, such as liquid nitrogen or helium, reaching temperatures of

around 80 K or 4 K. Furthermore, the STM housing unit also contains a hole and shutter for an adsorbate dosing line where adsorbates can be directed at the sample surface, dosing at a rate of approximately a layer per minute, as described further in this chapter.

2.2.2. Chamber 2

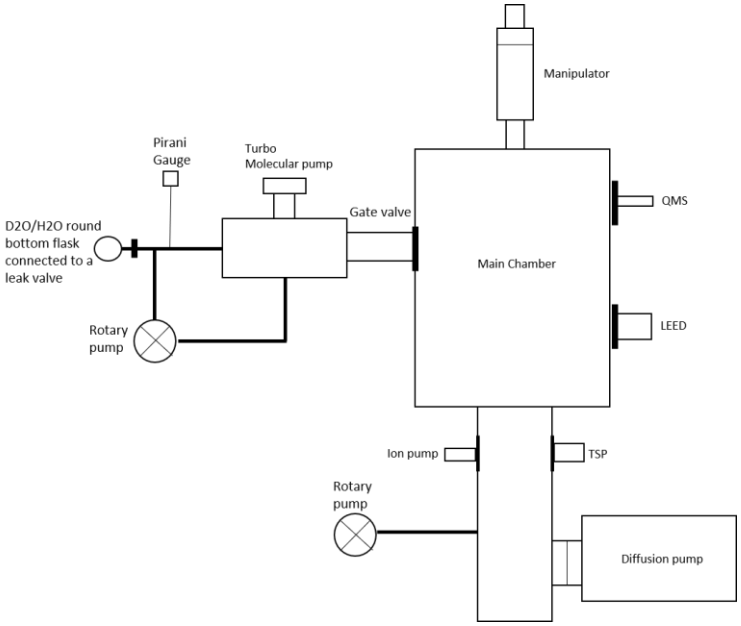

Figure 2. Simple schematic overview of the Ultra High Vacuum instrument used for LEED and TPD sample preparation and surface analysis.

The other UHV system in figure 2 consists of a three stage differentially pumped chamber with each stage independently cooled by water, with the third stage connected to the main chamber and additionally cooled by liquid nitrogen, which cryogenically pumps away any condensable gases. The main chamber is additionally fitted with a TSP which is fired periodically to further lower the pressure in the chamber, resulting in a base pressure as low as 10^{-11} torr. The chamber has been specially built with a turbomolecular pumped beamline, which is used to dose various adsorbates on the sample surface at a rate of approximately 0.4 layers per minute. The sample is suspended using tantalum wires between two tantalum posts to allow for conductive cooling when the manipulator cold trap is filled with liquid nitrogen. This chamber also contains LEED-AES optics (OCI multi-channel plate) with a dual microchannel plate amplifier to allow nA drain currents during LEED and avoid electron induced damage to the surface adsorbate layer. Furthermore, the chamber above contains a single manipulator that can translate the samples in the x, y and z directions, and rotate about θ due to the 360° rotatable seals.

2.3. Sample preparation

2.3.1. Preparation of a clean metal surface

Before experiments can take place, we must obtain a clean and well-ordered surface as the surface quality will have a significant impact on the binding of water. This was achieved by repeat cycles of sputtering for 10 minutes and annealing to various temperatures (specific temperatures found in each chapter). The sputtering process involved using an inert gas, such as argon and an ion gun to fire Ar^+ ions at the surface of the metal, which in turn removes the topmost layers and any contaminants present on the surface. It was important to heat the surface after sputtering so that the surface re-orders to form a flat surface. The sputter-anneal cycles were repeated regularly initially, and between experiments to ensure that the surface remained clean. Periodic oxygen treatments were also used in the initial stages to remove any carbon contaminants which may have diffused through the bulk while heating. This process consisted of dosing oxygen on the metal surface at a temperature of 500 K to liberate CO/CO_2, which can then be pumped away using the various pumps in the chambers mentioned above (fig. 1 and 2).

2.4. Surface characterisation

One of the most significant issues associated with studying metal-water interfaces, and certainly the one which has compromised many of the early ice film studies, is water's sensitivity to electron induced dissociation, which results in the re-structuring of the surface wetting layer, as mentioned in chapter 1. The use of some instruments, such as LEED, can induce dissociation, particularly on more reactive surfaces, such as Ni. However, if appropriate precautions are taken i.e. using a low current LEED with a channel plate amplified system, or rastering across a surface using a low bias voltage, these issues can be checked for by minimising the electron dose and translating the LEED spot across the surface. Using a few nA current and a defocused LEED beam, only the Ni(110) surface showed any appreciable damage on a timescale of 10s of minutes.

2.4.1. Temperature Programmed Desorption

Temperature Programmed Desorption (TPD) is a technique that allows one to understand the evolution and interactions between a gas and solid surface, thereby being a powerful tool in order to probe the binding energy of an adsorbate and surface reactions; for example, adsorption, surface substrate reactions and desorption.[9] This technique is especially important

in the field of catalysis, providing an understanding of how different gasses interact with the surface in order to evaluate the efficiency of the active sites present on the surface.[10, 11] The desorption kinetics of the surface structure in turn help one develop an understanding of how different structures form and evolve on different metal surfaces as a function of coverage and temperature. The nature of each of the different surface structures can then be further analysed using techniques such as Low Energy Electron Diffraction (LEED) and Scanning Tunnelling Microscopy (STM) to probe the structural arrangement.

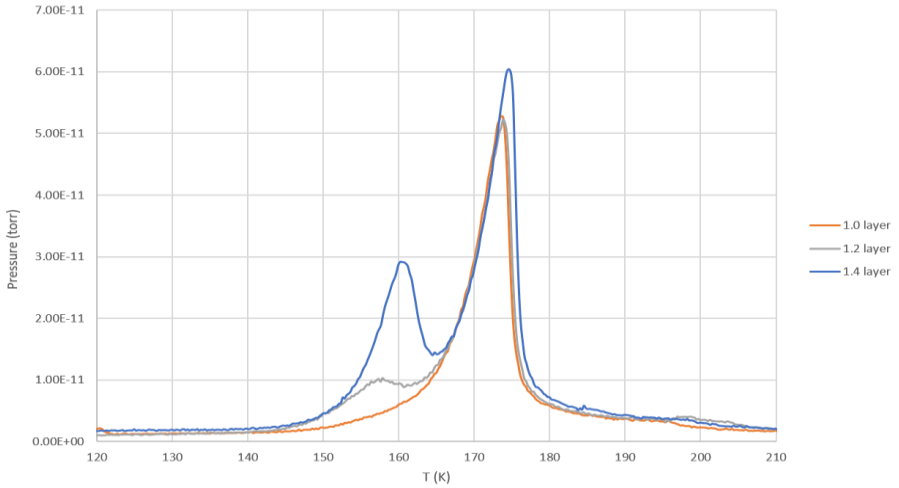

Figure 3. TPD spectra of various coverages of water heated on the Cu(511) surface. A single layer was defined as the amount of water needed to complete a single layer on the Cu(511) surface in the hexagonal 2D network, which exhibits a water density of 0.67 water per Cu surface atom.[12]

This technique involves dosing various amounts of water using a controlled molecular beam on the surface of a crystal that is held at 100 K. The amount of water that was adsorbed in our experiments was based on the calibration for a known 2D hexagonal network on a Cu(511) surface. Once water is adsorbed, a linear heating rate is then supplied via Ta wires which are spot welded to the suspended crystal, in turn the thermal energy is conducted from the solid interface into the thin water film at a constant rate (typically 1-2 Ks^{-1}). Upon heating, the Quadrupole Mass Spectrometer is set to monitor the pressure of D_2O/H_2O in the chamber as a function of time, which gives us a measure of the rate of desorption. Once a sufficient amount of thermal energy has been provided, some water may rearrange into a new structure whose formation is activated, for example by water dissociation to create a new H-bond structure, or all the water may desorb from the surface. The desorption of water results in an increase in partial pressure (monitored by the QMS), and once the majority of the gas has desorbed from the surface, the pressure of D_2O/H_2O will begin to drop significantly as most of the metal-water bonds will have been broken. However, if there is more than one layer of water on the surface, we will form two peaks, since the metal-water interactions are stronger than the water-water

interactions, causing the water above the first layer to desorb at a lower temperature as less energy is needed to remove them, as highlighted above in grey and blue (fig. 3).

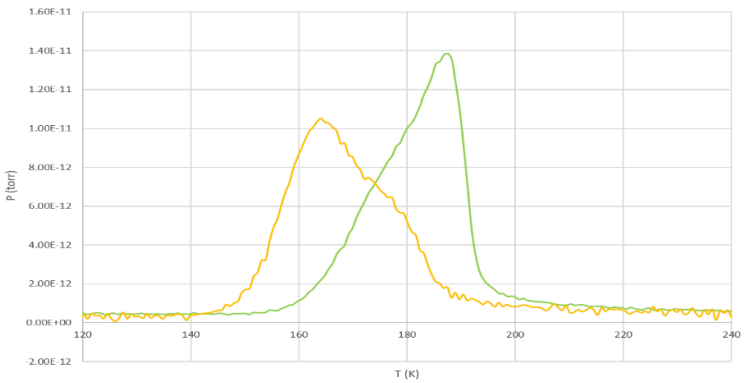

Figure 4. TPD spectra showing how a TPD profile for a fixed coverage of water (0.7 layers, relative to the calibrations on Cu(511) above) on a Pt(211) surface, with water on a clean Pt surface highlighted in green and an contaminated Pt surface highlighted in yellow. The TPD spectra shows how water on the surface is influenced by surface cleanliness, shifting to a lower temperature as the surface is not cleaned by repeat sputter-anneal cycles in between experiments.

In addition to the above, TPD was used to observe the surface cleanliness, this is because a clean surface will produce a well-defined peak as no other contaminants will influence the binding energy. A contaminated surface will generally produce a shallow broad curve rather than a steep narrow water peak (fig. 4), due to contaminates causing water to weakly adsorb to the surface, resulting in some water desorbing at a lower temperature. Alternatively a contaminant such as O may react to from OH, stabilising water to form a high T desorption peak.

Before TPD coverage sets were taken on various metal surfaces, the beamline was calibrated for water on Cu(511), which involved using a fixed D_2O/H_2O beam pressure over different lengths of time, until the closest TPD profile to a single layer was observed. This enabled a single-layer water dose to be defined as 0.67 water per Cu surface atom, taking ca. 0.4 layers per minute to dose water, which was based on the wetting of the first layer hexagonal structure on Cu(511).[12] Any coverage of more than a single layer creates an additional peak, as seen in grey and blue above (fig. 3), which enabled us to determine the closest coverage to a single layer. The calibrations were then monitored between different experiments to ensure that the calibrations for the coverage of water remained constant. We note that this was only used to estimate the coverage of water on the different metal surfaces relative to Cu(511), however, the known 2D wetting layer allowed us to form comparisons with the amount of water needed to form a single layer on other metal surfaces e.g. a 2D network on a different metal surface

would require a similar amount of water to that on Cu(511), which helps identify the structure of surface wetting layers. In contrast, the neighbouring chamber used STM analysis to determine the approximate coverage, dosing at a rate of approximately a layer per minute. This was achieved by monitoring a fixed pressure of water in the STM housing unit using the ion gauge over different periods of time until the closest coverage to a single layer was achieved. Although both chambers were used for different analytical techniques, both chambers dosed water at a similar rate, taking more than a minute to adsorb a single layer of water. It was important that the rate of adsorption was slow, as many of the structures reported in this thesis are coverage dependant, thus giving us more control over the structures formed.

2.4.2. Low Energy Electron Diffraction

Diffraction is a property of a wave, and therefore, if you change the energy of the electrons being fired at a surface it results in the changing of its wavelength. If one uses a higher energy, then it consequently reduces the wavelength of the electrons, and vice versa. The different wavelengths of the electrons create either constructive or destructive waves when fired at the surface, which can give information about the region you are sampling, as described below.

We used Low Energy Electron Diffraction (LEED) to develop an understanding and examine the structure of how thin ice layers evolve with a temperature in situ. The principles of LEED are fairly simple, a current is supplied to a photo-cathode in a LEED gun which causes the electrons to be excited, resulting in a collimated mono-energetic beam of electrons being fired at the surface. The elastically back scattered electrons are diffracted off the sample surface and detected across a fluorescent screen, which measures the angular intensity distribution, giving a reciprocal space pattern that represents the symmetry and the unit cell of the surface structure. The electrons directed at the surface can only penetrate a small number of surface layers, thus the surface structure is determined by the top atomic layers. The electrons cannot probe the crystal periodicity perpendicular to the surface unless LEED IV structure measurements are performed, limiting our understanding to two dimensions.

2.4.3. Scanning Tunnelling Microscopy

The scanning tunnelling microscope achieves its unsurpassed spatial resolution by exploiting the quantum phenomenon of tunnelling electrons from a scanning tip with atomic precision, allowing one to gain an atomic understanding of the structure and orientation of surface atoms. The first working scanning tunnelling microscope was invented by Binning and Rohrer in the 1980s at IBM Zurich Research laboratories,[13] who won a Nobel prize in physics for this

discovery. Their work changed our view of the world, turning conventional thinking upside down, which prompted many research studies into investigating atoms and molecules at the atomic scale.

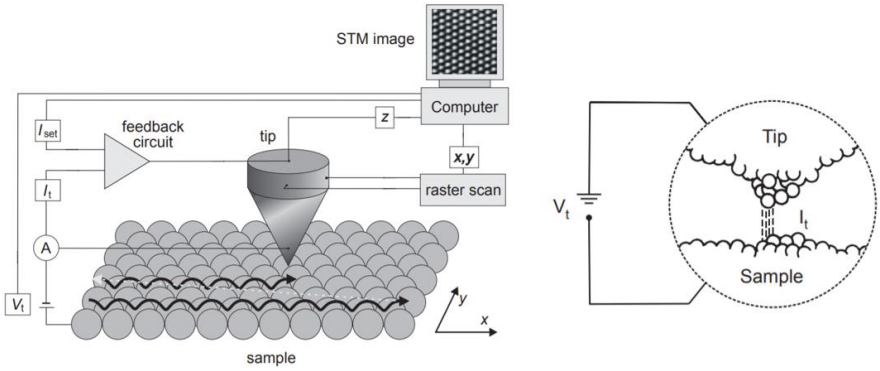

Figure 5. Simplistic schematic of the STM probe scanning over a surface. Adapted from.[14]

A bias voltage is used to influence the direction of the flow of tunnelling electrons from the tip to the conducting surface, for example; the polarity of a positive bias voltage causes the fermi level of the tip to be higher than the fermi level of the surface, which allows the electrons to tunnel from the tip through the vacuum to the surface unoccupied orbitals. However, this is only possible when the tip moves within angstroms of a conducting surface, as the process of quantum tunnelling is forbidden by classical mechanics, but when the tip-surface distance is very small electrons tunnel across a vacuum gap. This, therefore, allows electrons from the Fermi level of the tip to tunnel into vacant states on the surface atoms.

The current which flows between the tip and sample is hugely dependent on the tip-sample distance, this is because the current decays exponentially with distance away from the surface. The STM exploits this dependence of the tunnel current on the tip-sample distance to obtain height profiles of the sample using either, constant current or, constant height mode (fig. 5). In constant current mode, the tip-surface distance is constantly monitored using a feedback loop, which adjusts the height of the tip depending on the changes in current. These constant changes in the tip-surface distance can be used to create an image of the surface, which can be used to analyse the arrangement of atoms and any structures of adsorbates present. On the other hand, in constant height mode, the STM tip is kept at a constant height above the sample, measuring the change in current to create the image. The limitation with using constant height mode is that there needs to be minimal noise and the surface needs to be flat, otherwise the STM probe could potentially crash into the surface. As well as the above, the atomic resolution is dependent on how many atoms are tunnelling into surface atoms, as the fewer number of atoms the higher

the resolution. This is valuable for imagining an individual atom or a collective number of atoms in the surface plane of the sample, giving structural information i.e. lattice spacing or arrangement or atom size.

2.5. Conclusion

To conclude, the various techniques described in this thesis were essential to create a clear understanding of the structures being examined. Each of the chapters in this thesis contains further information about individual experimental procedures used for the preparation, and characterisation of each of the different metal surfaces to which they apply.

2.6. References

1. C. J. Knill and J. F. Kennedy, *Bioseparation*, 1999, **8**, 340-340.
2. M. Bowker, I. Z. Jones, R. A. Bennett and S. Poulston, *Surface Science and Catalysis*, eds. N. Kruse, A. Frennet and J. M. Bastin, Elsevier, 1998, vol. 116, pp. 431-439.
3. T. Keii and I. Okura, *Journal of Japan Society of Lubrication Engineers*, 1978, **23**, 192-195.
4. H. J. Zhai and L. S. Wang, *Journal of Chemical Physics*, 2005, **122**.
5. F. Huber, J. Berwanger, S. Polesya, S. Mankovsky, H. Ebert and F. J. Giessibl, Science, 2019, **366**, 235-+.
6. D. Borodin, I. Rahinov, P. R. Shirhatti, M. Huang, A. Kandratsenka, D. J. Auerbach, T. L. Zhong, H. Guo, D. Schwarzer, T. N. Kitsopoulos and A. M. Wodtke, Science, 2020, **369**, 1461.
7. H. Kasai, M. C. S. Escano, H. Kasai and M. C. S. Escano, *Physisorption at Surfaces*, *IOP Science*, 2016.
8. R. G. Quiller, T. A. Baker, X. Deng, M. E. Colling, B. K. Min and C. M. Friend, *Journal of Chemical Physics*, 2008, **129**.
9. R. J. Cvetanović and Y. Amenomiya, *Catalysis Reviews*, 1972, **6**, 21-48.
10. T. Ishii and T. Kyotani, *Materials Science and Engineering of Carbon*, eds. M. Inagaki and F. Kang, Butterworth-Heinemann, 2016, 287-305.
11. J. L. Falconer and J. A. Schwarz, *Catalysis Reviews*, 1983, **25**, 141-227.
12. C. Lin, N. Avidor, G. Corem, O. Godsi, G. Alexandrowicz, G. R. Darling and A. Hodgson, *Physical Review Letters*, 2018, **120**, 076101.
13. G. Binnig and H. Rohrer, *Reviews of Modern Physics*, 1987, **59**, 615-625.
14. A. Rønnau, *Thesis, Nanoscience center, University of Aarhus*, 2003.

Chapter 3

An investigation into the Structure of Intact Water on the Open Ni(110) Surface

3.1. Introduction

The use of Nickel, or Ni-alloys has been particularly relevant in the field of corrosion due to Ni exhibiting anti-corrosive properties, which is ideal for coating on metal surfaces that readily undergo oxidation in contact with water, such as Fe.[1-3] In order to use Ni effectively, one must first understand the interactions of water at its surface, which can help build improved coating that are more resistant to corrosion. Considering this, much research has gone into understanding the interaction of water, OH and other intermediate species, with studies investigating the structures and barriers associated with water on the Ni surface.[4] While studies on close packed Ni(111) faces have shown it to reversibly adsorb molecular water, other surfaces, such as Ni(110) have been studied at length as a result of its enhanced reactivity, with conflicting reports for the structure of water at low temperature showing that there is much still to be learnt. [5-7]

One of the first reports of a water structure on the Ni(110) surface was by Benndorf *et al*.[8, 9] who reported that a c(2x2) low energy electron diffraction (LEED) pattern exists in the temperature regime of 130 to 180 K. Coincidentally, a similar LEED pattern was observed on a Cu(110) by Bange *et al*. with the report suggesting that this LEED pattern was caused by the growth of a hexagonal bilayer of water. This gave Benndorf *et al*. an insight into the potential growth of water on the Ni(110) surface, and a basis for the arrangement of water.[10] This resulted in the following model of water proposed by Benndorf *et al*. consisting of a water bilayer arranged into a strained hexagonal lattice, compressed in the [110] direction and elongated in the [001] direction.[11] The arrangement contained O-O separations of 2.54 Å and 2.94 Å, similar to the O-O separations found in ice (~2.7 Å).[8, 12] Further to this, the study suggested that this arrangement is unfavourable at low coverages, due to the second layer being necessary for the construction of the hexagonal bilayer model.[8]

While this proposed structure by Benndorf *et al*.[9] may have been plausible, further studies using Electron Stimulated Desorption Ion Angular Distribution (ESDIAD), Reflection adsorption

Infra-Red Spectroscopy (RAIRS) and LEED by Callen et al. did not agree.[13] Instead, the study suggested that the structural model was composed of a single layer of water in a c(2x2) hexagonal arrangement, containing nearest neighbour separations of 4.3 Å.[14] This distance is much larger than the O-O distances in ice (2.76 Å), which indicated that the structure is composed of water with no intermolecular hydrogen bonding.[15] Further to this, Nuclear reaction analysis (NRA) data of water on Ni(110) at 180 K also disagreed with the bilayer model, with results indicating that the layer saturates at a coverage of 0.5 ML, which suggested that the second layer is not an intrinsic part of the c(2x2) structure.[8, 14]

Further investigations into the arrangement of water in the model described above using SEXAFS and NEXAFS by Pangher *et al*.[16] found that water favours the top sites with respect to the surface normal. The study gave evidence of a single O-Ni bond distance of 2.06 Å, which was similar to the distances found in calculations on Ni(111).[17] This result conflicted with the distorted bilayer model due to a second O-Ni distance being required for the construction of the c(2x2) bilayer model proposed by Benndorf *et al*.[9] thus agreeing better with the findings proposed by *Callen et al*.[18]

Although these models seemed plausible, further characterisation of water on Ni(110) by Pirug et al.[15] revealed that water dissociates in the temperature regime of 180 K and above, indicating that the previously proposed structures actually contain OH. Pirug et al. gained evidence for this using LEED, X-ray Photoelectron Spectroscopy (XPS) and Ultraviolet Photoelectron Spectroscopy (UPS) techniques, which made the concept of the pure H_2O bilayer proposed previously implausible.[14] These findings demonstrated the continued uncertainty that surround the adsorption of water on this surface, and whether water even adsorbs intact. Overall, there appears to be a general agreement within previous literature that the dissociation of water occurs at around 180 K on Ni(110), but the nature of adsorption considerably below remains unknown. Therefore, in this study, we will use more recent technological advances, such as DFT, STM and low current LEED to identify whether water adsorbs intact on the surface at much lower temperatures than those used previously, or spontaneously dissociates in contact with the surface.

Since there is a lot of uncertainty surrounding the interactions of water on the reactive Ni(110) surface, more inert surfaces that exhibit similar surface characteristics, such as Cu(110), can give an insight into the interactions that can be found on Ni at lower temperatures. Carrassco et al.[19] have shown that water does absorb intact on Cu(110), forming 1D pentagonal chains

that lie along the [001] direction at low temperature. Further analysis using DFT supports this, showing that water maximises the proportion of water molecules planar to the surface in this arrangement, whilst maintaining a relatively strong hydrogen bond with minimum strain. Since the lattice constant on Cu and Ni are very similar, it is also possible that water may adopt this structure at low coverage on Ni(110).

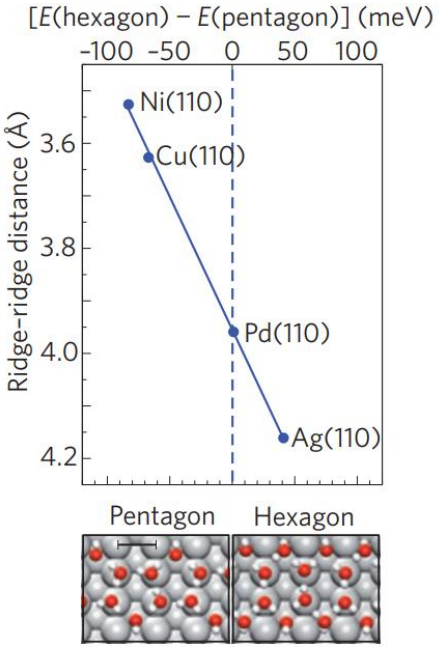

Figure 1. Illustration showing the expected outcome of waters arrangement on various (110) metal surfaces, based on DFT calculations. This graph compares a calculation for a face sharing hexagonal chain with a face sharing pentagonal chain, with results predicting that pentagons are favoured on Ni and Cu, and hexagons are favoured on surfaces with larger lattice spacings, including Pd and Ag. Adapted from.[20]

A recent study using DFT on open (110) surfaces has suggested that there is a strong correlation between favouring water hexamers vs pentamers and the lattice constant of a metal surface (fig. 1). This study found that metals with a larger lattice constant, such as Ag(110) prefer a hexagonal arrangement of water compared to metals with a smaller lattice constant, such as Cu(110) which prefer a pentagonal arrangement.[19, 20] Therefore, when assessing the arrangement of water on Ni(110), we may compare it to Cu(110) and the data above suggest that Ni(110) has an even larger preference to form a pentamer structure. Although this prediction seems reasonable, the structure and interaction of water at a metal interface cannot always be anticipated, for example, as in the early water adoption studies on Ru(0001), mentioned in chapter 1.[21-25] Moreover, one must also consider the difference in reactivity between Cu and Ni, as to the strength of the metal-water bond is a key factor to consider for the possibility of water forming 1D or 2D structures. Therefore, the many possibilities of what

water could do on Ni(110) leaves it unclear whether water will mimic its interaction with its neighbouring transition metal, Cu(110), or form structures that are different altogether.

The adsorption of water onto a surface reflects the conflict between maximising the binding energy to a surface while minimising the strain within the H-bond structure - water must accommodate both to grow in an ordered arrangement. Although this principle is now generally understood, little is known about how water does this on the reactive Ni(110) surface, with previous literature showing conflict for the arrangement of water and structures being misinterpreted. On the other hand, inert surfaces such as Cu(110), are comparatively better understood, with several different water and OH/H_2O structures having been reported on Cu(110).[19, 26-28] Therefore, understanding the adsorption on Ni(110) will reveal a more detailed molecular understanding of water adsorption on a reactive surface. For that reason, we have carried out measurements to combine global and local probes, such as LEED and STM with DFT calculations to determine the structure of water on this surface. In this chapter, we present results based on the LEED diffraction spots observed at 100 K, which allow us to come to a consensus about the c(2x2) diffraction pattern reported in early water adsorption studies, and helped to characterise the adsorption of water on the Ni(110) interface, clarifying the interpretation of the STM reported by *Gerrard*.[29, 30]

3.2. Experimental

LEED experiments were performed in a single stainless steel ultra-high vacuum (UHV) chamber with a base pressure $\leq 8 \times 10^{-11}$ torr. The Ni(110) surface was cleaned by cycles of Ar^+ ion sputtering using a discharge current of 20 mA and annealing to approximately 820 K, which removed any contaminants present on the surface. Four repeat cleaning cycles were necessary initially to give good surface quality, with two repeat surface cleaning cycles between each experiment. The sample was held on a manipulator between two tantalum wires that were spot welded to two tantalum posts, which cooled the crystal down to 100 K using liquid nitrogen as a cryogen. The chamber contained a LEED and quadrupolar mass spectroscopy instrument, which provided us with the ability to observe the lateral order of the surface water structures and define the coverage of water.

Before LEED experiments were taken on Ni(110), the beamline was calibrated for water on Cu(511) surface using TPD, which involved using a fixed beam pressure over different lengths of time, until the closest TPD profile to a layer on Cu(511) was observed. This enabled a single layer to be defined as 0.67 water per Cu atom, defined here as 1 ML water, based on the wetting

of the first layer hexagonal structure on Cu(511). We ensured that the calibrated beam position and UHV conditions, with respect to Cu(511), remained constant throughout the Ni(110) experiments. However, we note that this was only used to estimate the coverage of water on the Ni(110) surface, which allowed us to form comparisons with a known 2D wetting layer. A more detailed description of how water was dosed on the Cu(511) surface can be found in chapter 2.

Details of the STM experiment and DFT calculations can be found in the reports made by *Gerrard*.[29, 30]

3.3. Results and Discussion

3.3.1. Scanning Tunnelling Microscopy and DFT of the first water layer

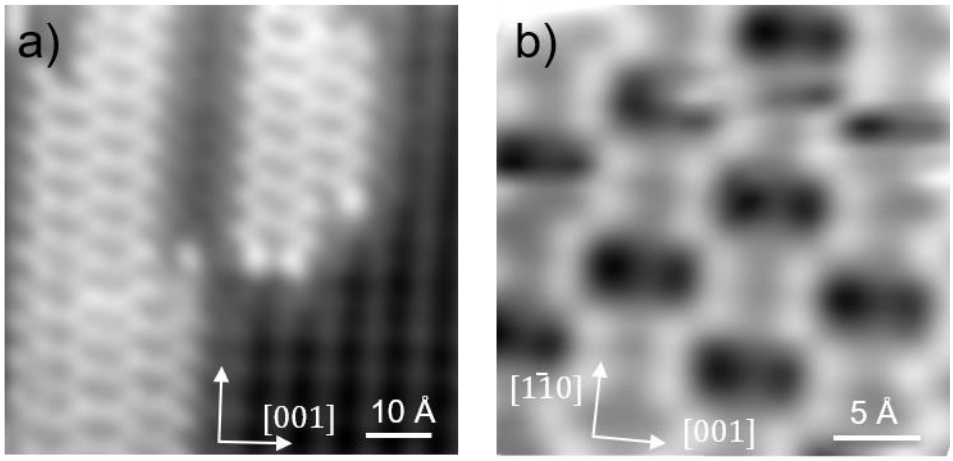

Figure 2. An STM image taken after water was dosed on the Ni(110) surface at 77K. a) the 'zig-zag' intact water chain. b) the 'Wiggly' water chain.

The STM images above were obtained by dosing water at 77 K on the Ni(110) surface (fig. 2), which shows intact water that sits in alternate pairs, or individually along the $[1\bar{1}0]$ direction. The zig-zag structure in figure 2a consists of water adsorbed on alternate sides of the Ni top sites, joined by hydrogen-bonded waters that zig-zag along in the $[1\bar{1}0]$ direction. Each of these chains is separated by a two times repeat in the $[001]$ direction (a distance too great to be explained by H bonding), creating a two times repeat in both the $[001]$ and $[1\bar{1}0]$ direction. On the other hand, the linear 'wiggly' chain (fig. 2b) consists of water with pairs of water molecules that alternate along each side of a Ni chain in the close packed direction with a four unit repeat (fig. 2b). Further STM analysis of both structures found that the zig-zag structure was the majority structure, with only small regions forming the wiggly chain structure. There

is also the presence of zig-zag chains that are staggered and out of phase with one another in the [001] direction, however, these chains appear much less than even the minority structure.

Further to this, we found that the wiggly chains disappeared over a small period of time at 80 K, converting into the (2x2) zig-zag chains, which suggested that the zig-zag structures is more stable structure. Although it appears that there is no water present on Ni rows between neighbouring chains in both structures, it is possible some of the water is not being imaged in between these chains. This question must be addressed as it seemed unlikely that regions of water would accumulate with one Ni missing row in between chains in a well ordered arragement, yet not fill the bare Ni row with water in between neighbouring chains. This behaviour is much different to any other water-metal interactions observed on previous surfaces, particularly Cu(110),[19, 27, 28] and implies a much lower first layer water coverage than on all other metal surfaces studied previously.

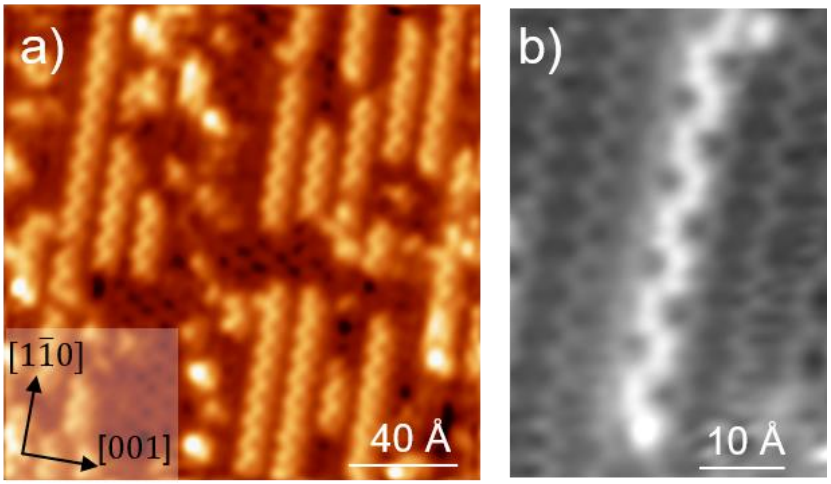

Figure 3. a) An STM image showing bright linear chains, taken at 77 K. b) A close up STM image of a bright linear chain filling the gap in between two zig-zag 1D chains, taken at 77 K.

STM reveals bright features that appear along the [1$\bar{1}$0] direction as the coverage is increased further, showing a linear structure with a very distinct and unusual shape (fig. 3). These bright features consist of regular chains with pairs of features on either side of the centre line of the gaps in between two zig-zag structures (fig. 2a). Furthermore, these chains have a characteristic arrangement, never being less than 4 Ni units apart in the [001] direction, and only forming in between adjacent (2x2) first layer chains, forming regions with a (4x4) period as the chains get denser. Interpreting this STM image further requires us to understand if this layer of water is binding above a row of bare Ni atoms, or if there are water molecules adsorbed on the surface

beneath this structure, as the bright chains in figure 3 have a large contrast difference to the structures in figure 2.

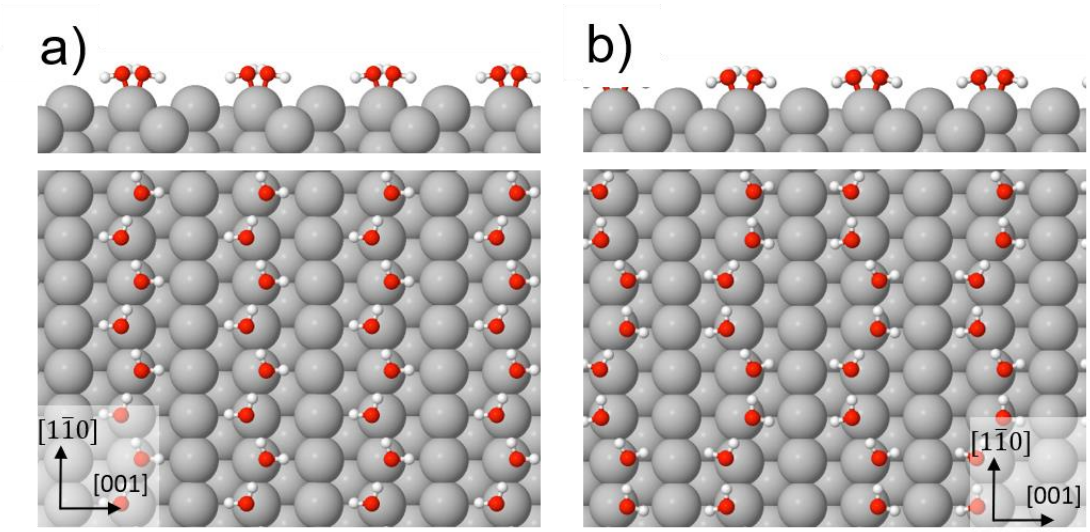

Figure 4. DFT calculations for the structures observed in figure 2, which shows the arrangement for water in the most favourable model, a) the zig-zag chains. b) the wiggly chains.

Further to the STM images in figure 2, DFT calculations suggested that both the zig-zag and wiggly chains contained intact water planar along the Ni top sites in the close packed direction. The zig-zag structure in figure 4a consists of water adsorbed flat on alternate sides of the Ni top sites, with each of the neighbouring chains separated by a row of bare Ni atoms to create a (2x2) structure. In contrast, DFT shows that the linear wiggly chain in figure 4b consists of pairs of flat water that alternate along each Ni side in the [1$\bar{1}$0] direction with a four unit repeat. The zig-zag structure has a slightly higher binding energy of 0.871 eV/water, compared to its slightly less stable wiggly structure (0.864 eV/water). Although the binding energies are very similar (0.034 eV/ water difference) in theory, practically we can see that the zig-zag structure is the favoured structure of water at 80 K. This would further suggest that if the temperature was raised slightly higher, so that water was more mobile during adsorption, it would be unlikely that the (4x4) structure would appear. This explained why we observe the wiggly chain structure converting into the more stable (2x2) arrangement when left over a short period of time in STM, as mentioned above. Furthermore, despite these structures having only two H-bonds per water, both chains displayed binding energies that are very slightly more stable than 2D hydrogen-bonded networks with three H-bonds per water, with a best bnding energy of 0.831 eV/water. Energy differences of this size are too low to be considered reliable, making it impossible to predict the behavior of water on Ni(110) from DFT alone.

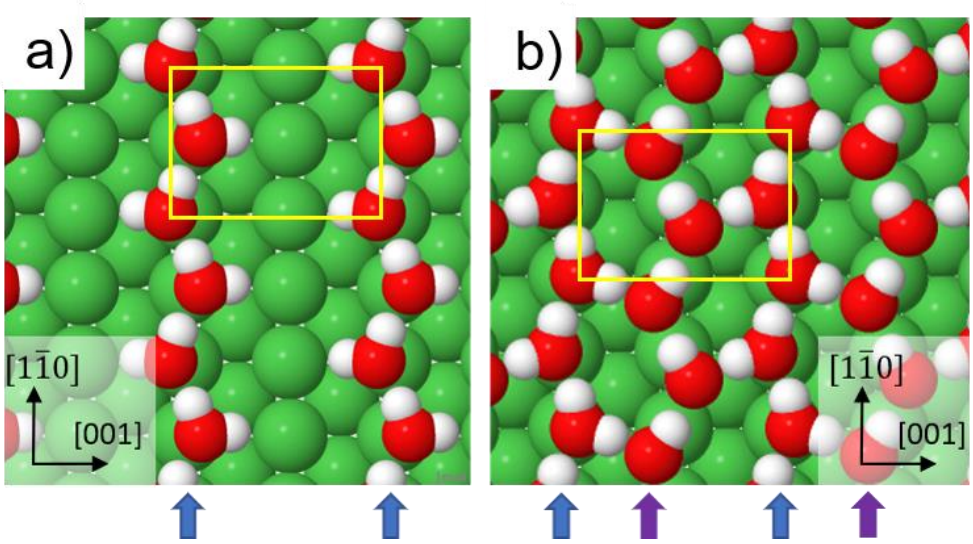

Figure 5. DFT simulation for the arrangement of water in figure 2a, with the blue arrows showing the position of the flat zig-zag water chains, purple the H-down water chains that run along the Ni top sites in the close packed direction, and unit cell highlighted in yellow, a) zig-zag chain. b) 2D (2x2) hexagonal network.

In order to understand whether the bright features grew on bare Ni rows, or atop water in the missing Ni rows in between neighbouring chains, we needed to understand the first layer structure further. Although the simple 1D zig-zag chains seem plausible, we do not know the water coverage associated with the STM images shown in Fig. 2, and these arrangements in figure 5 have a very low density, leaving half of the Ni sites unfilled. Therefore, further DFT calculations were undertaken to find an appropriate 2D layer that would form a network and join these linear 1D zig-zag chains, which could be used as a comparison to the low density chains in figure 5a. The calculations incorporated many arrangements for a hexagonal layer, since many metal surfaces have observed a hexagonal 2D layer to be stable,[19, 20, 31, 32] and previous literature reports a hexagonal structure for water on Ni(110).[9, 14, 33] DFT calculations found a stable hexagonal network with twice as much water on the surface (fig. 5b), formed of a highly buckled structure with chains of flat and H-down water along the close packed direction. It is apparent that both structures above share similar arrangements for water, as indicated by the blue arrow, which shows the positions of the intact flat water chains that have the same arrangement and spacing in both simulations on the Ni(110) surface (fig. 5). However, the hexagonal structure contains an addition H-down chain in between the flat zig-zag water chains, as indicated by the purple arrows in figure 5b. This distinct difference between the flat water chains and H-down chains in the hexagonal network, gives a potential reason for one of the chains to be a lower contrast than the other, which may cause only one of the chains being observed in STM.

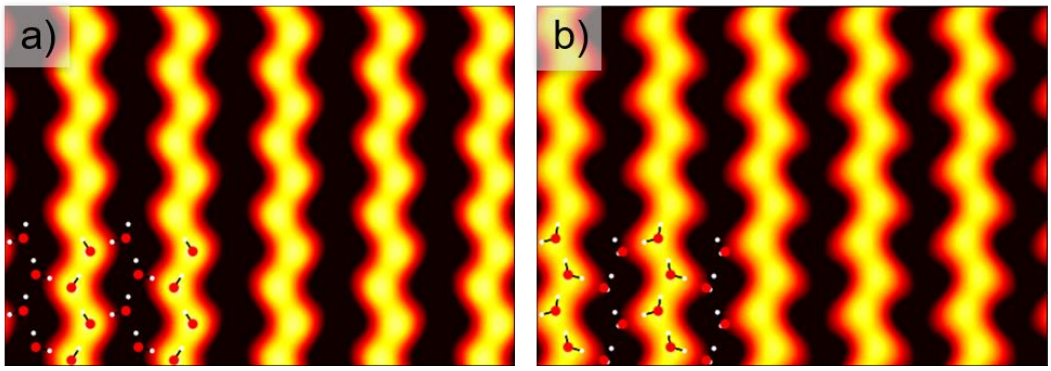

Figure 6. STM simulation of the hexagonal model, showing different bais voltages (± 0.1 V) could reveal the different chains of water in the [$1\bar{1}0$] direction in figure 5b. a) Image showing H-down water as bright zig-zag chains. b) Image showing the flat water as bright zig-zag chains.

Before any further experimental support was carried out, the Tersoff-Hamann approximation was carried out to try to simulate how the (2x2) zig-zag structure in figure 2a would be imaged in STM, and whether a (2x2) structure was caused by the hexagonal network. This type of simulation was used to further help us understand whether water would be present in between the missing Ni rows and provide supporting information for the (2x2) hexagonal network in figure 5b. The simulations shown in figure 6, display alternate orientations for water in bright and dark zig-zag chains with two different bias voltages for either orientation. The results supported the hypothesis that flat water zig-zag chains sit between bright H-down chains of water, and will image with a lower contrast to that of the neighbouring chain i.e. being invisible under some STM scan conditions. However, the STM data shows no sign of any features in between the (2x2) neighbouring chains, irrespective of tip changes or voltage, etc. Furthermore, assigning this structure to 2D islands of hexagonal water composed of flat and H down water leaves it unclear how to assign the wiggly chain structure (fig. 4b), since DFT calculations support no other structures that have the same relative stabilities to be formed along the Ni close packed direction. Since we can devise no other equivalent H-down water structures that would create this wiggly chain arrangement, and STM simulations for this (2x2) structure show only the upper H-down water. It is not possible to distinguish the structure of the complete (2x2) water layer from the arrangement in figures 5a and b, based on the STM images alone. Therefore, additional experimental evidence is required, for example, a calibration of the water coverage at which this first water layer completes and determination of the lateral ordering as a function of water coverage.

3.3.2. Low Energy Electron Diffraction

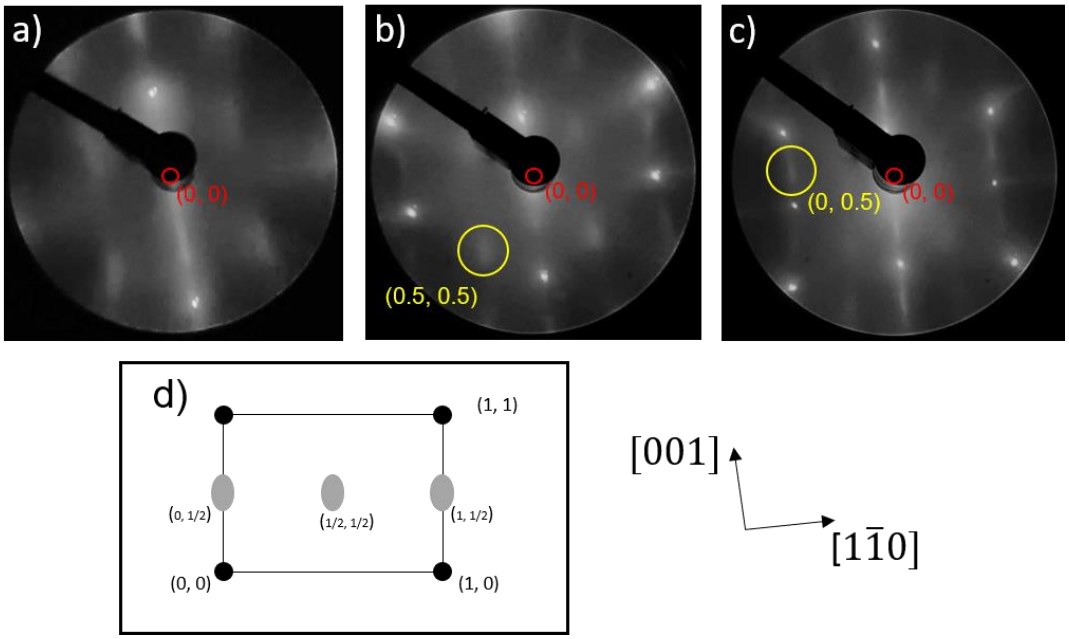

Figure 7. Shows LEED images for water adsorption at a coverage of ca. 0.5 ML, taken at 100 K. a) LEED pattern at 62 eV. b) LEED pattern at 79 eV. c) LEED pattern at 109 eV. LEED images contain red circles for the centred (0, 0) spot, with the diffraction spots at the half order positions highlighted in yellow. d) LEED illustration showing the combined diffraction patterns in figure a-c).

The lateral order of water on the Ni(110) surface was monitored using low energy electron diffraction, revealing that the same diffraction pattern persists up to ca. 0.5 ML, with the most intense half order beams being observed at ca. 0.5 ML (fig. 7a-c). The diffraction pattern at this coverage shows bright integer order spots for Ni with the presence of a streaked water overlayer, which consists of diffraction spots for water at the half order positions in both the [1$\bar{1}$0] and [001] direction (fig. 7d). These observations suggested that the water surface structure was composed of a (2x2) unit cell with a two times periodicity in both the [1$\bar{1}$0] and [001] direction. It is evident from these images above that there is more order in the [1$\bar{1}$0] direction, with streaking appearing to be observed considerably more in the [001] direction, compared to the [110] direction. This shows that there is a clear preference for water to contain a two unit repeat along the close packed [1$\bar{1}$0] direction, compared with the [001] direction at ca. 0.5 ML. The disorder along the [001] direction is consistent with 1D water chains being either in or out of phase with one another, since this is set not by any H-bonding but by weaker, next nearest neighbour, through surface interactions. So far this supports the STM data (fig. 2), giving evidence to support the (2x2) structure that leaves bare Ni rows in between adjacent

chains, with the presence of staggered zig-zag or disordered chains that are out of phase with one another in the [001] direction.

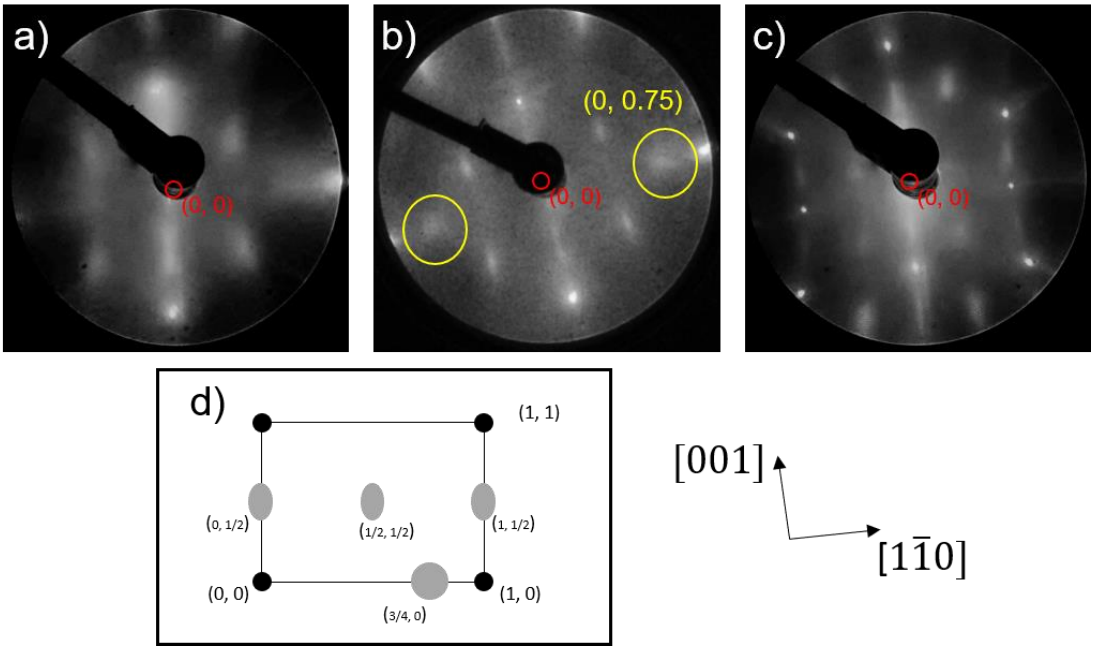

Figure 8. Diffraction pattern at various energies with a coverage of ca. 1.0 ML, and the centred (0, 0) diffraction spot shown in red. a) LEED pattern at 60 eV. b) LEED pattern at 63 eV, with the position of (0, 0.75) diffraction spots highlighted in yellow. c) LEED pattern at 109 eV. d) LEED illustration showing the combined diffraction patterns in figure a-c).

Further increasing the coverage over ca. 0.5 ML, we observed additional diffraction spots appearing at the quarter order positions for the water overlayer in the [1$\bar{1}$0] direction (fig. 8), with the most intense quarter order beams being at ca. 1.0 ML (fig. 8a-c). These quarter order spots indicate additional structure starting to appear above coverage of ca. 0.5 ML with a four unit repeat in the [1$\bar{1}$0] direction (fig. 8d), which is consistent with the four unit repeat up the chain in the second layer structure observed in STM (fig. 3). Above 1.0 ML, water creates a weak and diffuse diffraction pattern that fades with coverage, most likely due to disordered growth on top of the structure at 1.0 ML. These observations not only support the hypothesis that the surface saturates at ca. 0.5 ML, but also the (2x2) structure for the first layer evolving into the second layer structure above ca. 0.5 ML, with the characteristic four times periodicity along the [1$\bar{1}$0] chains. This is further supported by previous NRA, which suggested the surface saturates at a coverage of 0.5 ML on the Ni(110) surface.[14]

Since water has been reported to dissociate on the surface, we cannot use TPD to assess how much water is associated with the intact first layer, as TPD peaks will contain OH when water is heated on the surface. Fortunately, our beam calibrations for LEED on Ni(110) are based on

the adsorption of water on Cu(511), which exhibits a hexagonal high-density 2D layer at saturation with 0.67 waters per surface Cu atom. This allowed us to compare the water density on Ni(110) with a known 2D layer on Cu(511), which enables us to determine if the density at saturation on Ni(110) is similar to a 2D network, or the simple 1D zig-zag chains mentioned above. The presence of a high density layer on Ni(110), would result in the surface saturating at a coverage similar to that on Cu(511), as a comparable amount of water is needed for the growth of a 2D layer. This however is not observed on Ni(110), with LEED giving evidence that the surface saturates at a coverage of approximately half of the water density compared to that of a 2D layer on Cu(511). These observations rule out the suggestion that some of the waters on the surface may not be observed in STM, as the 2D structure would require more water and exhibit a higher density, similar to that on Cu(511). Further to this, these results suggest that the bright linear features observed in figure 3 above 0.5 ML is composed of linear chains that grow above the completed first layer and in between neighbouring 1D zig-zag chains, which helps us to decide between possible models in DFT. Moreover, these findings conflict with the early water adsorption studies for a c(2x2) bilayer on the Ni(110) surface, both due to the surface not saturating with a similar water density to that found on Cu(511) and LEED not showing just the centred c(2x2) diffraction spots. This, therefore, supports the fact that the surface saturates at a coverage of ca. 0.5 ML with a low density layer for a structure, with half the Ni atoms in the first layer structure remaining exposed.

3.3.3. DFT of second layer water

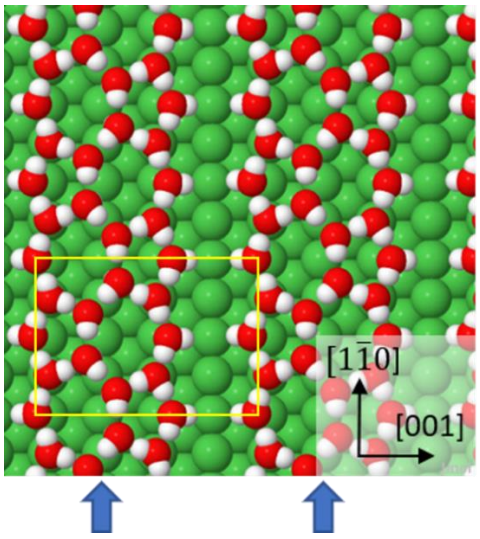

Figure 9. DFT simulation showing the proposed arrangement for water in figure 3, with the blue arrows showing the position of the bright chains of water that run along the Ni top sites in the close packed direction in figure 3, and (4x4) unit cell shown in yellow.

Since we have now established that the layer complets at half a monolayer to leave half the Ni atoms exposed in between neighbouring 1D chains, the additional water that forms the bright second layer chains (Figure 3) is clearly not adsorbing atop of water but is adsorbed in the missing water rows in the STM images in figure 2. This allows us to perform DFT calculations to determine the most stable arrangement of water in the bare Ni rows between the (2x2) zig-zag water chains, and the structure that was the most similar to the structure in figure 3. The resulting DFT calculations found that water fills in between two first layer water chains, forming alternating large and small rings along the Ni rows with a four unit repeat along the chain (fig. 9) above the bare Ni rows. This creates a characteristic pattern of pentamer and heptamer rings that alternate in the $[1\bar{1}0]$ direction, the chains appearing as isolated rows of water seperated by 4 units in the [001] direction to form a (4x4) unit cell (highlighted in yellow, fig 9). Water in this structure binds 0.68 Å above the flat zig-zag chains, with one hydrogen that poinst down towards the exposed Ni and O coordinating to the hydrogen of the original flat zigzag water chains. DFT simulations match closely with the structure observed in STM of the second layer structure, giving a similar binding energy (0.874 eV/water) from other 1D structures (0.837 eV/water) and 2D extended networks (0.831 eV/water) calculated on this surface.

The structures obtained by DFT help explain why it is not yet possible to adsorb an additional top layer of water to create a complete 2D network, water instead prefers to adsorb in between alternate pairs of zig-zag chains, seperated by one bare row of Ni. This is because the zigzag water chains along the outside of the pentamer-heptamer rings (figure 9) are tilted with the inside H pointing up and the outside H pointing down to the Ni. The addition of further water in between these chains was calculated to be less stable than the isolated pentamer-heptamer chains observed in figure 9. This was because the hydrogens that sit on the outside of the 2D chain would need to tilt upwards, bonding to the tightly bound second layer waters that run down the middle of the chain. This would therefore hinder the binding of the second layer, which was calculated to be less stable. This was consistent with the STM images in figure 3, showing no structure on either side of the isolated 2D chains, and bright linear features never being closer than 4 Ni rows apart in the [001] direction.

Despite Ni having a similar lattice constant to Cu, it is evident that the 1D pentagonal water rings predicted by DFT are not found on Ni(110) surface. Instead, we see water in the first layer forming simple zig-zag chains along alternating sides of the Ni top sites in the [110] direction, which is much different to the pentamer chains that extend across the [001] direction

on Cu(110). A distinct difference between both these water structures is the direction in which the chains grow, with water structures on Cu(110) growing along the [001] direction and the chains on Ni(110) growing along the close packed $[1\bar{1}0]$ direction. The key difference is the hydrogen bond coordination on Cu(110) compared to that on Ni(110), with water in the pentamer chains forming 2.67 H-bonds per water compared to two hydrogen bonds per water in the first layer structure on Ni(110). While this is desirable on Cu(110), DFT shows that Ni has a stronger water-metal interaction (0.63 eV/water) compared to that on Cu (0.49 eV/water), which more than compensates for the fact that the hydrogen coordination is lower on Ni(110). Furthermore, water on Cu(110) has two-thirds of the water adsorbed flat in the surface plane on the Cu top sites and one-third out of the surface plane in sites between the Cu ridges, which is a less favourable arrangement than that on Ni(110), which has all its water planar to maximise its Ni-water interaction. This is evident in previous literature, which shows that water planar to the surface is the most favourable orientation due to the lone pair $1b_1$ orbital on water interacting with the metal surface.[34] The low coordination number on Ni(110) is much different from any other intact water-metal adsorption study, but the chains are simular to the flat water backbone found in the 1D OH/H_2O chains observed on Cu(110).[26]

Previous literature studies on Ni(110) report a c(2x2) diffraction pattern for a hexagonal bilayer that is compressed in the $[1\bar{1}0]$ direction and elongated in the [001] direction. This directly contrasts with the data reported in this chapter, which clearly shows that intact water forms a (2x2) structure in the first layer structure. This is because we observed additional diffraction spots, not just c(2x2) diffraction spots, indicating the presence of a structure with a two unit repeat in both the $[1\bar{1}0]$ and [001] direction and not a centred structure. Furthermore, we find that this layer saturates at a coverage of approximately 0.5 ML to leave bare Ni rows in between simple 1D chains, which rejects the idea that a hexagonal bilayer is possible. Increasing the coverage to 1.0 ML, results in the same diffraction pattern persisting, but with the additional presence of a four unit repeat in the $[1\bar{1}0]$ direction. Both these unit repeats are supported by DFT calculations and experimental STM data, which further conflicts with the early water adsorption studies on Ni(110).[9, 14] Moreover, this study finds that the structure of water even above the saturation layer does not follow the LEED patterns and structures reported in previous studies, which suggests that the surface structure was altered by electron induced damage during LEED experiments in previous studies that were performed with conventional LEED optics that give much higher electron doses. These observations, however, do support some of the LEED data reported by Pirug et at. who reported the weak presence of addition

(½,½) diffraction spots in the [001] direction and concluded some of the water was dissociated in the c(2x2) structure.[33]

3.4. Conclusion

In this chapter, we have shown that a diffuse (2x2) diffraction pattern exists for isolated linear chains of water on the Ni(110) surface, which evolves into a (2x4) diffraction pattern for the growth of 2D isolated chains above the saturation layer at ca. 0.5 ML. These linear chains below ca. 0.5 ML are composed of flat water that sits planar to the surface in a zig-zag arrangement, extending along the $[1\bar{1}0]$ direction with each water chain separated from its neighbour by a row of bare Ni. However, we also find the presence of the minority wiggly chain structures that are composed of pairs of alternating flat waters that also run along the $[1\bar{1}0]$ direction below ca. 0.5 ML. Although these chains are observed in STM, the reduced stability of the chains compared to the zig-zag structure causes them to disappear over a short period of time, converting them into the favoured (2x2) zig-zag chains. Above saturation of this first layer, we find that water inserts into the gap between two (2x2) water chains to form isolated chains of a 2D water structure 3 Ni rows wide, which is composed of pentamer and heptamer rings in an alternating arrangement.

The reports in this chapter, therefore, show how the binding interaction on Ni is less constrained in the [001] direction, with 1D chains being driven by the short lattice repeat and strong Ni-water bonds, which hinder the formation of a 2D network and favours the formation of linear chains. This offers an insight into how water adapts its structure to bind differently on reactive surfaces, which bind water more strongly than inert surfaces, such as Cu(110). Furthermore, these structures reveal an exciting insight into the binding interaction that will have direct analogues on other tightly bound surfaces, including those that are highly corrugated that might favour the binding of water chains along the more reactive step edges.

3.5. References

1. W. R. Whitney, *Industrial & Engineering Chemistry*, 1925, **17**, 385-389.
2. M. N. Majeed, Q. A. Yousif and M. A. Bedair, *ACS Omega*, 2022, **7**, 29850-29857.
3. Q. F. Li, C. H. Li, L. K. Xu and G. Z. Liu, *Transactions of Nonferrous Metals Society of China*, 2007, **17**, S161-S165.
4. S. H and A. Tiwari, *The Journal of chemical physics*, 2014, **140**, 174704.

5. L. Zhu, C. Liu, X. Wen, Y.-W. Li and H. Jiao, *Catalysis Science & Technology*, 2019, **9**, 199-212.
6. M. Schulze, R. Reißner, K. Bolwin and W. Kuch, *Fresenius' Journal of Analytical Chemistry*, 1995, **353**, 661-665.
7. M. E. Gallagher, S. Haq, A. Omer and A. Hodgson, *Surface Science*, 2007, **601**, 268-273.
8. C. Nöbl, C. Benndorf and T. E. Madey, *Surface Science*, 1985, **157**, 29-42.
9. C. Benndorf and T. E. Madey, *Surface Science*, 1988, **194**, 63-91.
10. K. Bange, D. E. Grider, T. E. Madey and J. K. Sass, *Surface Science*, 1984, **137**, 38-64.
11. G. Benndorf, C. Nöbl and T. E. Madey, *Surface Science*, 1984, **138**, 292-304.
12. L. B. Skinner, C. Huang, D. Schlesinger, L. G. Pettersson, A. Nilsson and C. J. Benmore, *J Chem Phys*, 2013, **138**, 074506.
13. B. W. Callen, K. Griffiths, R. V. Kasza, M. B. Jensen, P. A. Thiel and P. R. Norton, *J. Chem. Phys.*, 1992, **97**, 3760-3774.
14. B. W. Callen, K. Griffiths, U. Memmert, D. A. Harrington, S. J. Bushby and P. R. Norton, *Surface Science*, 1990, **230**, 159-174.
15. G. Pirug, O. Knauff and H. P. Bonzel, *Surface Science*, 1994, **321**, 58-70.
16. N. Pangher, A. Schmalz and J. Haase, *Chemical Physics Letters*, 1994, **221**, 189-193.
17. H. Yang and J. L. Whitten, *Surface Science*, 1989, **223**, 131-150.
18. K. Griffiths, U. Memmert, B. W. Callen and P. R. Norton, *J. Vac. Sci. Technol. A-Vac. Surf. Films*, 1989, **7**, 2001-2004.
19. J. Carrasco, A. Michaelides, M. Forster, S. Haq, R. Raval and A. Hodgson, *Nature Materials*, 2009, **8**, 427-431.
20. J. Carrasco, A. Hodgson and A. Michaelides, *Nature Materials*, 2012, **11**, 667-674.
21. P. J. Feibelman, *Science*, 2002, **295**, 99-102.
22. N. S. Faradzhev, K. L. Kostov, P. Feulner, T. E. Madey and D. Menzel, *Chemical Physics Letters*, 2005, **415**, 165-171.
23. J. Weissenrieder, A. Mikkelsen, J. N. Andersen, P. J. Feibelman and G. Held, *Physical Review Letters*, 2004, **93**.
24. S. R. Puisto, T. J. Lerotholi, G. Held and D. Menzel, *Surface Review and Letters*, 2003, **10**, 487-492.
25. P. J. Feibelman, *Physical Review B*, 2003, **67**.

26. M. Forster, R. Raval, J. Carrasco, A. Michaelides and A. Hodgson, *Chem. Sci.*, 2011, **3**, 93-102.
27. Z. Pang, S. Duerrbeck, C. Kha, E. Bertel, G. A. Somorjai and M. Salmeron, *The Journal of Physical Chemistry C*, 2016, **120**, 9218-9222.
28. M. Forster, R. Raval, A. Hodgson, J. Carrasco and A. Michaelides, *Physical Review Letters*, 2011, **106**, 046103.
29. N. Gerrard, K. Mistry, G. R. Darling and A. Hodgson, *The Journal of Physical Chemistry Letters*, 2020, **11**, 2121-2126.
30. P. T. N. Gerrard.
31. C. Lin, G. Corem, O. Godsi, G. Alexandrowicz, G. R. Darling and A. Hodgson, *Journal of the American Chemical Society*, 2018, **140**, 15804-15811.
32. S. Duan, I. Y. Zhang, Z. Xie and X. Xu, *Journal of the American Chemical Society*, 2020, **142**, 6902-6906.
33. G. Pirug, O. Knauff and H. P. Bonzel, *Surface Science*, 1994, **321**, 58-70.
34. A. Michaelides, V. A. Ranea, P. L. de Andres and D. A. King, *Physical Review Letters*, 2003, **90**, 216102.

Chapter 4

An investigation into the Influence of Dissociation on the Open Ni(110) Surface

4.1. Introduction

Hydrogen is a more environmentally friendly resource than other finite resources, such as fossil fuels, as it does not contribute to the net amount of carbon dioxide released into the atmosphere.[1-3]Although the use of hydrogen has been widely accepted, the green nature of its production has been widely disputed. This is because processes that use fossil fuels to produce hydrogen tend to be more cost effective compared to more sustainable methods, such as the electrolysis of water.[4-7] Even though this method has shown much promise when using precious metals, their high costs and scarcity limit their application industrially.[8, 9] Therefore, to help solve this issue, research has gone into finding alternative, more cost-effective pathways using transition metals to produce high yields of hydrogen industrially.[10-12]

Many of these research studies have looked to water electrolysis using Ni-alloys for a more cost-effective method of producing hydrogen, due to nickel's reactivity playing a role in catalysing the splitting of water and the hydrogen evolution reaction (HER - $2H^{+}_{(aq)} + 2e^{-} \rightarrow H_{2(g)}$).[7, 13-20] Although Ni-alloys show much promise, further improvement is needed to enhance the HER efficiency, so that this process is just as efficient in producing hydrogen as those processes using fossil fuels.[1, 2, 21] Therefore, understanding the fundamental processes by which water splitting occurs at an Ni face is extremely desirable for developing prototype systems that can look at lowering the barriers associated with water, OH and other intermediate species.

In order to build molecular models for systems that incorporate water, one must consider the reactivity of a substrate surface and its surface arrangements. For example, Ni surfaces with hexagonal symmetry, such as Ni(111) have been seen to reversibly adsorb water.[22, 23] On other surfaces, such as Ni(110) the adsorption of water has been studied at length, as discussed in chapter 3, with studies giving evidence for the dissociation of water.[24-26] This is believed to be caused by Ni(110) exhibiting an increased reactivity at surface atoms with a low coordination number compared to Ni(111). Considering this, water may either adopt 1D or 2D structures that incorporate both hydroxyl and water on a Ni(110) surface. However, distinguishing

between pure water and mixed phases of water and hydroxyl experientially can be difficult, due to both water and hydroxyl exhibiting O-H bonds that display similar characteristic properties experimentally. Equally, the characterisation of a surface structure using DFT can be challenging, due to the many different hydrogen bond orientations and atom positions playing a significant role in determining the relative stability of a structure. Although a theoretical structure can have a good binding energy, experimentally this may not be the structure formed as it is very difficult, or perhaps currently impossible, to ensure you explore all of the possible structures and compositions available in an accurate DFT calculation. Therefore, both theoretical and experimental data go 'hand in hand' to produce the most robust conclusions for the behaviour of water on a reactive metal surface, such as Ni.

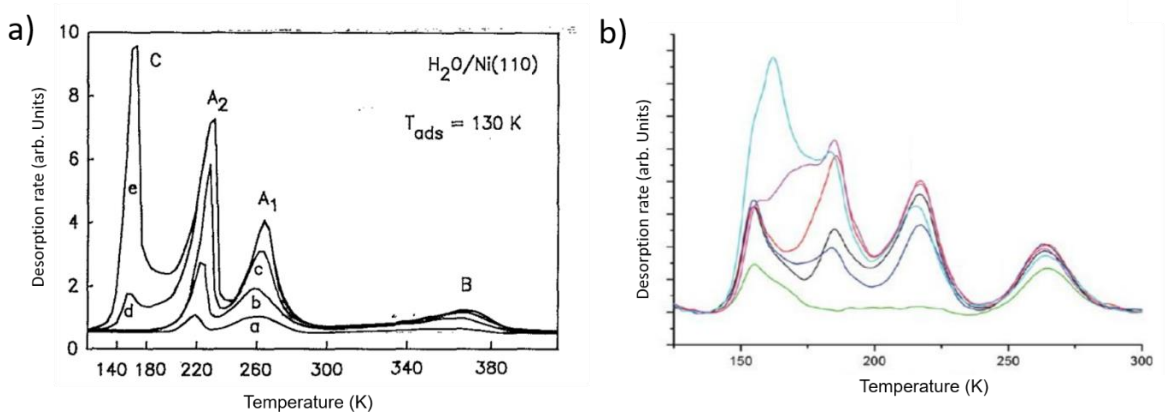

Figure 1. a) TPD spectra showing the desorption of water as it is heated on the Ni(110) surface, with coverage of water increasing from a to e. b) TPD spectra of water as it is heated on an oxygen pre-covered Cu(110) surface, with the coverage of water increasing from green to blue. Both TPD profiles above show how the binding energies of the surface structure evolves as the coverage increases. Adapted from. [25, 27]

Since there is little detailed structural information reported about the structures and H-bond network present in the temperature regime for dissociation on Ni(110), more inert surfaces that exhibit similar surface characteristics, such as Cu(110), can give an insight into the interactions that might be found on Ni. Cu(110) does not dissociate water but several different water and OH/H_2O structures can be formed by reaction of carefully controlled amounts of water and O.[27-29] The TPD data above (fig. 1), shows that both Ni(110) and Cu(110) share four characteristic TPD peaks, suggesting these surfaces have several structures that have different binding energies. It is clear that even though both surfaces exhibit similar desorption profiles, Ni(110) shows TPD profiles which are shifted to a slightly higher temperature compared to water on Cu(110). This is most evident with the final, high temperature TPD peak on Cu(110)

being observed at ca. 260 K and ca. 360 K on Ni(110), which is attributed to the stronger binding interaction on Ni compared to Cu. Moreover, this TPD peak on Cu(110) is associated with a pure OH phase, with experiments showing that water would not bind at such a high temperature, and previous reports observing OH dimers on the Cu surface.[27] This corresponding peak on Ni(110) at ca. 360 K is even higher and suggests that Ni also forms a pure OH phase, similar to that on Cu(110). With both of the TPD profiles highlighted above exhibiting similar TPD peaks (fig. 1), it seems possible that water and hydroxyl may form structures similar to those reported on Cu(110),[27] although the enhanced reactivity and greater binding interaction on Ni, along with the reduced lattice constant of the surface, may modify the detail of these structures from those formed on Cu.

There is further supporting evidence for the spontaneous dissociation of water on Ni(110) in previous literature by Pirug *et al*.[24] who gave evidence for the dissociation of water at 180 K using X-ray Photoelectron Spectroscopy (XPS) and Ultraviolet Photoelectron Spectroscopy (UPS). Further analysis using LEED at 180 K found that a c(2x2) diffraction pattern was observed in the temperature regime of 180 K, which suggested that this c(2x2) structure is composed of a mix of OH and water. This phase appears similar to the 2:1 water/OH c(2x2) network found on Cu(110), which would imply that, despite the reduced lattice spacing of Ni compared to Cu, the Ni(110) surface is able to also accommodate a c(2x2) arrangement, although the composition may differ due to Ni having an enhanced reactivity with respect to Cu. Moreover, this report further stated that water could be dissociating as low as 120 K, which would imply that all the TPD profiles reported by Callen *et al*.[25], as shown in the image above (fig. 1a), incorporate a mixed phase of water and hydroxyl. This would suggest that the water structures on Ni(110) are rather similar to those formed on Cu(110), with three different water/OH structures being associated with the TPD peaks observed above 180 K in figure 1.[27, 28]

Apart from the TPD profile and the LEED pattern reported above, there is no clear evidence for the structures that are present in the temperature regime where dissociation is possible on Ni(110). As well as this, existing LEED measurements are almost certainly influenced by electron induced dissociation, as is observed on other reactive surfaces when using conventional LEED systems. Therefore, we have chosen to investigate whether the increased binding strength on Ni(110), relative to that on Cu(110), will influence the structures adopted on the Ni surface, or whether they will be similar to those structures reported on Cu(110)

previously. To do this we used a combination of STM, LEED and TPD to allow us to come to a consensus about the interactions and structures present in the temperature regime for dissociation on Ni(110). In this chapter we report TPD and low-current LEED measurements, recorded at low electron exposure using a channel plate amplified LEED system to avoid the electron damage that was incurred in previous measurements. The LEED and TPD results presented here are discussed alongside the STM results that were performed in parallel by Gerrard. [30, 31]

4.2. Experimental

The conditions for dosing water, surface preparation, TPS and LEED are as given in chapter 3. The STM data were recorded by Gerrard and details of those measurements can be found in references. [30, 31]

4.3. Results and Discussion

4.3.1. Temperature Programmed Desorption

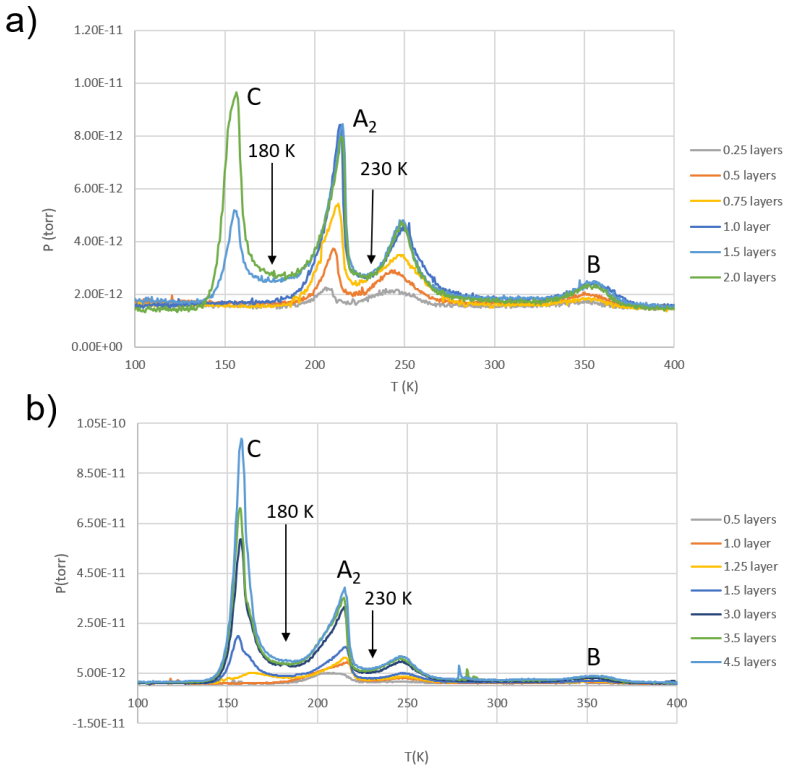

Figure 2. TPD for the various coverages of; a) H_2O adsorbed on the Ni(110) surface, heated at a rate of 2 K s^{-1}. b) D_2O adsorbed on the Ni(110) surface, heated at a rate of 2 K s^{-1}. All coverages indicated a thickness estimated from the completion of the Cu(511) layer, with one monolayer defined as the amount of water needed to complete a single layer on the Cu(511) surface in the hexagonal 2D network, which exhibits a water density of 0.67 water per surface Cu atom, very similar to the density of water in an ice Ih(0001) layer.

The water coverages on Ni(110) were increased gradually, using the calibrated molecular beam to deposit a known dose of water, and then the surface was heated at a rate of 2 K s^{-1}, resulting in four distinguishable TPD peaks (fig. 2), labelled peak C (155 K), A_2 (215 K), A_1 (245 K) and B (355 K) for coverages over a monolayer. Irrespective of coverage, we find that both TPD profiles for D_2O and H_2O follow the same trend with negligible differences, which suggests that the water/OH(OD) structures formed are equivalent with any isotope effect on the dissociation process having limited effect. The TPD profiles in figure 2, reveal the different binding energies of water as the structure evolves with temperature, i.e. the structure at peak B will have a higher binding energy than the structure at A_1 due to peak B appearing at a higher temperature. However, we must also consider that not all the water will desorb from the surface structure after each peak, some water may rearrange into a new, more stable structure whose formation is activated, for example by water dissociation to create a new H-bond structure.

It is clear from the TPD data in figure 2 that the TPD profiles on Ni(110) are similar to those TPD profiles formed by the reaction of water and O on Cu(110) in figure 1b. However, the corresponding peaks on Ni(110) lie 20 to 70 K higher than that on Cu(110), which is evidence of a higher surface-water binding energy on Ni(110) and is consistent with the idea that OH is present on the surface. Therefore, it is likely that these peaks on Ni may also be associated with the same types of structures, or identical structures to that on Cu. The structures formed on Cu(110) that correspond to the desorption peaks in the temperature regime of ca. 160, 200 and 260 K are the (2:1) water/OH c(2x2) hexagonal network, (1:1) water/OH 1D chains and OH dimers in a pure OH phase respectively.[32] Considering this, the peak at 360 K on Ni(110) is likely to be associated with a pure OH phase, as water would not be bound at a temperature as high as this and a pure OH phase can also be observed on Cu(110).

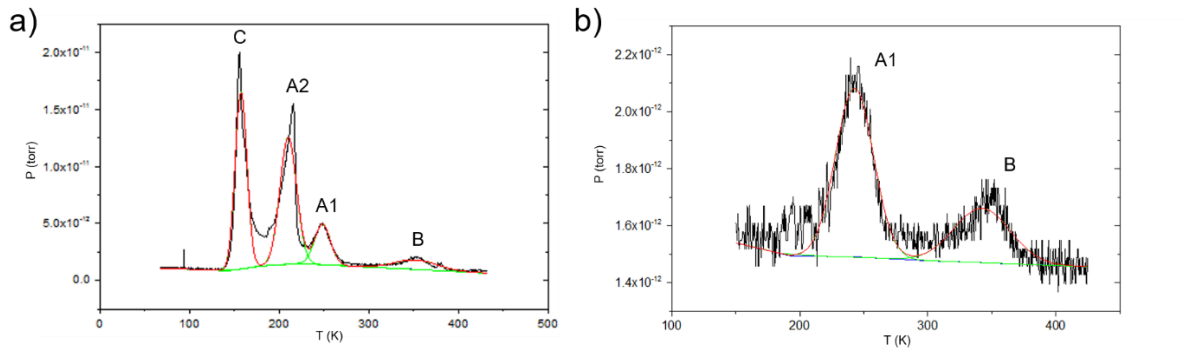

Peak	Intergration area	Intergration percentage (%)
C	2.95E-10	40.4 ± 1.7
A2	3.00E-10	41.1 ± 1.7
A1	9.04E-11	12.4 ± 1.7
B	4.41E-11	6.0 ± 1.7

Peak	Intergration area	Intergration percentage (%)
A1	2.20E-11	67.6 ± 0.9
B	1.05E-11	32.4 ± 0.9

Figure 3. a) An integrated TPD profile of a single layer of water on the Ni(110) surface. b) An integrated TPD profile of 0.25 of a layer of water on Ni(110) surface in the temperature regime of 150 to 430 K. The table below each TPD spectra shows the total integrated area and percentage, with the percentage errors taken from subtracting different baselines off the spectra.

To get a more detailed idea as to whether the composition of the water/OH structures present on Ni(110) are similar to those observed on Cu(110), we integrated each of the TPD profiles to calculate the approximate ratio for the amount of water desorbed in each phase. For example, if the structure at A1 is the same as the 1:1 water/OH structure on Cu(110), then we would expect the size peak B (pure OH phase disproportionation) to be half that of A1. However, this is reliant on the assumption that no more dissociation occurs during the course of heating the surface from A1 to B, otherwise, the size of peak B will be greater and more similar to that of peak A1. We note that there is some variability in the values in figure 3 due to the errors associated with subtracting the baseline to obtain integrated areas.

Integration of the desorption peaks at both coverages (fig. 3b) reveals an approximate ca. 2:1 ratio between the size of peaks A1 and B, indicating that for each water that desorbs from the A1 phase, half as much water desorbs from the B peak associated with pure OH disproportionation. This data supports the idea that the A1 phase is composed of a structure with an approximate 1:1 ratio of water/OH, from which water desorbs as the surface is annealed past the A1 phase to leave just OH on the surface. An identical 1:1 water/OH composition is observed for the A1 structure on Cu(110) after the reaction of O and water,[27] where spontaneous dissociation does not occur. This result supports the hypothesis that a similar structure is formed in the A1 phases on both Cu(110) and Ni(110).

In contrast, the ratio between A2 and A1 in figure 3b is greater (ca. 3:1) than that of A1 and B (ca. 2:1), which indicates there is much more water desorbing from the A2 phase than A1. This ratio is different to the corresponding $2H_2O$:1OH c(2x2) structure on Cu(110), which might suggest that the amount of water present in the surface structure that forms the A2 desorption peak is greater than a 2:1 ratio and different to the structure observed on Cu(110) in this region. However, since peak C and A2 have significant overlap, it is hard to estimate the exact composition for the structure prior to the A1 phase, as there is going to be a large amount of variability in the compositions estimated.

4.3.2. Low Energy Electron Diffraction

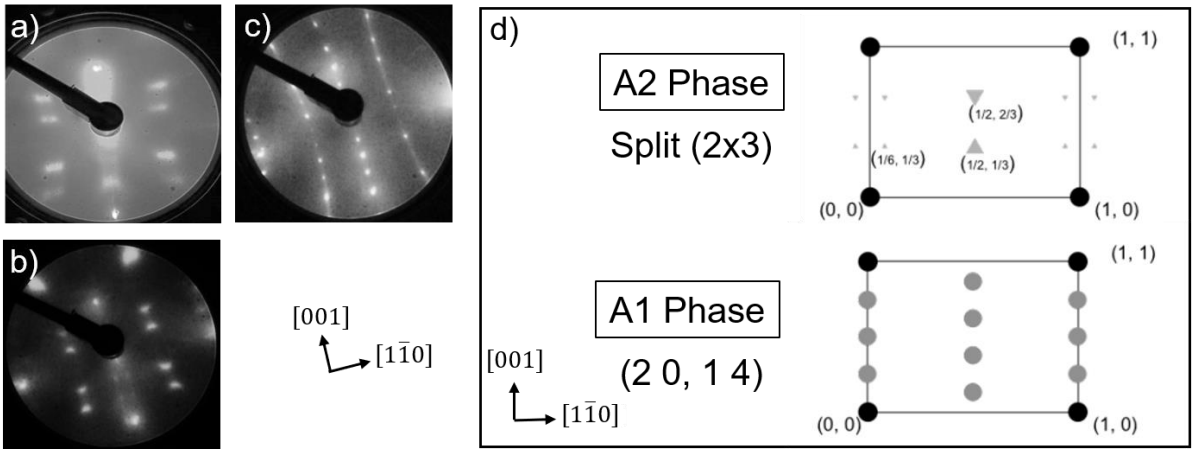

Figure 4. LEED pattern taken after 1.0 layer was deposited at 100 K and the surface was annealed to 180 K at a rate of around ~1 K s^{-1} to form the A2 phase. a) LEED pattern at 49 eV. b) LEED pattern at 59 eV. c) LEED pattern taken after 1.0 layer was deposited at 100 K and annealed to 220 K at a rate of around ~1 K s^{-1} (63 eV) to form the A1 phase. d) LEED illustration showing the diffraction pattern for both the A2 and A1 phases.

Once water was dosed on the surface at 100 K, it was then heated to different temperatures to initiate dissociation and remove excess water, which resulted in the diffraction patterns shown

in figure 4. As water starts to desorb prior to the A2 phase, we find half order diffraction spots which are split along the [001] direction to form a (2x3) repeat with additional splitting that appears to correspond to the length of ca. 6 times the Ni repeat along the $[1\bar{1}0]$ direction (fig. 4a, b and d). Although we observe ca. 6 times repeat in the $[1\bar{1}0]$ direction, the weak presence of the diffraction spots indicates that there is no strong preference for the structure to contain this repeat, likely due to a lack of order. These diffraction features are observed in the temperature regime prior to and during the desorption of water in the A2 peak. It is clear that the diffraction pattern for the A2 structure of water/OH in figure 4a is very different to the corresponding structure at ca. 160 K on Cu(110) which shows a c(2x2) hexagonal network of ($2H_2O$+1OH). Instead, we find a LEED pattern for a structure that is not centred with a regular 3 unit repeat in the [001] direction, which is larger than the 2 unit repeat on Cu.

As peak A2 completes and the A1 phase is formed, we find additional streaking start to appear in the [001] direction to produce a LEED pattern that can be defined as (2 x n), where n is dependent on the initial water coverage. Heating from a coverage ≥1 layer results in a well-defined LEED (2 0, 1 4) pattern for the A1 phase (fig. 4c and d), indicative of a well-ordered surface structure. One of the potential reasons for this to occur is if the structures formed at low coverage repel each other, increasing their separation from one another, compared to a higher coverage where structures are closer together and form a more ordered structure with a regular repeat. An obvious example of this behaviour is the formation of Ag-O-Ag chains on Ag(110).[33] Although the LEED pattern in figure 4c indicates a well-ordered pattern, it is not yet clear as to whether this structure is different to or the same as the 1:1 water/OH chains observed on Cu(110) at 200 K, as we only have an indication of the composition so far. Heating further above the A1 phase gave no LEED pattern for the pure OH phase, indicating this phase has no long range order.

Now that we have a clear idea of the phases present on Ni(110) from TPD and LEED studies, the structure of these phases was investigated further by STM to learn about the local arrangement of water and OH; this was carried out by Gerrard.[30, 31]

4.3.3. Scanning Tunnelling Microscopy

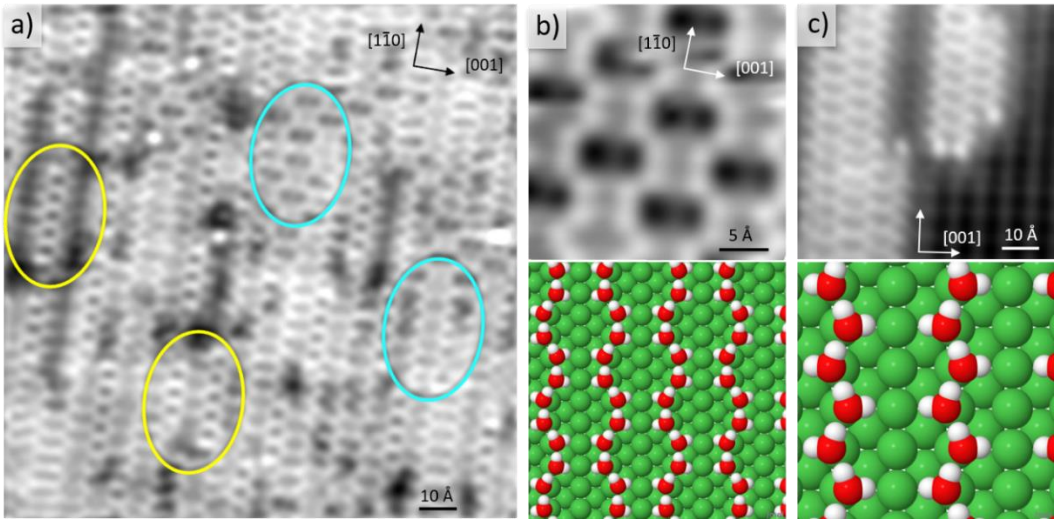

Figure 5. a) STM image showing the water structures formed after water was deposited at 77 K and heated to 183 K, just prior to the A2 desorption peak (fig. 2), and then cooled to 80 K. The regions in blue represent (b) the wiggly chain structure and (c) the zig-zag chains, which is observed for intact water at 80 K, as seen in chapter 3. The regions in yellow highlight the structure of water that characterises the A2 phase.

The STM image in figure 5 shows the structure of water after it is heated to 183 K, just (30 K) below the desorption peak of the A2 phase (fig 2). Note that the time scale for heating the Ni(110) surface in the STM is much slower than during thermal desorption, ca. 1 K min^{-1} in the STM compared to 2 K s^{-1} for TPD's taken in figure 2. Therefore, decomposition and desorption will be more advanced in STM images in contrast with the thermal desorption spectrum for any particular anneal temperature.

While a significant proportion of the surface can be attributed to a mixture of different types of intact 1D water chains, with examples marked in blue in Fig. 5, the rest of the surface at 183 K forms short face sharing hexamer chains (see yellow marked regions) that only appear above 150 K. This shows the transition from the intact water phase to a mixed water/OH phase as the intact structures start to decompose. STM analysis of both the intact water chains and the structure containing hexamer units shows that the intact water chains are considerably longer (ca. 80 Å) than these hexamer units, before a defect or different structure appears. This may suggest that the intact phase forms a more stable and ordered structure, or the structure is less strained than the hexagonal regions, which results in the structure having to break. However, complete removal of the intact phase is needed to analyse the hexagonal regions further, as the transition from the intact phase to the partially dissociated phase is still ongoing.

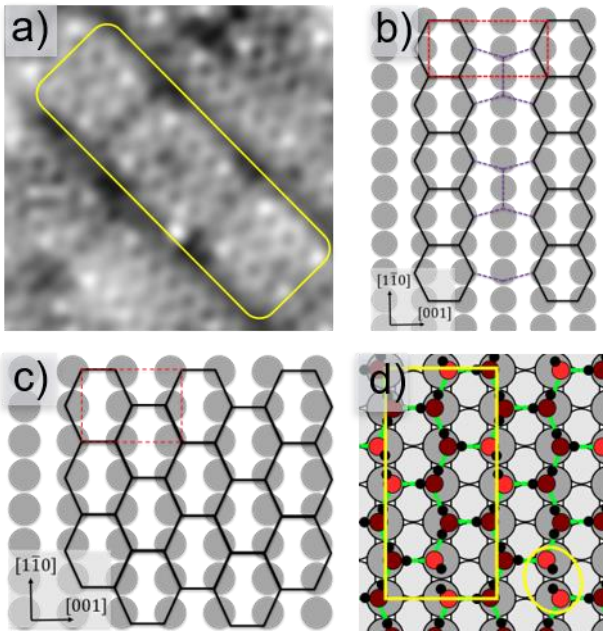

Figure 6. a) STM image that shows details of the local (2x3) arrangement in the A2 phase formed after extended annealing at just below 200 K, highlighted in yellow. b) Illustration showing the registry of the two hexagonal rows in bold and the possible intermediate structure decorating the vacant Ni rows in purple, with the (2x3) unit cell highlighted in red. c) Illustration showing the structure of water/OH on the Cu(110) surface with the c(2x2) unit cell highlighted in red. d) Illustration showing a c(2x2) hexagonal network calculated in a p(2x6) unit cell containing Bjerrum defects, which is highlighted yellow. Adapted from.[27]

Prolonged annealing just below 200 K resulted in the complete removal of the intact water structures, leaving short-range hexamer rows that have intermediate structure in between, rarely being more than 6 units (30 Å) in length in the [1$\bar{1}$0] direction before a defect or different structure continues. As a matter of fact, these units with limited order have a strong preference to appear three Ni repeats apart in the [001] direction; an example is displayed above in yellow (fig. 6a), forming structures with a local (2x3) arrangement. These (2x3) domains are composed of hexagonal rows that are somewhat different to the structure in between, showing contrast changes between the higher contrast hexagonal rows and the lower contrast intermediate structure, which suggests that the network is corrugated. It is less clear as to the arrangement of water/OH in the intermediate structure, but some detail of bigger rings can be observed along the centre of two hexagonal rows and the presence of smaller ring structures (fig. 6a), as highlighted in the centre structure of the yellow box shown in fig. 6a. Further analysis of the ring structures, shows that some of the bigger ring structures have a diameter of approximately 2.5 Ni atoms in the close packed direction, which confirms that there is no adsorbate bound on some of the Ni atop sites in between the hexagonal rows where the bigger ring structure are

present. These STM images are consistent with the LEED observations prior to desorption of the A2 peak (fig. 2), which shows a diffraction pattern for a structure with a (2x3) unit cell and a splitting corresponding to ca. 6 units in length in the $[1\bar{1}0]$ direction (fig. 4a and b).

In contrast to Ni(110), a simple c(2x2) hexagonal network can be found on Cu(110) at ca. 160 K, as seen in figure 6c, which is composed of face sharing hexagons with a 2:1 ratio of water/OH. Each of the hexagons is compressed in the [001] direction and elongated in the close packed direction to form slightly distorted hexagonal structures. Furthermore, this structure is stabilised by Bjerrum defects, an example of these defects is circled in yellow above (fig. 6d), and shows two neighbouring OH groups that are adjacent to one another, acting as H-bond acceptors to two neighbouring waters. This structure sacrifices one of the H-bonds due to OH being a poor donor and a better acceptor, which results in the structure being stabilised by the number of OH acceptors that are tightly bound to the surface.

In the c(2x2) network on Cu(110), water/OH molecules zig-zag along every Cu atop site in the close packed direction, forming hydrogen bonds along adjacent Cu rows in the [001] direction. These molecules that hydrogen bond across the [001] direction are positioned so that two molecules sit in the inner Cu atop sites, forming hydrogen bonds to the adjacent Cu row in a two unit repeat in the close packed direction (fig. 6d).[27] Decreasing the separation distance in the [001] direction from 3.6 Å on Cu(110) to 3.5 Å on Ni(110), we see hexagonal rows that have adsorbate missing in between, which creates the structure mentioned above (fig. 6a and b). This suggests that the structure cannot accommodate the necessary O-O spacings in between the hexagonal rows on the smaller Ni-Ni spaced template, leaving bare Ni atoms along the centre of two hexagonal rows. More specifically, a c(2x2) hexagonal arrangement would be too compressed in the [001] direction, which results in the structure forming a (2x3) arrangement. This behaviour is similar to that found in the intact water structures found at 77 K, with structures leaving bare Ni rows in between chains due to the unfavourable separation distance of water on adjacent Ni rows, an idea which is supported by DFT.[31] Therefore, the most obvious suggetion is that water forms the arragement in between the hexagonal rows highlighted in purple in figure 6b, which is based on STM images on Ni(110) (fig. 6a) and previous strain relief features that are known to be form alongside hexagonal structures on a Ni(111),[34] Cu(511),[35] Pt(111) [36] and a SnPt surface.[37] The regular interruption of the face sharing hexagonal chains every ca. 6 Ni units along the $[1\bar{1}0]$ direction can likewise be interpreted as the Ni substrate spacing causing strain in this direction that is greater than that on Cu(110), which is able to form a well ordered hexagonal network.

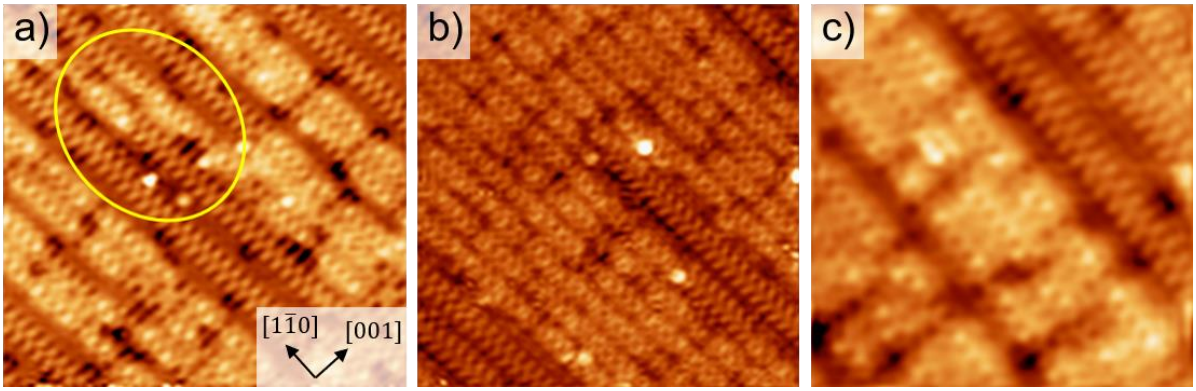

Figure 7. Structures of water formed after the surface was annealed to 200 K and cooled to 80 K. Images a-c) show regions of water remodelling from the 2D structure into the 1D zig-zag structure as the coverage decreases into the A1 phase from the A2 phase, with the conversion highlighted in yellow.

As the surface is gradually heated further to 200 K, STM images show that regions of 2D structure start to disappear as water dissociates and desorbs, converting water from the 2D structure into 1D zig-zag structures (fig. 7). This results in the breakdown of large islands of water into smaller units of 5 or 6 rings along the [1$\bar{1}$0] direction and a smaller number of (2x3) regions of 2D water. As the temperature rises further, we find an increased number of 1D chains on either side of the isolated hexagonal (2x3) domains, with the chains becoming the majority surface structure as the temperature continues to increase. Annealing the surface to 220 K results in the complete removal of all the 2D structures from the surface, leaving ordered 1D chains that characterise the A1 phase.

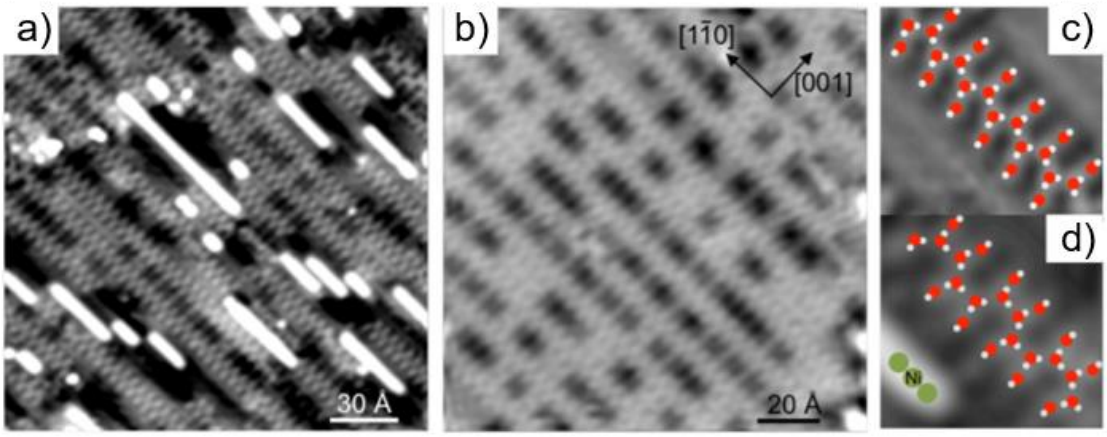

Figure 8. STM images showing the structure present on the Ni(110) surface in the A1 phase, after annealing the surface to 220 K and completing the decomposition of the A2 phase. a) STM image of a low coverage showing H_2O-OH chains and high contrast added Ni rows. b) STM of a high coverage showing well-ordered H_2O-OH chains in a (2 0, 1 4) structure that is formed from the desorption and dissociation of coverages over one monolayer. c) A 'Z' zig-zag chain and d) a 'P' type chain with a structural model superimposed on the STM images to highlight the arrangement of H_2O/OH.

Heating the surface to 220 K orders the 1D chains into an anti-phase arrangement with the chains separated by ≥4 Ni atoms along the [001] direction (fig. 8). Even at a higher coverage, the chains are never any closer than 4 Ni rows apart, which suggests a repulsive interaction is present between the chains. This repulsive interaction is evident at lower coverages, which is expected if the chains want to reduce their chain-chain repulsion, forming structures with no regular repeat. This agrees with LEED analysis, with streaked diffraction patterns at coverages less than a layer due to many chains preferring to maximise their chain separation, only at coverages close saturation do we see the highly ordered (2 0, 1 4) LEED pattern (fig. 4b).

The 1D chains can be broken down into two different types of chains, an example is shown in figures 8c and d. The 'Z' zig-zag chain is the majority surface structure, consisting of a flat-water backbone with open branched OH that bind in the Ni bridge sites. Water is bound flat along the atop Ni sites, alternating either side of the atop positions, with each water hydrogen bonding in the direction away from the chain axis to the nearest neighbour OH (fig. 8c). Conversely, in the H_2O-OH 'P' chains, water alternates in pairs along the close packed direction with a four times repeat, creating a 'pinch' type structure (fig. 8d). This structure appears less often than the 'Z' type structure, which suggests that the stability of the 'P' type chain is less than the 'Z' type chain. However, the core structure on both chains is held together via a flat water backbone that alternates down the atop Ni sites with OH bonded in the neighbouring Ni bridge sites, stabilising both types of chains. Both these structures have been suggested by DFT on Cu(110) to be the most stable arguments, and since the lattice parameter on Ni is similar to that found on Cu, it seems the same structure forms. Both these structures mentioned above are in good agreement with the STM and DFT measurements for the 1:1 water/OH chains found on Cu(110) at 220 K,[27] and therefore this supports the TPD integrations in figure 3, which indicates that the A1 phase is composed of a 1:1 ratio of water/OH on Ni(110) (fig. 3).

In addition to the water/hydroxyl chains, we also observe high contrast features that run along the $[1\bar{1}0]$ direction, similar to those seen after dissociation on Cu(110),[28] which suggests that these linear features can be attributed to monoatomic Ni wires. Although these Ni wires run along the exposed Ni regions where no H_2O/OH is present, there seems to be no correlation as to the length or periodicity of each of the Ni wires, only that they often are present next to the H_2O-OH chains. These bright linear features do not appear on clean Ni(110) and have been suggested to be stabilised by hydrogen on Cu(110) in previous lierature.[38]

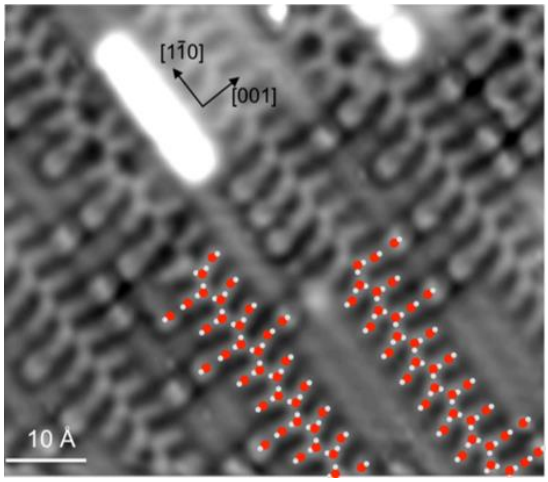

Figure 9. STM image just before the decomposition of the A1 phase (just above 220 K), showing 1D 1:1 water/OH branched chains with additional OH features either side. A structural model has been superimposed on the STM image to highlight the proposed arrangement of H_2O/OH.

After annealing the surface just above 220 K to allow some structural decomposition of the 1D chain, STM reveals some additional features on either side of the 1D chains that start to appear progressively as decomposition continues (fig. 9). These additional features are caused by the presence of surface OH that decorate some OH groups along the 1D chain, forming OH dimers as the coverage increases beyond the 1:1 ratio of the H_2O/OH chains. Annealing the surfaces to temperatures above 245 K, leaves the surface exclusively with OH, which is stable up to 350 K. We were not able to get a clear image of the pure OH phase on Ni(110) due to the surface being highly stepped, possibly induced by oxygen, which made it hard to distinguish the OH molecules on the surface. Similar OH dimers to those observed here at the edge of the water/OH chains were found on Cu(110) in the pure OH phase, with both OH lying flat in the short bridge sites.[27]

While early measurement on Ni(110) found a c(2x2) or sometimes c(2x4) or (2x6) diffraction pattern at 180 K,[24, 25, 39] our low-current LEED found a (2x3) diffraction pattern in the temperature regime for these structures. This LEED pattern reported at 180 K (A2 phase) does not form a centred unit cell, but a (2x3) unit cell, which agrees with STM analysis for the local hydrogen bonded structure. Despite the presence of OH, under no conditions do we create a c(2x2) arrangement or any of the other structural arrangements mentioned above. Since there has been a variety of structures reported, with none using other techniques that probe local hydrogen bonded structures, there is no clear evidence as to whether water forms any of the LEED patterns mentioned above. This direct contrast is probably attributed to the high-current LEED instruments used in conventional LEED studies, which compromised the surface

arrangement and LEED pattern by electron-induced damage. Furthermore, the distorted c(2x2) hexagonal network of alternating OH and water groups reported by Pirug *et al*.[24] cannot be supported by our analysis of the local structure of water on Ni(110) surface at 180 K. Instead, we find short-range structures that are formed of two hexagonal rows that are somewhat different to the structure in between, containing a (2x3) unit cell that is rarely more than 6 units in length in the $[1\bar{1}0]$ direction. Therefore, this shows how easily the structure of water can be altered by the dose of electrons on a reactive surface, which is one of the issues associated with conventional analytical studies, causing structures to be misinterpreted and studies to have a variety of outcomes.[40, 41]

4.4. Conclusion

In conclusion, TPD found four distinguishable TPD peaks that match closely with previous literature studies, labelled peak C (155 K), A_2 (215 K), A_1 (245 K) and B (355 K) for coverages over a monolayer, with evidence to support 1:1 water/OH structures in the A1 phase. Apart from the TPD data, the results discovered in this chapter are much different to those reported in previous literature studies on Ni(110), as we find no LEED patterns at any given temperature that correspond to a centred (2x2) unit cell. As a matter of fact, we found that a diffraction pattern for a (2 x 3) repeat with additional splitting that appears to correspond to the length of ca. 6 times the Ni repeat along the $[1\bar{1}0]$ direction exists prior to the A2 phase. Further annealing the surface prior to the A1 phase, resulted in LEED showing a (2 0, 1 4) LEED pattern at ca. 230 K for coverages ≥ one layer, with no other ordered diffraction patterns being observed above the A1 phase. Unlike previous studies, our LEED measurements were confirmed by STM, showing a partially dissociated (2x3) 2D network prior to the A2 phase, and 1:1 water/OH 1D zig-zag chains with a (2 0, 1 4) unit cell prior to the A1 phase. Although a diffraction pattern was not observed above the A1 phase, STM found OH dimers appearing above 245 K, which showed a high affinity to adsorb to the exposed branched OH in the zig-zag chains before the surface was left exclusively with OH, which is stable up to 350 K. The use of low-current LEED measurements enabled us to determine initially whether the structure of water on Ni(110) using a lower dose of electrons was different to what has been proposed previously. This technique helped us to avoid electron-induced damage, with our results concluding that the LEED measurements reported in conventional Ni(110)-water studies have been altered by the dose of electrons.

Although previous literature suggested the Ni lattice parameter could accomodate a c(2x2) arragement, just as Cu(110) does, our results suggest that this outcome was altered by the high dose of electrons, which has been avoided in this study due the surface wetting layer being exposed to a very low dose of electrons using a channel plate amplified LEED system. Instead, we find that the Ni surface template cannot accommodate the longer O-O separations in a hexagonal network, forming hexagonal chains with reasonable registry to the Ni template at the expense of the structure in between the hexagonal rows. The most obvious suggestion as to the structure in between in the hexagonal rows is highlighted in figure 6b, which shows a structural arrangement composed of seven and five membered rings, and is based on previous strain relief features that are known to be form alongside hexagonal structures on a Ni(111),[34] Cu(511),[35] Pt(111) [36] and a SnPt surface.[37] Therefore, although the Ni surface template is too strained for a simple c(2x2) network, the smaller surface template of Ni relative to Cu is able to mimic the corresponding structures on Cu(110) below the A1 phase. [28]

4.5. References

1. M. Wang, Z. Wang, X. Gong and Z. Guo, *Renewable and Sustainable Energy Reviews*, 2014, **29**, 573-588.
2. I. E. Agency, *World Energy Outlook*, 2019.
3. I. Staffell, D. Scamman, A. Velazquez Abad, P. Balcombe, P. E. Dodds, P. Ekins, N. Shah and K. R. Ward, *Energy & Environmental Science*, 2019, **12**, 463-491.
4. P. J. Megía, A. J. Vizcaíno, J. A. Calles and A. Carrero, *Energy & Fuels*, 2021, **35**, 16403-16415.
5. G. Abuin, R. Coppola and L. Diaz, *Electrocatalysis*, 2019, **10**, 17-28.
6. A. Landman, S. Hadash, G. E. Shter, A. Ben-Azaria, H. Dotan, A. Rothschild and G. S. Grader, *Advanced Functional Materials*, 2021, **31**.
7. S. Takenaka, Y. Orita, H. Umebayashi, H. Matsune and M. Kishida, *Applied Catalysis a-General*, 2008, **351**, 189-194.
8. C. Li and J.-B. Baek, *ACS Omega*, 2020, **5**, 31-40.
9. H. Jung, S. Choung and J. W. Han, *Nanoscale Advances*, 2021, **3**, 6797-6826.
10. Y. Li, L. Zhou and S. Guo, *EnergyChem*, 2021, **3**, 100053.
11. J. Yu, Y. Dai, Q. He, C. Cheng, Z. Shao and M. Ni, *Applied Physics Reviews*, 2020, **7**, 041304.
12. T. Wu, M.-Z. Sun and B.-L. Huang, *Rare Metals*, 2022, **41**, 2169-2183.

13. A. Haryanto, S. D. Fernando, S. D. F. To, P. H. Steele, L. Pordesimo and S. Adhikari, *Energy & Fuels*, 2009, **23**, 3097-3102.
14. A. Meena, M. Ha, S. S. Chandrasekaran, S. Sultan, P. Thangavel, Ahmad M. Harzandi, B. Singh, J. N. Tiwari and K. S. Kim, *Journal of Materials Chemistry A*, 2019, **7**, 15794-15800.
15. B. H. R. Suryanto, Y. Wang, R. K. Hocking, W. Adamson and C. Zhao, *Nature Communications*, 2019, **10**, 5599.
16. J. X. Qian, L. R. Enakonda, W. J. Wang, D. Gary, P. Del-Gallo, J.-M. Basset, D. B. Liu and L. Zhou, *International Journal of Hydrogen Energy*, 2019, **44**, 31700-31711.
17. A. Aliyev, G. G, U. Gurbanova, D. Babanly, V. Fateev, I. Pushkareva, D. Tagiyev, B. Фатеев, О. Алексеева, С. Коробцев, Е. Серегина, Т. Фатеева, А. Григорьева and А. Алиев, *Chemical Problems*, 2018, **16**, 283-306.
18. C.-C. Hu, C.-H. Tsay and A. Bai, *Electrochimica Acta*, 2003, **48**, 907-918.
19. R. Solmaz and G. Kardaş, *Energy Conversion and Management*, 2007, **48**, 583-591.
20. L. Xiao, S. Zhang, J. Pan, C. Yang, M. He, L. Zhuang and J. Lu, *Energy & Environmental Science*, 2012, **5**, 7869-7871.
21. A. Eftekhari, *International Journal of Hydrogen Energy*, 2017, **42**, 11053-11077.
22. M. Schulze, R. Reißner, K. Bolwin and W. Kuch, *Fresenius' Journal of Analytical Chemistry*, 1995, **353**, 661-665.
23. L. Zhu, C. Liu, X. Wen, Y.-W. Li and H. Jiao, *Catalysis Science & Technology*, 2019, **9**, 199-212.
24. G. Pirug, O. Knauff and H. P. Bonzel, *Surface Science*, 1994, **321**, 58-70.
25. B. W. Callen, K. Griffiths, R. V. Kasza, M. B. Jensen, P. A. Thiel and P. R. Norton, *The Journal of Chemical Physics*, 1992, **97**, 3760-3774.
26. N. Pangher, A. Schmalz and J. Haase, *Chemical Physics Letters*, 1994, **221**, 189-193.
27. M. Forster, R. Raval, J. Carrasco, A. Michaelides and A. Hodgson, *Chem. Sci.*, 2011, **3**, 93-102.
28. M. Forster, R. Raval, A. Hodgson, J. Carrasco and A. Michaelides, *Physical review letters*, 2011, **106**, 046103.
29. J. Carrasco, A. Michaelides, M. Forster, S. Haq, R. Raval and A. Hodgson, *Nature materials*, 2009, **8**, 427-431.
30. N. Gerrard, *The University of Liverpool, PhD Thesis*, 2019.
31. N. Gerrard, K. Mistry, G. R. Darling and A. Hodgson, *The Journal of Physical Chemistry C*, 2020, **124**, 23815-23822.

32. P. A. Thiel and T. E. Madey, *Surface Science Reports*, 1987, **7**, 211-385.
33. M. Taniguchi, K.-i. Tanaka, T. Hashizume and T. Sakurai, *Surface Science*, 1992, **262**, L123-L128.
34. A. Shiotari, Y. Sugimoto and H. Kamio, *Physical Review Materials*, 2019, **3**, 093001.
35. C. Lin, G. Corem, O. Godsi, G. Alexandrowicz, G. R. Darling and A. Hodgson, *Journal of the American Chemical Society*, 2018, **140**, 15804-15811.
36. G. Zimbitas, S. Haq and A. Hodgson, *The Journal of Chemical Physics*, 2005, **123**, 174701.
37. N. Gerrard, C. Gattinoni, F. McBride, A. Michaelides and A. Hodgson, *Journal of the American Chemical Society*, 2019, **141**, 8599-8607.
38. Y. Shi, B. Y. Choi and M. Salmeron, *The Journal of Physical Chemistry C*, 2013, **117**, 17119-17122.
39. C. Benndorf and T. E. Madey, *Surface Science*, 1988, **194**, 63-91.
40. P. J. Feibelman, *Science*, 2002, **295**, 99-102.
41. C. Clay, S. Haq and A. Hodgson, *Chemical Physics Letters*, 2004, **388**, 89-93.

Chapter 5

An investigation into the Structure of Water on the Stepped Cu(110) surface

5.1. Introduction

In most real-life cases, metal surfaces will never be entirely flat, they will contain many surface defects, such as steps, terraces or gain boundaries. Therefore, understanding how these defect sites play a role is important in forming an understanding of whether they have a positive or negative impact on processes, such as water dissociation. For pragmatic reasons, the influence of surface defects, particularly steps, are often neglected when experimental studies address the interaction between water and a solid metal surface. Defects are considered a part of the background, and therefore little is known about how the steps play a role in the nucleation and dissociation of water. Recent theoretical studies suggest that the presence of defects on transition metal surfaces provide low-coordinate sites that reduce the barrier to dissociation[1-3]. In light of this, stepped metal surfaces have gained much attention with the hope of understanding how these high-index surfaces compare to flat surfaces. Although this has been predicted to be the case, most previous water adsorption studies on transition metal surfaces reported the structures formed on plane surfaces, not at, or near, the step edge, which brings the question of how does water interact on a corrugated surface and how does this compare to a flat surface?

Not only do transition metals make good catalysts, but they also provide an ideal surface environment to study chemical reactions, such as the dissociation of water. This reaction plays a crucial role in the water gas shift reaction,[1] where the spitting of water is the rate-limiting step for the conversion of carbon monoxide and water into carbon dioxide and hydrogen, which is then used in the synthesis of methanol.[4,5,6, 7] Typically, this process uses a Cu catalyst to provide an alternative pathway for the reaction, resulting in a lower activation energy for the rate-determining steps i.e. water dissociation and hydrogen recombination, making a more efficient catalyst.[2, 8] The metal interface determines the overall activity of the catalyst, but other factors such as the type of surface (stepped or flat) and surface preparation can also significantly affect the lifetime of the catalyst. In order to improve the catalytic activity and lifetime of a catalyst in industrial processes that incorporate metals (as catalysts) and water, it

is important that we understand how water interacts at the metal interface, both stepped and flat. Therefore, in this chapter, we have chosen to investigate the interaction between water and a stepped Cu(110) surface, in the hope to address the theoretical predictions mentioned above and understand the differences with a planar Cu(110) surface.

Due to the lack of research on stepped metal surfaces, the adsorption of water on flat metal surfaces has been comparatively better understood. However, in order to form direct comparisons between both flat and stepped metal surfaces, we must first understand the interactions on a flat metal surface. Although water has been observed to form intact structures on flat metal surfaces, our picture of how this layer is structured has changed considerably over the last decade. Originally, it was thought that water forms intact structures similar to that of bulk ice, creating a single bilayer of hexagonal water on the metal surface, however more recent studies have found that this is not generally the case. Instead, recent studies revealed that some of these hexagonal structures were actually a mix of water and hydroxyl, contradicting the original theory mentioned above.[9-14] For example, in early water adsorption studies it was thought that water formed an ordered intact structure at 165 K on Ru(0001). This (√3x√3)R30° structure was based on LEED images, and at the time it was assumed that this structure consisted of intact water resembling the hexagonal structure of bulk ice.[15, 16] However, it was later proposed from DFT that this (√3x√3)R30° structure was more stable being made of a mix of water and OH, rather than pure water, and this finding brought about a flurry of interest into the dissociation of water and the structures formed.[17, 18]

Following this, many partially dissociated structures with various structural compositions have been observed on flat metal surfaces.[4, 10, 14, 19] For example, on flat Cu(110), studies have observed a partially dissociated hexagonal network forms as water is heated on an oxygen pre-adsorbed Cu surface, consisting of a 2:1 ratio of H_2O:OH and is stable up to ca. 180 K.[10, 20] On other surfaces, such as Ni(110), water has been seen to dissociate at around 150-180 K, again forming face-sharing hexagonal domains. These hexagonal structures are interrupted by strain relief features that bisect the partially dissociated network to accommodate the longer O-O spacing compared to the relatively short Ni-Ni lattice spacing.[4] The studies mentioned above find that water will dissociate no lower than 150 K on Ni(110), and 160 K on Cu(110), but it is not yet known how a stepped surface compares to a more reactive Ni(110) surface and flat metal surface Cu(110) surface.

Although literature DFT studies have reported steps to make a significant contribution to lowering the dissociation barrier,[2, 21] it is not yet known how these stepped sites compare experimentally to a planar surface, or other more reactive surfaces, such as Ni. This chapter will discuss this topic further, comparing the structures formed on a stepped Cu(110) surface to planar counterpart, and further comparing how the interaction at these steps maybe more or less similar to Ni(110). Low temperature STM was used to explore the behaviour of water at the stepped Cu sites, with results showing that water forms intact 1D pentagonal chains at 77 K, extending out from the top step edge and never growing any closer than four Cu rows apart in the close packed direction. Above 100 K, we find that water dissociates into a partially dissociated water network consisting of ordered hexagonal domains decorated by branched OH, and OH/H_2O chains. Dissociation as low as 100 K has not been reported previously on flat Cu surfaces, indicating that the stepped Cu(110) surface induces dissociation by lowering the activation energy. These findings suggest that the reactivity of the Cu steps is similar to more reactive surfaces, such as Ni(110), with both surfaces showing that water dissociated when heated without the presence of co-adsorbates, such as oxygen, to initiate dissociation.

5.2. Experimental

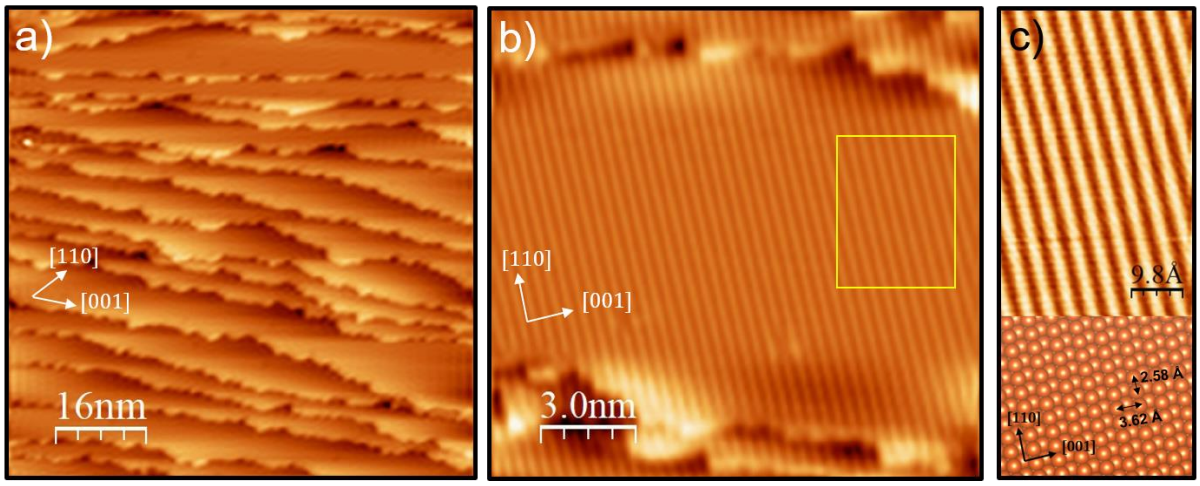

Figure 1. a) An STM image showing the disorder in the size of terraces found on the stepped Cu(75, 78, 1) surface. b) An STM image of one of the terraces on the stepped Cu(75, 78, 1) surface. c) A close up image of the region highlighted in figure b) (in yellow), showing the regular Cu rows on the terrace with the structural model below.

In this study, we used a stepped Cu(110) crystal which had an average step spacing of 75 atoms (~200 Å) apart. The large terrace size results in relatively weak step-step interactions, with insufficient through-surface interaction to organise the steps, generating disorder in the step spacing between the terraces and the presence of kink and defect sites along the step edge. The

disordered step array found on this Cu(75,78,1) crystal is considered a better model for the kind of step arrays that might populate a disordered Cu(110) surface formed on a real catalyst particle (fig. 1a) than a highly stepped surface. This surface is very different to other stepped surfaces, such as Cu(511) which exhibits an ordered array of close packed steps separated by terraces that are three atoms wide, small enough for the steps in the Cu(511) crystal to organise into a more ordered surface.[22] Although the step array found on this stepped surface is disordered, the terraces do exhibit some ordering along the [001] direction (fig. 1c), which is ideal for the growth of ordered structures of water.

The surface was cleaned by repeat cycles of sputtering-annealing, which consisted of sputtering the surface for 10 minutes to remove the topmost layers, followed by the surface being heated to 500 K. The coverages were estimated by STM, using the average fraction of the surface covered by water to create an estimate of the surface saturation.

5.3. Results and Discussion

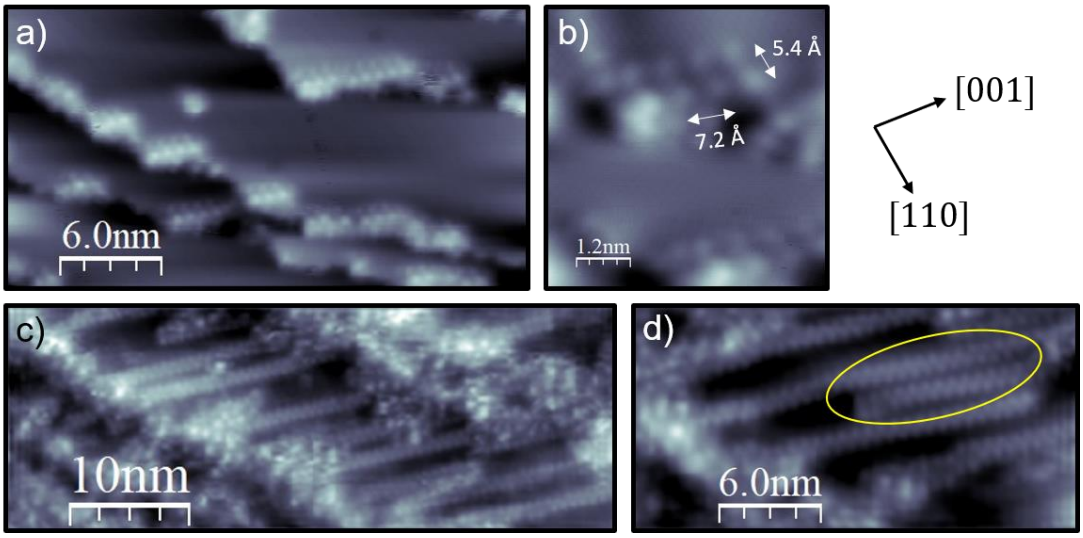

Figure 2. Water adsorption at 77 K on a stepped Cu(110) surface after ca. 0.2 layers of water was dosed on the surface. a) shows 1D water structures growing from each of the Cu(110) step edges. b) close up image of a 1D chain. Water adsorption at 77 K on a stepped Cu(110) surface after ca. 0.8 layers of water was dosed on the surface. c) show disordered water clusters accumulating at the step edge with ordered zigzag chains growing out from the steps in the [001] direction. d) close up of the zigzag chains that grow from the step edge, highlighted in yellow.

The STM images in figure 2 were obtained by dosing various coverages of water on the stepped Cu(110) surface at 77 K. The high resolution images show that water nucleates from the top step edge (fig. 2a), forming 1D linear water chains that slowly extend out along the terrace in the [001] direction as the coverage increases (fig.2). These small zig-zag domains of water can be attributed to intact water chains which grow exclusively along the [001] direction

(perpendicular to the Cu rows). At ca. 0.8 ML coverage, water forms disordered clusters of water along the step edge, with zig-zag 1D chains extending out in the terrace. The water chains are rarely less than 4 (~10 Å), or 6 (~15 Å) units apart; an example is shown in the region highlighted above in figure 2c. The depression and lateral separation of the adjacent bright features measure a distance of 7.2 Å along the [001] direction and 5.4 Å in the close packed direction at both coverages (fig. 2b), matching closely with the measurements for the pentagonal chains of water on flat Cu(110) at 77 K in figure 3, reported by Carrasco *et al.* [23-25]

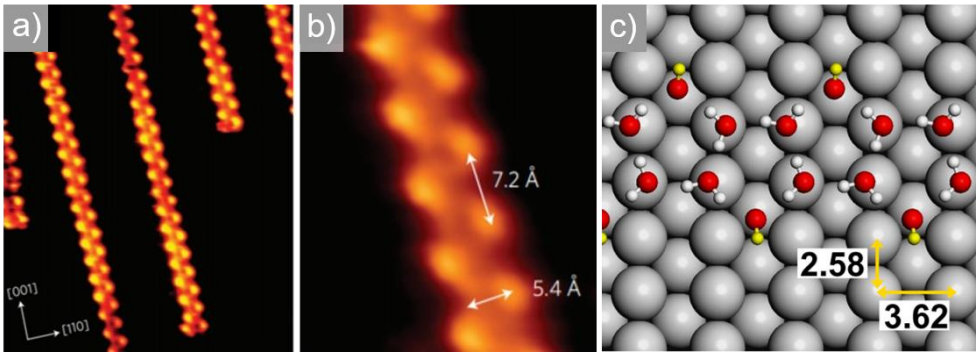

Figure 3. a-b) An STM image taken at 100 K showing water chains growing along the [001] direction on flat Cu(110). c) DFT calculation of the proposed arrangement of intact water in the pentagonal chain. Adapted from.[24]

Further DFT analysis reported by Carrasco *et al.*[24, 26] of these pentamer chains on flat Cu(110), shows that two flat out of 3 waters are flat in the atop Cu sites with one H-down water completing the H-bonded network in the Cu ridge (fig. 3c). This forms edge-sharing pentamer rings, with each ring alternating with one OH bond on water pointing up away from the surface, creating alternating bright features in STM. This reveals a zig-zag arrangement in STM (fig. 3a and b), due to the water molecules planar to the surface having a much lower contrast to the H-up molecules, which is also observed in figure 2. Water in this arrangement has its largest proportion of water molecules planar to the surface in this favoured orientation, which exhibited the lowest energy structure of all those tested and gave evidence of strong surface-water and hydrogen bond interactions.[24] More specifically, the Cu-Cu spacing of the surface is slightly shorter than the equilibrium O-O separation of a hydrogen bonded structure, and therefore it is less favourable to have two waters next to one another on Cu. This results in water wanting to zig-zag up the chain in a lower dimensional structure as Cu cannot accommodate the correct O-O spacing.

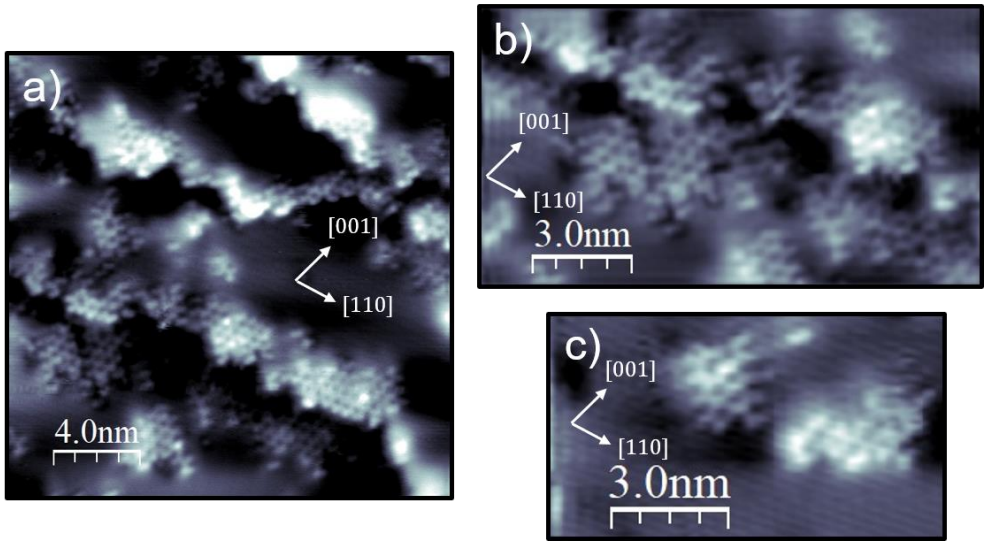

Figure 4. a) STM image showing the structures formed after ca. 0.5 ML of water is heated to 100 K, and then cooled to 77 K. b) close up image of the structures at the step edge. c) close up image of the structures on the terrace.

Water adsorbed at 77 K was then heated to 100 K which led to the formation of small hexagonal domains, with branched and zig-zag chain structures extending out from each of the hexagonal domains on the lower and upper terrace. These structures indicate the presence of a partially dissociated hexagonal network with OH and OH:H_2O chains extending out from each of the domains (fig. 4), similar to that on flat Cu(110).[10, 27] It is evident in previous literature that many of these partially dissociated structures are stabilised by the presence of hydroxyl molecules, which is supported by DFT.[26] This also must be the case here on this stepped Cu(110) surface, with the presence of H-bonded hydroxyl molecules within the 2D network acts as a strong H bond acceptor, stabilizing the water adsorption sites. Furthermore, the OH molecules have a preference to decorate the exposed edges of the partially dissociated structures, due to OH being a poor proton donor but a very a good acceptor, thus forming strong H-bonds along the outside of the water domains.[20, 28]

Dissociation on the flat Cu(110) surface does not typically occur until the surface temperature is above at least 160 K,[27] however our results show the presence of a dissociated c(2x2) network at as low as 100 K. If we compare our stepped surface to the flat Cu(110) and Ru(0001) systems (mentioned above), we find that the stepped Cu surface dissociates water at least 60 K lower, which shows that the presence of the steps has lowered the activation energy for this process to occur, compared to a flat metal surface.[4, 10, 17]

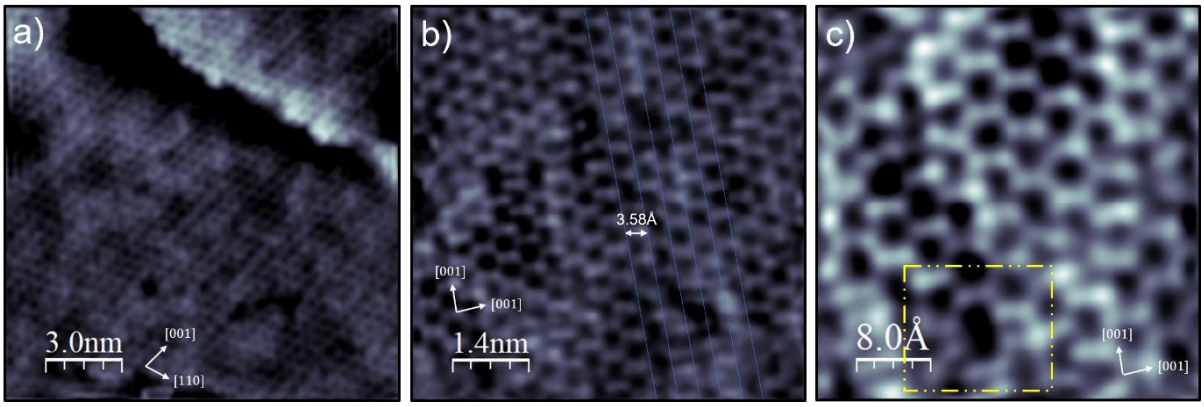

Figure 5. a) STM images showing the structures formed after (ca. 1 ML) water is heated to 140 K, and then cooled to 77 K on the stepped Cu(110) surface. b) STM image of the hexagonal network on a Cu terrace, with an overlayer showing an equivalent spacing of 3.58 Å in [001] direction. c) close up image of the hexagonal network with a region highlighted in yellow where larger rings have formed.

The structures seen at 100 K (fig. 4), where water first dissociates, are rather disordered, but by heating the surface to 140 K they can be ordered further into an extended 2D network (fig. 5). We note that the hexagonal network does contain some defects, such as smaller and bigger ring structures (fig. 5c), which differs from the preferred hexagonal commensurate structure. The measurements for the hexagonal structure of water in figure 5, are in line with previous literature findings of a partially dissociated hexagonal c(2x2) network on flat Cu(110), which further supports our findings of partial dissociation below 100 K.[10, 28] However, the composition of our structure, compared to the structure in previous studies may vary as we do not know the level of dissociation caused by the steps. Moreover, these findings mentioned above suggested that we have water/OH in a c(2x2) network with adsorbate bound adjacent to one another on neighbouring rows of Cu in the close packed direction and on adjacent Cu atop sites, similar to that found on flat Cu(110).[10, 27]

We have shown that even for a corrugated surface such as Cu(110) the presence of steps can have a significant impact on the dissociation process by lowering the activation energy barrier. A recent DFT study on flat Cu(111) and stepped Cu(321) supports this idea.[2] This study found that the dissociation energy barrier was lower when the steps were present on Cu(321) than on flat Cu(111), resulting in a rate constant for the stepped surface being approximately 3 orders of magnitude greater than the flat surface. They predicted that the presence of the steps decreases the activation energy barrier for the rate-limiting step, which is associated with the dissociation of water into H* and OH* and the recombination of hydrogen.[21, 29] This prediction is consistent with our experimental conclusion that the presence of steps lowers the energy

barrier to dissociation, suggesting that stepped surface is able to provide these conditions at a lower temperature than a flat terrace, which is unreactive at 100 K.

It is useful to contrast the behaviour of water during adsorption on this stepped Cu(110) surface and on a Cu surface with a more ordered step array. The stepped Cu(511) surface serves as an ideal template for the growth of a buckled hexagonal network, due to the surface providing strong step-step interactions and regular terrace spacing of 6.6 Å, matching closely to bulk ice.[30] In contrast, the composition of this network on Cu(511) is much different to that on Cu(110), with the network on Cu(110) being composed of both hydroxyl and water. Furthermore, as water is heated on the Cu(511) surface it does not dissociate, despite the presence of steps, as seen in chapter 2. This suggest that the dissociation barrier on stepped Cu(511) surface is relatively high compared to that on stepped Cu(110), as water would rather desorb intact on Cu(511) than dissociate in contact with the surface as it is heated. This could be attributed to the many defect and kink sites that are present on Cu(110), something that is caused by a lack of step-step interactions which provide binding sites with a lower activation energy for dissociation to occur. This is comparatively dissimilar to the step arrays found on Cu(511), and since dissociation does not occur on this surface, these results suggest that the type of step, whether its ordered or disordered can have a significant impact on the dissociation process. Therefore, this study suggests that the type of step array found on metal surfaces is important when considering the type of dissociation catalyst to use, as dissociation is favoured on weakly interacting, disordered steps, not regular step arrays which have fewer active sites.

On more reactive surfaces, such as Ni(110) water dissociates below 160 K even on the ordered surface, forming isolated water/OH hexagonal (2x3) domains that are rarely more than 6 units (30 Å) long in the $[1\bar{1}0]$ direction before a defect or different structure continues.[4] Although this arrangement of water/OH is different compared to that on stepped Cu(110), the reactivity is similar, with both surfaces showing that water dissociated when heated without the presence of co-adsorbates, such as oxygen to help initiate dissociation. This directly contrasts flat Cu(110) surfaces, which requires the presence of oxygen to create a partially dissociated water/OH structure, otherwise, water will desorb intact on the clean flat Cu terraces.[31, 32] This gives an insight into how defect sites, in this case, steps can provide sites that are just as reactive as other surfaces that are considered to be more reactive than Cu, which reaffirms the fact that the steps play a key role in lowering the barrier for dissociation. Therefore, this shows that steps are an important factor to consider in the field of catalysis, particularly when assessing suitable metal catalysis that can help promote the dissociation of water.

5.4. Conclusions

To conclude, this study shows that water nucleates on the top step of the Cu(110) surface, before extending across the terrace in the [001] direction as the coverage increases. As intact water is heated to 100 K or above, the H-bonded structure evolves from the linear edges sharing pentamer chains at 77 K into a partially dissociated 2D cyclic network, comprising a hexagonal c(2x2) structure with branched OH and OH/H_2O chains extending out from the small domains. The partially dissociated phase orders up further into an extended network as it is heated to 140 K, with some larger ring structures that differ from the commensurate structure. The hexagonal structure is stabilized by the presence of H-bonded hydroxyl molecules within the network, which acts as a strong H-bond acceptor stabilizing water adsorption. Onset dissociation at such a low temperature reflects the complex kinetics associated with dissociation/desorption of a corrugated surface, compared to a flat surface with no periodic change in the surface binding energy.

To summarise, we have shown that the increased number of step defects has a positive influence on the dissociation process, compared with a more planar surface, by reducing the barrier to dissociation. It is true that planar surfaces still contain a small number of steps with large terraces, however it is clear from our study that increasing that number can lead to a more effective dissociation catalyst. Finally, the dissociation of water at clean metal surfaces appears to occur more readily at atomic rough areas, such as fcc(110) faces or steps, than the atomic smooth areas (terraces). Dissociation does not take place on the smoother flat regions of the surface and only at the steps.

5.5. References

1. H. Prats, P. Gamallo, R. Sayós and F. Illas, *Physical chemistry chemical physics*, 2016, **18**, 2792-2801.
2. J. L. C. Fajín, M. N. D. S. Cordeiro, F. Illas and J. R. B. Gomes, *Journal of Catalysis*, 2009, **268**, 131-141.
3. R. Peköz and D. Donadio, *The Journal of Physical Chemistry C*, 2017, **121**, 16783-16791.
4. N. Gerrard, K. Mistry, G. R. Darling and A. Hodgson, *The Journal of Physical Chemistry C*, 2020, **124**, 23815-23822.
5. J. L. C. Fajín, M. N. D. S. Cordeiro, F. Illas and J. R. B. Gomes, *Journal of Catalysis*, 2010, **276**, 92-100.

6. A. Y. Rozovskii and G. I. Lin, *Topics in Catalysis*, 2003, **22**, 137-150.
7. S. H. D. Lee, D. V. Applegate, S. Ahmed, S. G. Calderone and T. L. Harvey, *International Journal of Hydrogen Energy*, 2005, **30**, 829-842.
8. D. J. Suh, C. Kwak, J.-H. Kim, S. M. Kwon and T.-J. Park, *Journal of Power Sources*, 2005, **142**, 70-74.
9. A. Hodgson and S. Haq, *Surface Science Reports*, 2009, **64**, 381-451.
10. M. Forster, R. Raval, A. Hodgson, J. Carrasco and A. Michaelides, *Physical Review Letters*, 2011, **106**, 046103.
11. L. Guillemot and K. Bobrov, *The Journal of Physical Chemistry*, 2011, **115**, 22387-22392.
12. T. Kumagai, M. Kaizu, H. Okuyama, S. Hatta, T. Aruga, I. Hamada and Y. Morikawa, *Physical Review B*, 2010, **81**, 045402.
13. T. Schiros, L. Å. Näslund, K. Andersson, J. Gyllenpalm, G. S. Karlberg, M. Odelius, H. Ogasawara, L. G. M. Pettersson and A. Nilsson, *The Journal of Physical Chemistry C*, 2007, **111**, 15003-15012.
14. M. Forster, R. Raval, J. Carrasco, A. Michaelides and A. Hodgson, *Chem. Sci.*, 2011, **3**, 93-102.
15. D. L. Doering and T. E. Madey, *Surface Science*, 1982, **123**, 305-337.
16. P. A. Thiel and T. E. Madey, *Surface Science Reports*, 1987, **7**, 211-385.
17. C. Clay, S. Haq and A. Hodgson, *Chemical Physics Letters*, 2004, **388**, 89-93.
18. Y. Huang, X. Zhang, Z. Ma, W. Li, Y. Zhou, J. Zhou, W. Zheng and C. Q. Sun, *Scientific Reports*, 2013, **3**, 3005.
19. I. Hamada, T. Kumagai, A. Shiotari, H. Okuyama, S. Hatta and T. Aruga, *Physical Review B*, 2012, **86**, 075432.
20. C. Ammon, A. Bayer, H. P. Steinrück and G. Held, *Chemical Physics Letters*, 2003, **377**, 163-169.
21. R. Peköz, S. Wörner, L. M. Ghiringhelli and D. Donadio, *The Journal of Physical Chemistry C*, 2014, **118**, 29990-29998.
22. C. Lin, G. Corem, O. Godsi, G. Alexandrowicz, G. R. Darling and A. Hodgson, *Journal of the American Chemical Society*, 2018, **140**, 15804-15811.
23. T. Yamada, S. Tamamori, H. Okuyama and T. Aruga, *Physical Review Letters*, 2006, **96**, 036105.
24. J. Carrasco, A. Michaelides, M. Forster, S. Haq, R. Raval and A. Hodgson, *Nature Materials*, 2009, **8**, 427-431.

25. P. J. Feibelman, *Nature Materials*, 2009, **8**, 372-373.
26. J. Carrasco, A. Hodgson and A. Michaelides, *Nature Materials*, 2012, **11**, 667-674.
27. M. Forster, R. Raval, J. Carrasco, A. Michaelides and A. Hodgson, *Chemical Science*, 2012, **3**, 93-102.
28. J. Ren and S. Meng, *Journal of the American Chemical Society*, 2006, **128**, 9282-9283.
29. D. Donadio, L. M. Ghiringhelli and L. Delle Site, *Journal of the American Chemical Society*, 2012, **134**, 19217-19222.
30. E. R. Batista and H. Jonsson, *Computational Materials Science*, 2001, **20**, 325-336.
31. T. Schiros, S. Haq, H. Ogasawara, O. Takahashi, H. Öström, K. Andersson, L. G. M. Pettersson, A. Hodgson and A. Nilsson, *Chemical Physics Letters*, 2006, **429**, 415-419.
32. Haq. S, *Unpublished data, University of liverpool, Surface Science, 2009*.

Chapter 6

An investigation into the Structure of Water on a Stepped Pt(211) Surface

6.1. Introduction

Fossil fuel is a finite resource that contributes to global warming by releasing carbon dioxide into the atmosphere. In order to mitigate this damage, we must find alternative fossil-free energy applications that can not only reduce the net carbon dioxide emissions but also reduce the demand for this limited resource.[1, 2] One possible solution that can provide a source of clean carbon-free energy is the hydrogen fuel cell, which creates no adverse environmental impact during operation as the only by-products are simply water, heat and energy.[1-3] With hydrogen fuel cells being carbon-neutral, this type of fuel cell technology has also gained a lot of attention in the automotive industry, due to the industry having a significant contribution to the net burning of fossil fuels.[4, 5] The hydrogen fuel cell works by using a catalyst to separate the hydrogen into protons and electrons at the cathode, which is then combined with oxygen at the anode, releasing the stored chemical energy, water and heat. Although this process works well, a lot of energy is lost in heat transfer during the operation of the cell, consequently reducing the overall efficiency.

Recent studies have looked to solve this problem by the use of improved proton exchange membranes and new catalysts, which have shown potential in the field of fuel cell technology, producing cells with higher energy output and lower operating temperature.[6] The membrane insulates against electrons whilst allowing protons to travel through the catalyst-coated membrane to participate in redox reactions at the surface. One of the coatings typically used on the surface membrane is Platinum, due to Pt having the best catalytic activity of all pure transition metals.[7, 8, 9] Taking this into consideration, much research has gone into understanding the reactions occurring on a Pt surface and their involvement in fuel cell technology.[10, 11] In particular, there is great interest in reactions involving barriers associated to the formation of water from O, OH and H species on ideal surfaces, and more complex surfaces that might populate a fuel cell catalyst.[1, 10-13] In order to understand the reaction mechanisms involved with the formation of water on a Pt-coated proton exchange membrane

(PEM), one must first look at the different intermediate formed, the structures, barriers and interactions associated with water on the Pt surface.

Many of the first research studies investigating the interaction of water with a Pt surface looked for a surface that would facilitate the growth of a simple ice-like layer, over a more complex 2D network composed of many different ring structures. A reason for wanting a simpler structure is that there would be fewer specific geometries and binding environments to understand, giving one a better understanding of the interactions present on the Pt face. With this in mind, numerous studies have investigated water on the flat Pt(111) face, in the hope that the hexagonal surface template would provide a commensurate layer similar to that of bulk ice.[13, 14] Although this seemed theoretically possible, many experimental studies found that water adopted an array of pentagonal, hexagonal and heptagonal rings with a (√37x√37)R25.3° structure at low coverage, restructuring into a (√39x√39)R16.1° arrangement as the surface saturated (fig. 1).[14-17] This result indicates water forms a more complex network than anticipated, due to the structures containing many more binding environments than the simple hexagonal layer. Although a hexagonal wetting layer did not form on the flat Pt(111) surface, a bulk hexagonal wetting layer was found to form on a stepped Cu(511) surface in a different study.[18] This stepped surface provided an excellent template for understanding the binding environments and bond geometries adopted by water at the stepped Cu surface. However, so far there has been little study of water at stepped Pt surfaces, particularly by local probes (e.g. STM and AFM). Therefore, in order to see how water and OH bind on these surfaces, we have chosen to investigate the interaction of water with a stepped Pt(211) surface, to see whether the surface adopts a simpler first layer structure, which will in turn help us to gain a better understanding for the type of interactions present with water and OH on a fuel cell catalyst mimic.[9, 19]

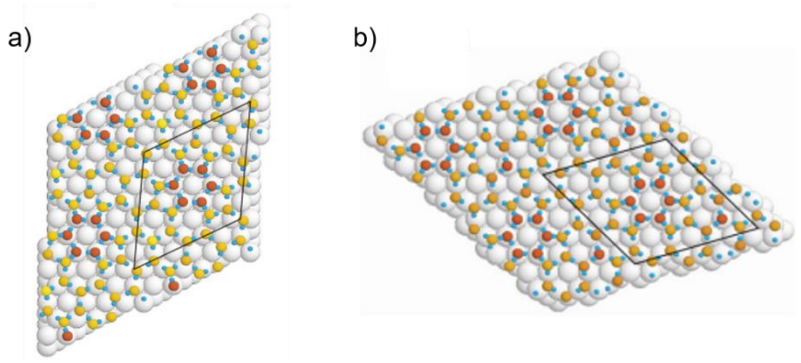

Figure 1. a) DFT image of waters overlayer on the Pt(111) surface(√37x√37)R25.3° structure. b) DFT image of waters overlayer on the Pt(111) surface(√39x√39)R16.1° structure. The figures above show showing the tightly bound, flat waters close to the Pt surface in dark orange, with the rest of the network sitting slightly higher shown in yellow. Adapted from.[14]

To gain a better understanding of how a stepped Pt(211) face will fare, one must first understand how water interacts in more detail on its close packed (111) face. Previous studies have shown that water adopts a (√37x√37)R25.3° structure at low coverage (fig. 1a), further restructuring into a (√39x√39)R16.1° structure as the surface saturates (fig. 1b).[14] The low coverage structure consisted of a combination of waters that bind either planar or H-down onto the surface, forming five, six and seven membered rings. Only a small fraction of water in this network adopted the desired hexamer units, creating low-lying tightly bound water rings alternating with high-lying water rings that sit slightly above at a 30-degree rotation. As the coverage increases, the layer completes with a mix of pentamer and heptamer rings that bridge these high and low-lying hexagonal units (fig. 1), forming the large unit cells. Both these arrangements of water were supported by DFT, which suggested that it was energetically favourable to have water flat and tightly bound (highlighted in dark orange), with the rest H-bond network (highlighted in yellow) optimising bond geometries (fig. 1). However, the structural consequence of the networks described above is that further growth of water atop the first wetting layer is impossible without substantial molecular rearrangement of the first layer.[14, 20-22] Therefore, it was clear that water on this surface does not form the simple hexagonal ice structure that many studies thought it would, forming a more complex 2D structure with many more binding environments which is more difficult to understand and study in detail.

On other corrugated surfaces, such as Ni(110), we observe 1D chains that do not interact with one another, with each chain separated by a row of bare Ni. Regardless of the fact that this structure only contains two hydrogen bonds per water, DFT calculations showed that the 1D chains are 0.034eV/water more stable than other 2D hydrogen bonded networks, containing

three hydrogen bonds per water. The question is, does this also occur on other corrugated surfaces, particularly those with a small terrace width that may encourage the formation of 1D chains, rather than bridging across the steps. Scanning tunnelling microscopy observations at Pt steps have indicated that water initially adsorbs at the step edges, forming one dimensional hydrogen bonded chains.[23] Analysis by Endo et al.[24] of water at Pt steps has suggested that 1D growth occurs on the narrow Pt(211) surface, forming chains along the step edges that do not bridge across the (111) steps into a 2D structure. These reports were based on O K-NEXAFS signals for water at 532.9 eV, comparing resonances that corresponded to the OD bond orientation perpendicular to the step lines and hydrogen bonds which extend in a zigzag arrangement along the steps. These signals were used to interpret bond geometries and the position of water on the Pt(211) surface, which lead them to believe that simple 1D zigzag chains grow along the step edges. Further analysis using DFT showed two optimized 1D chains, both containing a single strand of water that alternates in a zigzag manner along the top edge of the (100) step sites. The two different structures showed that water either sits atop the step Pt atoms, alternating either side of the Pt atom with water either planar to the surface or alternating H down and planar, both containing one hydrogen bond donor and acceptor per water.[24] Another study investigating the relative adsorption and dissociation energies of water on the Pt(211) surface, also proposed that simple 1D hydrogen bonded chains grow on this surface. The DFT calculations in this study used different configurations and sizes of 1D hydrogen bonded chains, with water preferentially accumulating at the step rather than the (111) terrace sites.[25] What these studies all have in common is the fact that they suggest that simple 1D growth will be adopted over the growth of a 2D structure on the Pt(211) surface.

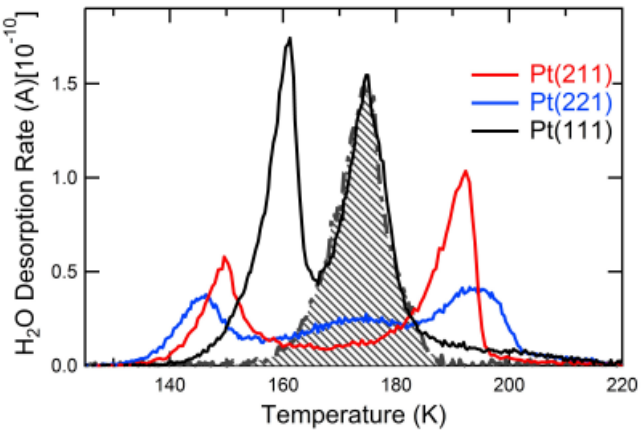

Figure 2. Temperature programmed desorption (TPD) spectrum of water on various Pt surfaces. Adapted from.[26]

In the hope of understanding more about the interactions of water on stepped Pt surfaces, including those reported above, Juurlink et al.[9] and Badan et al.[26] investigated the binding of water on different Pt surfaces using TPD, comparing the planer Pt(111) surface to the stepped (211) and (221) surfaces. The purpose of using the two different stepped faces was to see whether the slight change in terrace width and step symmetry had a significant role in the bonding and structure of water. The TPD profile of the (111) face (highlighted in black, figure 2) showed that water created two distinct peaks, with the monolayer at desorbing ca. 175 K and multilayer at ca. 160 K, and a temperature difference with ca. 15 K. Although the Pt(211) surface (highlighted in red, figure 2) followed a similar trend of two desorption peaks for the monolayer (ca. 190 K) and multilayer (ca. 150 K), the temperature spread was much greater (c.a. 25 K) than for the flat Pt(111) face. The same was not observed for Pt(221), which showed three distinct desorption peaks at ca. 145 K, ca. 170 K and ca. 195 K (highlighted in blue, figure 2).[26] This study suggested that the distinct differences in TPD profiles were attributed to different binding environments, step symmetries and increased terrace spacing from 2.5 atoms on Pt(211) to 3.5 atoms on Pt(221). [27, 28] Further analysis of these peaks, lead them to believe that water was not bound on the (111) terrace sites on Pt(211), proposing a linear structure that is unlikely to bridge across the (111) steps due to a distance too great for hydrogen bonding to explain, but grows along the Pt steps edge. This study finally suggested that the Pt(211) surface does not only provide a bad anchor for hexagonal water structures, but also was not able to provide any clear supporting evidence for the 1D zigzag chains reported by Endo et al.[24]

These reports mentioned above, question whether the structure of water has been misinterpreted on the Pt(211) surface, with water either adopting a different structure entirely or 1D hydrogen bonded chains, similar to those suggested above. Although some literature studies believe that simple 1D zigzag chains grow on this surface, there are no conclusive reports to confirm these proposed structures, including the fact that the surface does form an appropriate template for the growth of 2D water. Therefore, we have chosen to investigate a stepped Pt(211) surface, both to understand how water wets this surface and what reaction intermediates will be present on a stepped fuel cell catalyst. The findings in this chapter demonstrate waters preference to form pseudo 1D chains with rings on the terrace at low coverage, and not simple 1D chains. Increasing the coverage further, we start to see regions where there is two times periodicity on adjacent steps with limited order in the $[\bar{1}11]$ direction. These regions show a surface structure that has a small propensity to form a 2D network, forming only small (2x1) regions that are in phase with little order between adjacent steps.

6.2. Experimental

The surface was prepared in a UHV system comprised of two chambers that were connected via a gate valve; one was used for sample preparation and characterisation, and the other for sample analysis. The sample preparation involved sputter-anneal cycles and the sputtering process consisted of bombarding the surface with a beam of monatomic Ar^+ ions, followed by the surface being heated to 1000 K to re-order the Pt surface. The analysis chamber contained an STM cryostat, which is capable heating at a rate of 1 K min^{-1}, and cooling down to 77 K using liquid nitrogen. The STM provided us with the ability to visualise the surface on the monoatomic scale, further helping establish whether the surface was clean. The coverages using STM were approximated using the STM images to estimate coverage.

TPD and LEED analysis was undertaken in a separate UHV chamber, which consisted of a single chamber that was used for sample cleaning and analysis. The same sample preparation methods were used in this chamber to eliminate any changes in surface conditions, with the surface being annealed to 1000 K in between TPD experiments. The sample was held on a manipulator between two tantalum wires that were spot welded to two tantalum posts, which cooled the crystal down to 100 K using liquid nitrogen as a cryogen. The chamber contained a LEED and quadrupolar mass spectroscopy instrument, described in chapter two, which provided us with the ability to observe the lateral order of the surface water structures. Before TPD coverage sets were taken on Pt(211), the beamline was calibrated for water on Cu(511) surface, which involved using a fixed beam pressure over different lengths of time, until the closest TPD profile to a layer on Cu(511) was observed. This enabled a single layer water dose (ca. 1.0 ML) to be defined as 0.67 water per Cu surface atom, which was based on the wetting of the first layer hexagonal structure on Cu(511).[18] During the experiments we ensured that the calibrated beam position and UHV conditions used for Cu(511) remained constant throughout the Pt(211) experiments. However, we note that this was only used to estimate the coverage of water on the Pt(211) surface, which allowed us to form comparisons with a known 2D wetting layer. A more detailed description of how water was dosed on the Cu(511) surface can be found in chapter 2, explaining the process used.

6.3. Results and Discussion

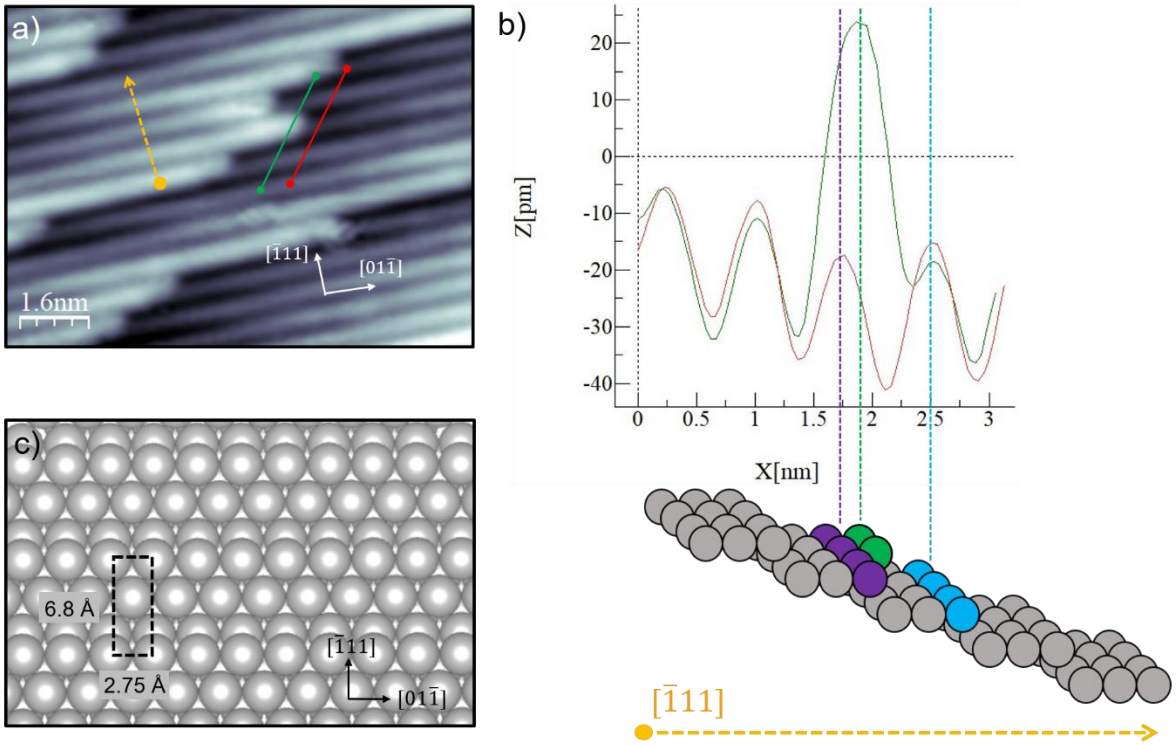

Figure 3. a) STM image showing regularly spaced rows of Pt atoms filling each of the terraces, with the step direction highlighted in orange, and two line profiles highlighted in green and red. b) Shows two merged line profiles that were taken from figure a), illustrating the position of the addition Pt row on the Pt(211) surface. c) A simulated image of the Pt(211) surface with the unit cell highlighted black.

The STM image above (fig. 3a), shows a clean stepped Pt(211) surface which is built from extremely narrow terraces, with each step showing up as bright lines that are separated by the terrace width of two and a half atoms (6.8 Å). Whilst the terraces exhibit a hexagonal (111) symmetry, the step sites show a (100) symmetry and are potentially more reactive sites for water adsorption.[9] This surface therefore provides a model for the kind of step arrays that might populate a stepped region of a Pt(111) surface (fig 3a).

Investigating the position of additional bright rows of Pt protruding from the edge of terraces on the Pt(211) surface enables us to determine the step direction of the surface. This is because any additional Pt rows will always choose to sit in the highest coordination sites, for example, sites below the Pt step edges will have a coordination number of six, compared to three atop the step edge, resulting in the additional row sitting below the step due to the higher coordination stabilising the additional Pt rows. This can be observed in STM images (fig. 3a), by placing line profiles across terraces with an additional row (highlighted in green), and comparing it with the line profile of the neighbouring rows without the additional Pt row

(highlighted in red). The merging of both line profiles shows that the additional row sits closer to the first step, highlighted in purple, than the second step, highlighted in blue (fig. 3b). This therefore shows that the topmost layer decreases with each step edge, facing along the line in the [$\bar{1}$11] direction highlighted in orange (fig. 3b and c).

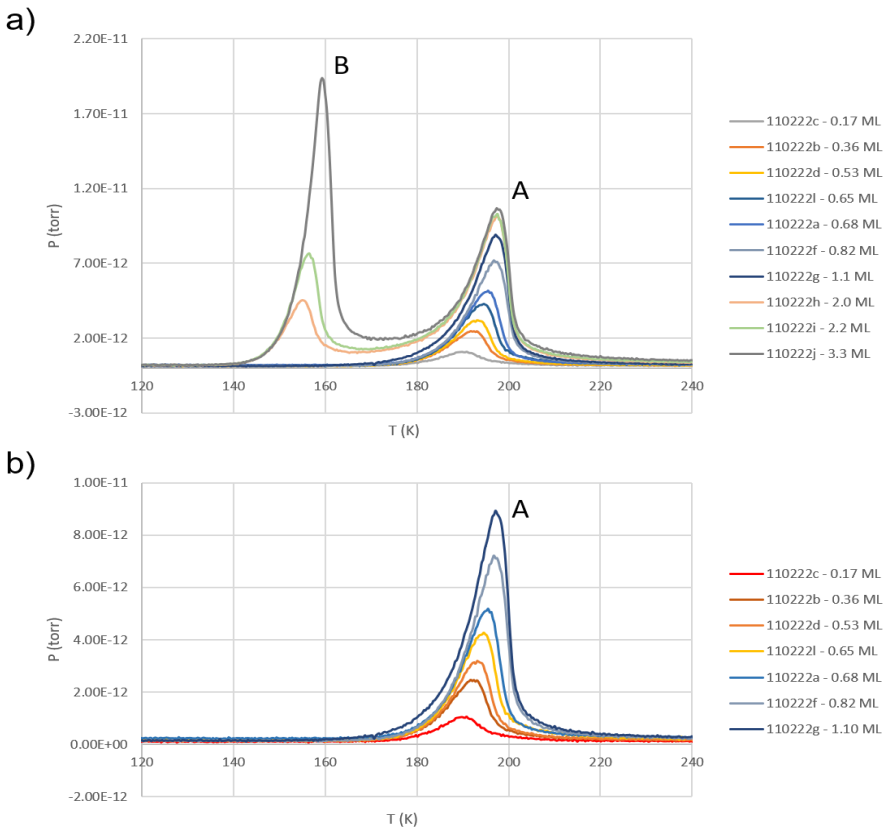

Figure 4. Thermal desorption for various coverages of water on the Pt(211) surface: a) TPD profiles of coverages above the monolayer (B) and below the monolayer (A). b) TPD profiles of coverages below 1.1 monolayer. All coverages indicated a thickness estimated from the completion of the Cu(511) layer. One monolayer was defined as the amount of water needed to complete a single layer on the Cu(511) surface in the hexagonal 2D network, which exhibits a water density of 0.67 water per Cu surface atom.[18]

The water coverage on the Pt(211) surface was increased gradually using our calibration for one layer of water (described in our experimental section, chapter 2), which gave the approximate coverage of water on the Pt surface. The surface was then heated at a rate of 1 K s^{-1}, resulting in two distinguishable TPD peaks, peak A (ca. 195 K) and peak B (ca. 150 K) for coverages over one monolayer (fig. 4a), showing a clear distinction between the binding energy of the water-water and Pt-water interactions. These TPD profiles shown above (fig. 4), are in line with previous literature findings for water on Pt(211), supporting the presence of intact water on our Pt(211) surface.[9, 26] Leading edge analysis of the TPD profile for coverages below

1.0. ML (fig. 4b), shows that the leading edge does not change, indicating that the surface is composed of a structure or structures, with a similar binding energy. In regards to the completion of a layer, we find some inconsistencies with previous literature, with our TPD coverages showing that the surface completes its layer with a similar density to that on Cu(511).[18] The presence of low density 1D hydrogen bonded chains, for example, as suggested in previous literature, would create coverages much lower than those shown above, due to water only adsorbing to half the number of exposed Pt atoms on each of the terraces.[9, 24, 25] The saturation coverage of ca. 1.0 ML strongly suggests that the water structures formed on Pt(211), are composed of a high-density layer, with a similar density to the 2D layer found on Cu(511), which has a hexagonal of 2D water network at saturation. Moreover, the absence of any evidence of a change in binding energy with coverage strongly implies that any low dimensional structures that might be formed at low coverage have a similar binding energy to that of the 2D layer formed as the coverage reaches 1.0 ML.

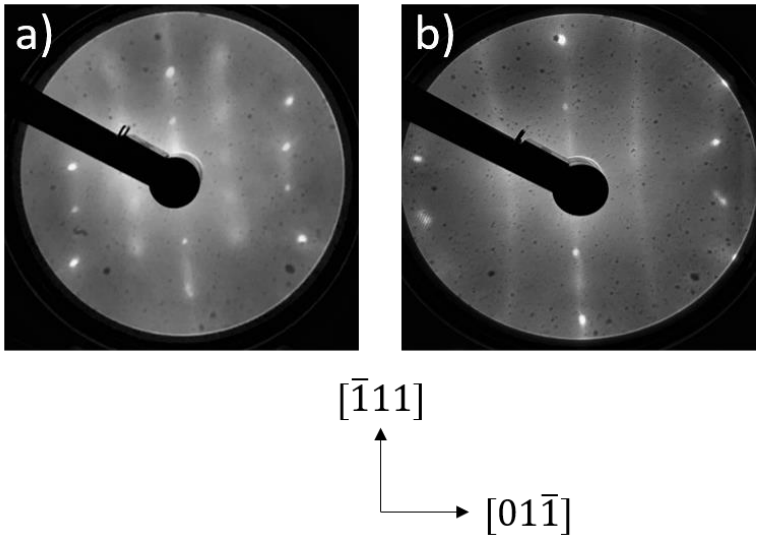

Figure 5. a) LEED images obtained by annealing ca. 0.4 ML of water to 160 K on the Pt(211) surface, taken at 90 eV. b) LEED image obtained by annealing ca. 0.7 ML of water to 160 K on the Pt(211) surface, taken at 69 eV.

The lateral order of the first layer was monitored using low energy electron diffraction, showing bright Pt integer order spots with the presence of a partially ordered water overlayer (fig. 5). Annealing ca. 0.4 ML to 160 K, revealed diffuse diffraction spots at the half order positions in the [01$\bar{1}$] direction, indicating two times periodicity and a (2x1) diffraction pattern. Further increasing the coverage to ca. 0.7 ML, resulted in the water diffraction spots at the half order positions becoming fainter and streaked in the [$\bar{1}$11] direction. This suggests the amount of disorder in the surface wetting layer has increased, compared to the [01$\bar{1}$] direction, where

streaking is absent, even at high coverage. This suggests that we have some order along the step direction on the Pt(211) surface implying a structure with a two-unit repeat. In contrast, the increased disorder perpendicular to the step direction at ca. 0.7 ML suggests that we have less of the step structures in registry with one another at a higher coverage. These findings are supported by STM analysis of water on the Pt(211) surface, showing a lack of order in the $[\bar{1}11]$ direction as the coverage increases, something we will further elaborate in this chapter.

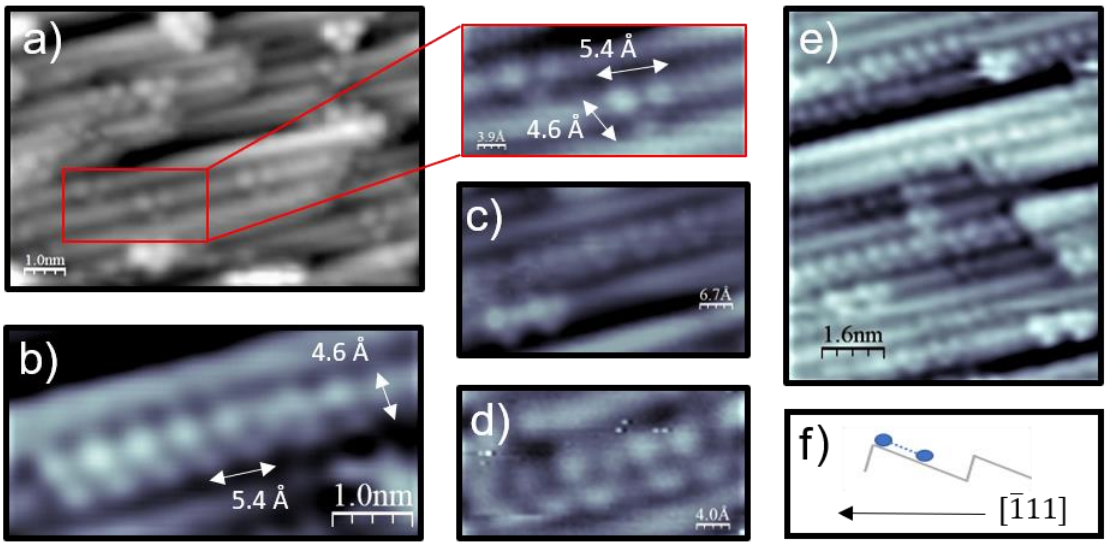

Figure 6. The STM images above were obtained by heating a low coverage of water on the Pt(211) surface to various temperatures, with all structures seen to be stable up to 160 K. a) Water adsorption at 77K on the Pt(211) surface after surface annealing to 120 K, showing individual structures of water imaged as trimers. b) Water adsorption at 77K on the Pt(211) surface after surface annealing to 140 K, showing a pseudo 1D chains of water. c) shows the water structures in a) arranged next to one another, forming linear rows with an irregular spacing. d) STM image showing ordered linear zigzag chains with an irregular regular repeat in the $[01\bar{1}]$ direction. e) Water adsorption at 77K on the Pt(211) surface after surface annealing to 140 K, showing a mix of the structure seen in figure a) to c). f) illustration showing that water sits at the step edge on the Pt(211) surface, with no apparent structure below the step.

The STM images above show structures that are not simple 1D chains (fig. 6), as structures are seen to grow along two alternating sites parallel to the steps, with the structures along the step edge being typically brighter than the structures that feature on the terrace. The bright features have a repeat distance of 5.4 Å in the $[0\bar{1}1]$ direction and 4.6 Å in the $[\bar{1}11]$ direction, which is smaller than the spacing of one terrace (6.8 Å). These bright features in figure 6, give evidence of structures that lie solely along one terrace, with bright features that point towards the upper terrace and along the step edge with no clear structure below the step (fig. 6f). This distance of 5.4 Å in the $[01\bar{1}]$ direction is equivalent to the spacing of two Pt atoms, and is in accordance with the ordering seen in LEED (fig. 5a). Further to this, the distance of 5.4 Å is

too large for two adjacent water molecules to bind directly (fig. 6a and b), due to the average H-bond distance of ice being ca 2.75 Å, which suggests that there must be intermediate water in between these bright features.[29, 30] The same is true in the $[01\bar{1}]$ direction, which points to the fact that there is a more complex structure present along the step edge, compared to that of a simple 1D chain. Although these are clearly not simple linear chains, we are not able to image the structure in between these bright features but we do find structures that image in STM as either individual trimers (fig. 6a), or linear zigzag chains of trimers (fig. 6b). Further analysis of these structures suggests that water has no obvious preference to want to form zigzag pseudo 1D chains which contain a regular two-unit repeat (fig. 6b) or linear rows of individual trimers with an irregular spacing (fig. 6c), and the additional features remains disordered along the chains. Although the zigzag chains seem to be the more ordered structure, we often observe some form of chain interruption in the arrangement of the bright features, showing irregularly spaced linear features, as seen in figure 6d. This shows that these regularly spaced linear zigzag chains with a two times repeat in the $[01\bar{1}]$ direction also contains a certain degree of disorder. These observations suggest that, even after annealing to 160 K, water clusters remain somewhat disordered, with little drive to form a single structural arrangement on the Pt(211) surface.

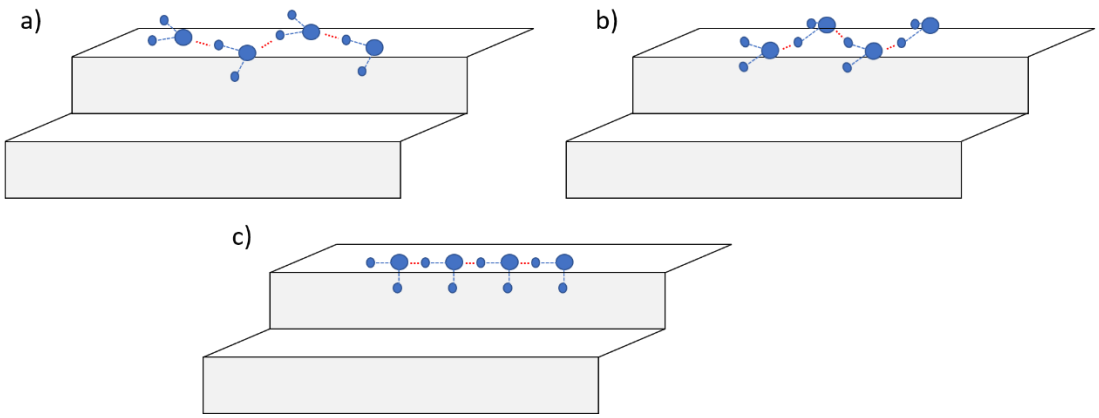

Figure 7. a-c) Shows an illustration of the potential arrangements for water along the step edge, with water with covalent O-H bonds highlighted in blue, and hydrogen bonds highlighted in red.

The illustrations shown above in figure 7 show potential arrangements for water along the Pt(211) step edge, which are based on a combination of previous DFT reports on stepped Pt(211) and Pt(533).[24, 25, 31, 32] Figure 7a shows water alternating with one water-OH positioned H-down over the step, opposing the step dipole, with its other water-OH bond pointing along the step and hydrogen bonding to adjacent water above the step in a buckled arrangement. Figure 7b shows water molecules in a zigzag arrangement planar to the surface, with one water having its OH group point out over the step edge in an alternate arrangement. Figure 7c shows

water forming a linear chain along the step edge, with each OH group pointing down over the step, opposing the step dipole.

STM is sensitive to the change in height of water on the surface, and to the electronic environment of the atom, resulting in contrast changes due to water having different positions relative to the surface plane. In our STM data, we see contrasting changes along the step edge with a two-unit repeat, most likely due to a buckled structure along the step edge with two different height profiles. This is not consistent figure 7c, which has all waters at the same height, and a structure that does not alternate with a two unit repeat along the Pt step edge, which is observed in both STM and LEED. Although figure 7b does contain a two unit repeat and an alternate arrangement, it does not contain any buckled water, making it less likely to display regular bright features with twice the Pt spacing along the step. This is because individual waters with a similar height profile will likely produce a similar contrast in STM, which results in every water being observed, creating bright features every 2.7 Å, which is not consistent with our 5.4 Å observed in STM (fig. 6b). In contrast to both these structures, figure 7a does contain a buckled arrangement for water with a two-times repeat for twice the Pt spacing, making it the most likely candidate to create the bright features along the step edge. This arrangement is supported by DFT calculations, which suggest that the hydrogen pointing down opposite to the step dipole stabilises the chain above.[24, 25, 31, 32] Not only has this been reported on stepped Pt surfaces, but also on stepped Cu(511), with DFT calculations pointing to the fact that the water aligned H-down over the step edge stabilises water along the terrace.[18]

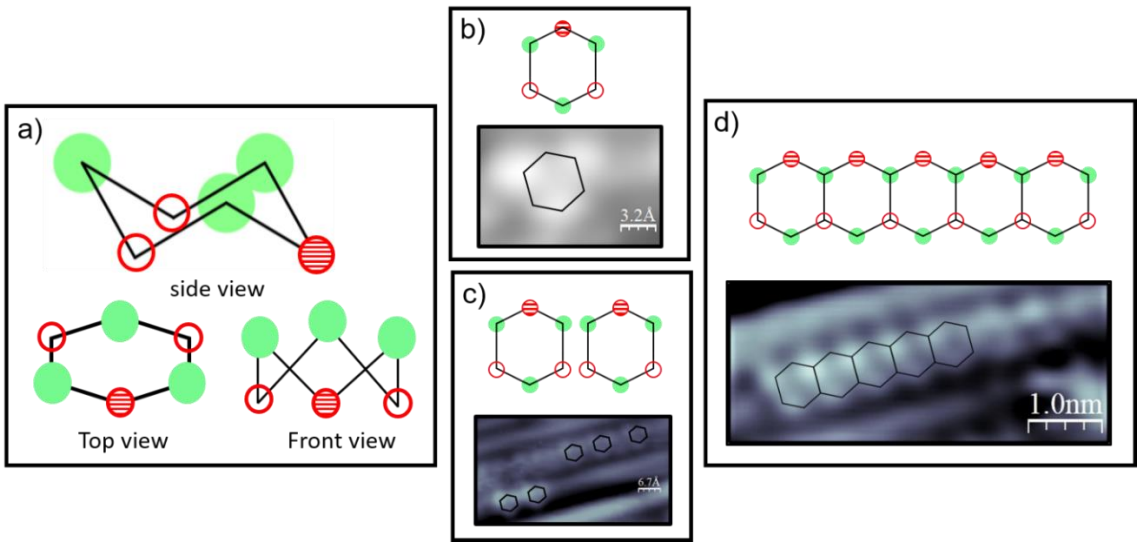

Figure 8. a) Illustration showing various views of a buckled hexagonal ring, with three waters in the upper layer shown in green, and three waters in the lower layer shown in red (with the water that is H-down over the step edge highlighted with a red strip). b) STM image showing an isolated water structure which is imaged as a trimer, with the outline of a hexagonal ring. c) STM image showing irregularly spaced linear rows of isolated water structures that are imaged as a trimer, with the outline of hexagonal rings. d) STM image of water chains that are imaged as regularly spaced zigzag features, with the outline of a linear hexagonal chain. The hexagonal structures above the STM images show positions of the individual water molecules that were imaged in green, and waters that were not imaged in red (with the water that is H-down over the step edge highlighted with a red strip).

Further to the above, we can see that we have a buckled zigzag chain that is stabilised by water-OH groups that point out and over the step edge with a two-unit repeat, with additional structure along the terrace joined to these chains, as seen in STM (fig. 6). In order for water to have additional bright features along the terrace with a similar contrast to water along the step, water must not only be position higher than the adjacent waters along the terrace, but also must be H-up. The fact that the additional bright features along the terrace lie directly in between the bright features along the step edge, suggests that these structures are similar in size and shape to that of a distorted hexagonal ring (fig 8b). A buckled hexagonal ring would not only cause water to alternate along the step edge, but would also result in a single bright feature appearing on the terrace, directly in between the two bright features along the step (fig. 8b). This is because a buckled hexagonal ring contains three positions where water sits higher with possible water-OH groups points away from the surface (highlighted in green, figure 8a), which causes high contrast bright features to appear compared to the other waters in the structure that sit lower (highlighted in red, figure 8a). This not only explains the trimer features appearing in STM (fig. 8b), but also the linear zigzag features that exhibit a two-unit repeat (fig. 8d).

Overall, these findings show that individual water molecules highlighted in green sit higher in the vacuum than water highlighted in red (fig.8). Although the water molecules highlighted with a red stripe also sits along step, the H-down over the step edge results in a lower contrast compared to its neighbours. Since STM data shows one bright feature along the terrace (highlighted in green), it is plausible to assume that this water must be H-up and positioned higher than its neighbouring waters along the terrace (highlighted in red). Therefore, this shows that we have stabilised zigzag chains along the step edge, with the formation of hexagonal rings along the terrace, with STM showing that water hexamers can either be positioned irregularly along the chain (fig 8c), or in a more ordered continuous hexamer chain along the $[01\bar{1}]$ direction (fig 8d).

Morgenstern et al.[33] found hexagonal rings of water imaged as timers on Ag(111) surface, which was caused by the upper layer of water in a buckled hexagonal ring, with every second water not being able to be imaged in STM, due to being lower to the surface substrate compared to the upper layer. On surfaces with similar reactivity to Pt(211), such as Pt(533), water has been calculated to form buckled hexagonal rings along the step edge, which have been shown to be considerably (0.112 eV) more stable than simple zigzag chains (0.31 eV).[32] These hexagonal rings on Pt(533) contain three waters in the upper layer and three in the lower layer in a buckled arrangement, with water alternating along the step edge. In addition to this, the DFT calculations by Koper et al.[32] show that the water along the step edge of the isolated buckled hexagonal ring prefers to have a single water orientated H-down over the step, with water on the adjacent terrace in the upper layer (directly opposite) having a double acceptor geometry, leaving it pointing H-up. The other water in the upper layer along the terrace sits flat on the terrace, allowing it to adopt either in a single or double donor arrangement, and ensuring it sits below the H-up water. This is highly similar to the arrangement of water proposed along the step edge in this chapter (fig. 7a), providing supporting evidence not only for a buckled hexagonal arrangement of water, but also for the buckled arrangement of water along the step edge. Since both of these substrate surfaces mentioned above exhibit similar step symmetry and reactivity, this strongly suggests that the trimer and zigzag chains observed in our STM data are composed of bucked hexagonal rings of water. However, due to the terrace spacing on Pt(211) being 1 atom smaller than Pt(533), these hexagonal rings on Pt(211) will extend very close to the next Pt step. These results above provide evidence for structures that are more complex than the simple 1D hydrogen bonded chains suggested in previous literature.[24, 25]

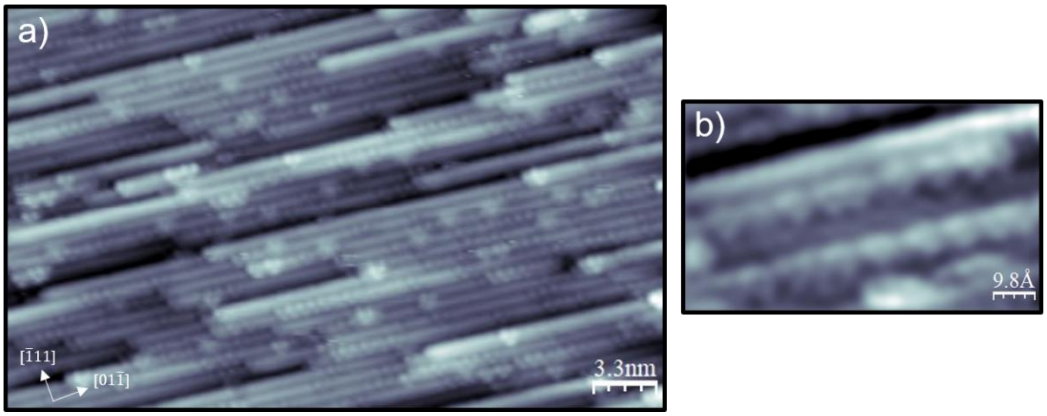

Figure 9. a) Water adsorption at 77K on the Pt(211) surface after surface annealing to 140 K, showing low coverage water chains. b) Water adsorption at 77K on the Pt(211) surface after surface annealing to 160 K, showing low coverage water chains 160 K.

When we increase the coverage, we still see some of the large pseudo 1D linear structures growing along the step edge (fig. 9a and b), but with no regular repeat on adjacent steps. These linear zigzag chains in figure 9 and 6c, show chains that are ca. 14 Pt atoms in length, which implies that there is relatively long range order along the step. This suggests water has a strong propensity to form pseudo 1D linear zigzag structures over bridging across adjacent steps. This behaviour is unlike other stepped surfaces, such as Cu(511), which form chains that are four atoms in length at low coverage, and two at high coverage, forming a 2D network.[18]

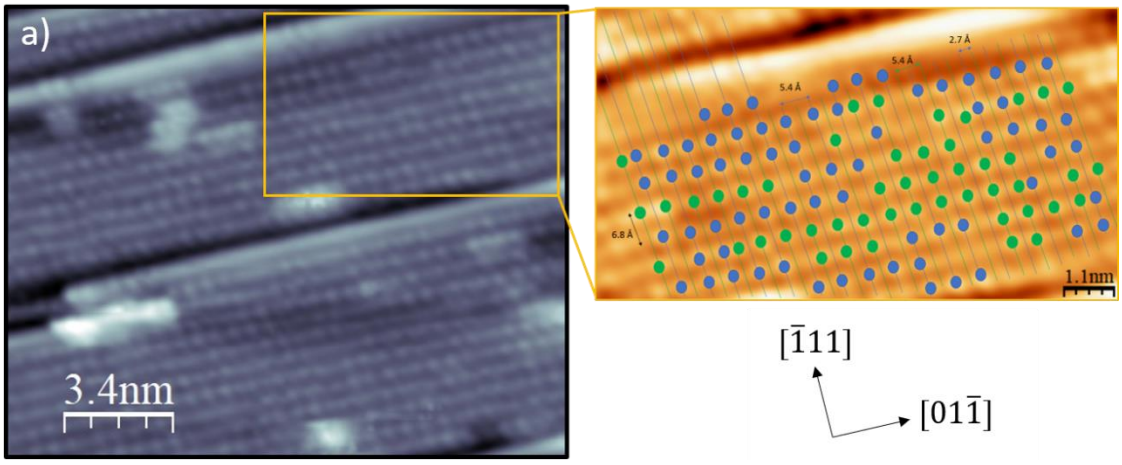

Figure 10. a) STM image that was obtained by annealing a coverage close to the saturation to 160 K. b) is taken from a region in figure a), highlighted by the orange box, which shows all the bright (2x1) features that are in phase with one another in the [$\bar{1}$11] direction in green and blue.

Increasing the coverage further, we observe water covering the surface with a network of bright linear features that contain a 6.8 Å separation in the [$\bar{1}$11] direction (corresponding to the step spacing), and 5.4 Å in the [01$\bar{1}$] direction (fig. 10). The regular (2x1) rows contain a two times

periodicity along the steps and show regions that are in phase, or out of phase along adjacent steps, as indicated in figure 10 (highlighted in green and blue). Many of these regular bright features extend across ca. 30 Å in the $[01\bar{1}]$ direction before the linear features end or change phase, which is considerably greater than the number of linear features in phase along the $[\bar{1}11]$ direction. This suggests that the order between adjacent steps is rather weak compared to the $[01\bar{1}]$ direction, which indicates that stronger bonds are forming along the steps. Not only this, but the fact that many of these (2x1) structures on adjacent steps are not in registry, suggests that these linear features are not joined by hydrogen bonds directly to the neighbouring steps.

Although we can no longer see structure in between adjacent steps, there is no reason to believe that the water that was previously mentioned has disappeared. One possible reason why we are only seeing water along the step edge, maybe because we have water along every adjacent step, which shadows any water sitting on the terrace. In contrast, at lower coverage (fig. 6), this is not the case, showing water not only along the step edge, but also along the terrace. Assuming this is true, figure 10 shows many chains that are out of phase with one another, showing a weak propensity to form a well-ordered network, and a greater propensity to form linear 1D chains. This is evident in LEED, showing a clear two unit repeat in the $[01\bar{1}]$ direction, with streaking appearing in the $[\bar{1}11]$ direction as the coverage increases from 0.5 to 0.7 ML (fig. 5), caused by a lack of order. In spite of this, it is possible linkage across adjacent steps may be a result of the waters pointing down over the step forming hydrogen bonds onto the adjacent terrace. However, we observe no clear evidence to support a strong propensity for this to occur along adjacent steps, since there is a high degree of disorder in the chains in the $[\bar{1}11]$ direction.

Our evidence leads us to suggest that the structures observed above, cannot accommodate the growth of water along the $[\bar{1}11]$ direction, showing a stronger propensity to form long linear 1D chains along the step, and therefore preventing the growth of an ordered 2D network. This behaviour is unlike other stepped surfaces, such as Cu(511), which forms chains along the step edge that are four atoms in length at low coverage, and two at high coverage, ideal for water to bridge across steps regularly into a 2D network.[18] This is likely because Pt binds water more strongly at the step edge, forming chains of water considerably longer on Pt(211), compared to Cu(511). This stronger binding interaction along the Pt step edge compensates the lack of H-bonding in the $[\bar{1}11]$ direction, which explains why we see water favouring the growth of 1D chains over the growth of a 2D network, despite having a similar terrace spacing to Cu(511). This type of behaviour is also observed on Ni(110), with 1D chains being driven by the short

lattice repeat and strong Ni-water bonds, which hinder the formation of a 2D network and favours the formation of linear chains.[34] Not only this but the slightly larger terrace spacing of 0.2 Å on Pt(211) compared to that on Cu(511), may hinder the water bridging across the steps, due to the hydrogen bonds having to stretch more in the $[\bar{1}11]$ direction on Pt(211). This therefore displays how the strength of the binding interactions can influence the structures along metal steps, even though both surfaces exhibit terraces with similar spacings and similar step symmetries.

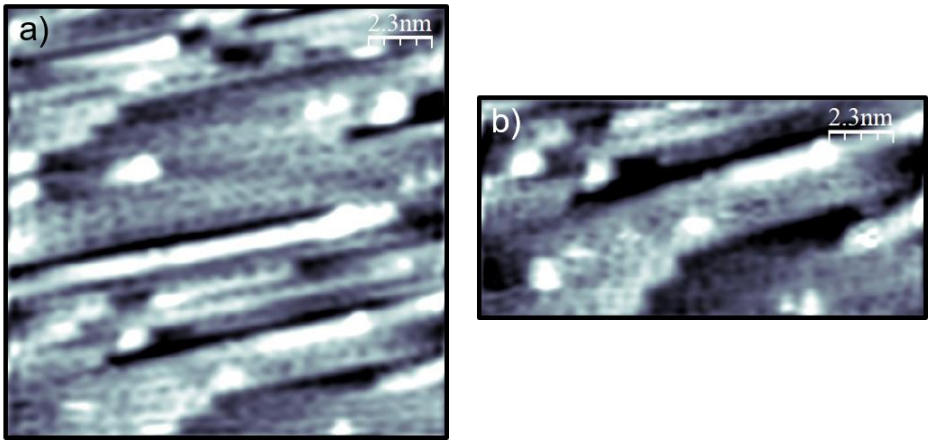

Figure 11. a) An STM image showing a 2D wetting layer just above saturation of the layer on Pt(211), which was annealed to 160 K on the Pt(211) surface. b) close up of the bottom of figure a).

Saturation of the Pt(211) surface with water occurs just above 1.0 ML (relative to the monolayer on Cu(511)), results in a 2D network of water which has lost much of its registry along adjacent steps, revealing a rather disordered system composed of rings (fig. 11). This system has now lost much of its order, which is caused by the surface structure compressing to allow further water to bind to the surface. This is evident in our TPD data, showing the leading edge in figure 4b shifting lower just above the saturation layer (1.10 ML) compared to the layers below a layer, which indicates that the surface structure is less stable. Although Pt(211) contains the same number of atoms along the terrace as Cu(511), it has 10-20% more water per unit cell, rather than two per unit cell seen on Cu. STM shows that water on Pt(211) does not conform to the same level of order as the structures seen on Cu(511), which forms a well-defined hexagonal network with many unit cells in registry with one another.[18] A possible explanation for this is that the terrace spacing on Pt(211) is slightly larger (0.2 Å) than that on Cu(511), which means that hydrogen bonds on Pt(211) are stretched, and less able to form strong linkages between adjacent rows that extend across the whole surface, compared to Cu(511).

6.3.1. Discussion of the structure with previous literature

To summarise, our data shows structures at low coverage that are not simple linear 1D water chains, but structures that are more complex, extending along the $[01\bar{1}]$ direction at the top of the step edge with a larger wider than a simple 1D chain in the $[\bar{1}11]$ direction. The water structures observed in STM image as either individual trimers (fig. 6a), or linear zigzag chains (fig. 6b), both containing bright features with a distance of 5.4 Å apart in the $[01\bar{1}]$ direction and 4.6 Å apart in the $[\bar{1}11]$ direction. These arrangements are probably composed of either, single hexamers for the individual trimers, or linear hexagonal chains for the linear zigzag features, as is illustrated in figure 6e and f. As the coverage increases, we start to see regions where there is two times periodicity along adjacent steps with limited order in the $[\bar{1}11]$ direction. These regions show a surface structure that has little propensity to form a 2D network, forming only small (2x1) regions that are in phase with limited order between adjacent steps (fig. 10). Above the saturation of this structure, water creates a network that has lost much of its registry along adjacent steps, revealing a rather disordered system composed of 2D rings (fig. 11) that show no order in LEED.[36]

Previous literature suggests that single strand 1D chains grow along the step edges of the Pt(211) surface, forming chains that are unlikely to bridge across the (111) steps.[24, 35] As well as this, studies report that water will not be bound on the (111) terraces sites, forming linear structures that cannot be made of rings, or support the growth of a 2D network due to the surface providing a poor anchor for the growth of a hexagonal base.[9, 26] This directly contrasts with the data reported in this chapter, which clearly shows that simple 1D chains do not exist on the Pt(211) surface. The presence of simple chains would result in water only adsorbing to half the number of exposed Pt atoms along each of the terraces, and the layer saturating the surface with a very low-density of water. Although this is possible, our TPD results show otherwise (fig. 4), finding that water saturates the surface with a water density similar to that on Cu(511) (0.67 water per Cu surface atom). The surface layer on the Cu(511) surface is composed of a high density of water, with water not only bound on weak (100) terrace sites, but also tightly along the step edges to form a buckled hexagonal network across the three atom wide terraces.[18] Since Pt(211) also has a similar size terrace spacing (fig. 3c), and TPD points to the fact that the surface saturates with a similar or slightly greater water density, compared to Cu(511), it is clear that the water structure that saturates this surface is also likely to be a 2D network.

We find further evidence that conflicts with previous literature studies in our STM data (fig. 6 and 8), with structures showing clear evidence that a more complex structure must be present on this surface, most likely rings. This is supported by TPD data, mentioned above, which suggests that the density of the pseudo 1D chains must be much greater than the simple 1D chains reported by Endo et al.[24] Further analysis of these more complex chains, leads us to believe that these structures are in fact composed of pseudo 1D zigzag chains that form hexagonal rings on the terrace, forming small networks on adjacent step with coverage. An explanation for this, arises from water along the steps stabilising the water molecules adsorbed along the (111) terrace sites, which enables a water structure to grow along the neighbouring row. This type of behaviour has been reported previously on Cu(511), with water-OH groups pointing down next to the Cu step, stabilising the less favourable waters on the (100) terrace sites below. The stability of the step sites, combined with increasing the hydrogen coordination along the terraces, is sufficient to support bridging across the step.[18] This is a feasible explanation for Pt(211) also, with data pointing to the fact that hexagonal rings grow along the Pt terraces, forming short range 2D networks at higher coverage with an average H-bond coordination number greater than two.

Badan et al. [9, 26] proposed that the three-atom wide terraces on Pt(211) would be too narrow to support the binding of a 2D structure, particularly the growth of a hexagonal base, due to the (111) terraces sites being unfavourable binding sites for a 2D structure to exist. Our results reject the idea that the terraces are intrinsically too narrow to bind water, with STM and TPD indicating that a higher density structure composed of hexagonal rings grow on the surface, further supporting water bound on the (111) terrace sites. Instead it seems likely that the failure to form an ordered 2D network that extends across the steps is driven by the over-riding preference to bind water at all the step sites on Pt(211), whereas 2D networks that wet the steps all leave vacant step sites unfilled.

6.4. Conclusion

In this chapter, we have investigated the adsorption of water on a stepped Pt(211) surface in the hope of settling the conflicting theories for water's arrangement in previous literature studies. Although only experimental studies have been used in this investigation, local probes, such as STM, have already revealed an exciting insight into the structure of water that forms on the stepped Pt(211) surface.

This investigation concludes that we find no evidence for simple linear 1D chains on the Pt(211) surface, as originally proposed.[9, 24, 25] Instead, our data supports the growth of chains of buckled hexagonal rings that can either be positioned irregularly along the terrace, or in a more ordered continuous hexamer chain along the $[01\bar{1}]$ direction. Furthermore, it is clear that there is much disorder in the growth of water, with STM data showing ordered linear zigzag chains with a regular repeat in the $[01\bar{1}]$ direction being interrupted by the growth of isolated rings of water, or a change in the regular repeat. This behaviour extends out as the surface is covered with water, showing many linear chains out of phase along adjacent steps, with a stronger propensity to form 1D chains over an ordered 2D network. This type of behaviour is intrinsically different to other stepped surfaces, such as Cu(511), which exhibit a similar step spacing to that on Pt(211), and a more ordered hexagonal 2D network.[18] This shows how the binding of water along the step can influence the wetting behaviour, showing that water with a stronger binding energy along the step has a greater propensity to want to form extended 1D chains, much like the behaviour of water reported on Ni(110), disrupting the ability to form a 2D network.[34] We hope that in future work on Pt(211) DFT will reveal more about the behaviour of water, with the aim to learn more about the binding environments and bond geometries that might populate a stepped Pt- PEM fuel cell catalyst.

6.5 References

1. L. Peng and Z. Wei, *Engineering*, 2020, **6**, 653-679.
2. S. Fukuzumi, Y. Yamada and K. D. Karlin, *Electrochimica Acta*, 2012, **82**, 493-511.
3. M. Yue, H. Lambert, E. Pahon, R. Roche, S. Jemei and D. Hissel, *Renewable and Sustainable Energy Reviews*, 2021, **146**, 111180.
4. S. S. Penner, *Energy*, 2006, **31**, 33-43.
5. P. Chen and M. Zhu, *Materials Today*, 2008, **11**, 36-43.
6. M. T. Y. Paul, M. S. Saha, W. L. Qi, J. Stumper and B. D. Gates, *International Journal of Hydrogen Energy*, 2020, **45**, 1304-1312.
7. A. B. Laursen, A. S. Varela, F. Dionigi, H. Fanchiu, C. Miller, O. L. Trinhammer, J. Rossmeisl and S. Dahl, *Journal of Chemical Education*, 2012, **89**, 1595-1599.
8. M. D. Wodrich, B. Sawatlon, M. Busch and C. Corminboeuf, *Accounts of Chemical Research*, 2021, **54**, 1107-1117.
9. C. Badan, M. T. M. Koper and L. B. F. Juurlink, *The Journal of Physical Chemistry C*, 2015, **119**, 13551-13560.

10. G. Luna-Sandoval, G. Urriolagoitia-C, L. H. Hernandez, G. Urriolagoitia-S and E. Jimenez, *Imperial College*, 2011.
11. P. Quaino, F. Juarez, E. Santos and W. Schmickler, *Beilstein Journal of Nanotechnology*, 2014, **5**, 846 - 854.
12. A. R. Zeradjanin, A. Vimalanandan, G. Polymeros, A. A. Topalov, K. J. J. Mayrhofer and M. Rohwerder, *Physical Chemistry Chemical Physics*, 2017, **19**, 17019-17027.
13. N. Gerrard, C. Gattinoni, F. McBride, A. Michaelides and A. Hodgson, *Journal of the American Chemical Society*, 2019, **141**, 8599-8607.
14. S. Nie, P. J. Feibelman, N. C. Bartelt and K. Thürmer, *Physical Review Letters*, 2010, **105**, 026102.
15. A. Glebov, A. P. Graham, A. Menzel and J. P. Toennies, *The Journal of Chemical Physics*, 1997, **106**, 9382-9385.
16. S. Haq, J. Harnett and A. Hodgson, *Surface Science*, 2002, **505**, 171-182.
17. S. Standop, A. Redinger, M. Morgenstern, T. Michely and C. Busse, *Physical Review B*, 2010, **82**, 161412.
18. C. Lin, G. Corem, O. Godsi, G. Alexandrowicz, G. R. Darling and A. Hodgson, *Journal of the American Chemical Society*, 2018, **140**, 15804-15811.
19. M. Morgenstern, J. Muller, T. Michely and G. Comsa, *Zeitschrift Fur Physikalische Chemie-International Journal of Research in Physical Chemistry & Chemical Physics*, 1997, **198**, 43-72.
20. A. Picolin, C. Busse, A. Redinger, M. Morgenstern and T. Michely, *The Journal of Physical Chemistry C*, 2009, **113**, 691-697.
21. G. A. Kimmel, N. G. Petrik, Z. Dohnálek and B. D. Kay, *The Journal of Chemical Physics*, 2007, **126**, 114702.
22. G. A. Kimmel, N. G. Petrik, Z. Dohnálek and B. D. Kay, *Physical Review Letters*, 2005, **95**, 166102.
23. M. Morgenstern, T. Michely and G. Comsa, *Physical Review Letters*, 1996, **77**, 703-706.
24. O. Endo, M. Nakamura, R. Sumii and K. Amemiya, *The Journal of Physical Chemistry C*, 2012, **116**, 13980-13984.
25. R. Peköz and D. Donadio, *The Journal of Physical Chemistry C*, 2017, **121**, 16783-16791.
26. C. Badan, Y. Heyrich, M. T. M. Koper and L. B. F. Juurlink, *The Journal of Physical Chemistry Letters*, 2016, **7**, 1682-1685.

27. M. L. Grecea, E. H. G. Backus, B. Riedmüller, A. Eichler, A. W. Kleyn and M. Bonn, *The Journal of Physical Chemistry B*, 2004, **108**, 12575-12582.
28. D. C. Skelton, R. G. Tobin, G. B. Fisher, D. K. Lambert and C. L. DiMaggio, *Journal of Physical Chemistry B*, 2000, **104**, 548-553.
29. T. K. Ghanty, V. N. Staroverov, P. R. Koren and E. R. Davidson, *Journal of the American Chemical Society*, 2000, **122**, 1210-1214.
30. I. Ignatov and O. V. Mosin, *Journal of Medicine, Physiology and Biophysics*, 2014, **4**, 58-80.
31. N. Nagatsuka, N. Shibata, T. Muratani and K. Watanabe, *The Journal of Physical Chemistry Letters*, 2022, **13**, 7660-7666.
32. M. J. Kolb, J. Wermink, F. Calle-Vallejo, L. B. F. Juurlink and M. T. M. Koper, *Physical Chemistry Chemical Physics*, 2016, **18 5**, 3416-3422.
33. K. Morgenstern and J. Nieminen, *Physical Review Letters*, 2002, **88**, 066102.
34. N. Gerrard, K. Mistry, G. R. Darling and A. Hodgson, *The Journal of Physical Chemistry C*, 2020, **124**, 23815-23822.
35. D. Donadio, L. M. Ghiringhelli and L. Delle Site, *Journal of the American Chemical Society*, 2012, **134**, 19217-19222.
36. K. Mistry, N. Gerrard and A. Hodgson, *The Journal of Physical Chemistry C*, 2023, **127**, 4741-4748.

Chapter 7

An investigation into the Structure of Water on an Oxygen Pre-covered Cu(511) Surface

7.1. Introduction

Before the reports by Lin et al.[1] there was little structural information that discussed the interactions of water on a stepped Cu surface, with the report showing that water forms a buckled hexagonal layer on a corrugated Cu(511) surface, similar to bulk ice, I_h. This finding showed that the interactions of water at steps, which has been neglected for the past few decades in many studies, showed greater potential to grow an ice-like layer than many, if not all, the other planar metal surfaces reported previously.[2-5] Moreover, despite the presence of steps it was further found that the corrugated surface did not dissociate water, which directly contrasts the predictions in many theoretical studies that show that the presence of steps will induce dissociation by lowering the activation energy barrier.[6-8] Instead, this stepped Cu(511) surface showed that the dissociation energy barrier is higher than anticipated, suggesting that there is much more to to be learned about how water interacts on this stepped surface. This surface is also considered a better model for the kind of step arrays that might populate ordered regions on a real Cu catalyst particle. In view of the above, we have chosen to investigate whether the presence of oxygen will induce the dissociation process and to discover if the structures formed will mimic those found other Cu surfaces,[2, 5] or form different structures due to the unpredictable behaviour of water on this surface.

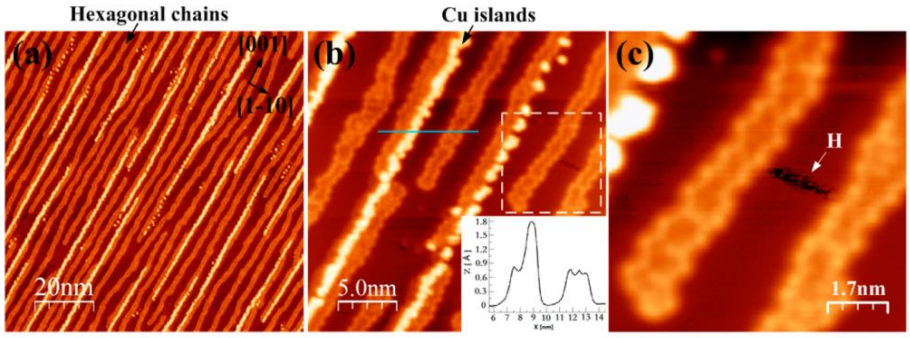

Figure 1. STM image of water and oxygen, after water was dosed on an (0.12 ML) oxygen pre-covered Cu(110) surface and annealed to 155 K. a-c) Adapted from.[2]

In order to understand whether water will form similar structure to those observed previously, it is useful to first understand the interaction between water and oxygen on a more planar surface, such as Cu(110). Previous studies investigating the reaction of oxygen and water on a flat Cu(110) surface have found that water forms hexagonal chains with the occasional defect ring structures at 155 K using a low coverage of water and 0.12 layers of oxygen (fig. 1). Increasing the coverage of water resulted in the structure forming a more ordered c(2x2) hexagonal network, which was reported by Forster et al.[9] as described in chapter 5.

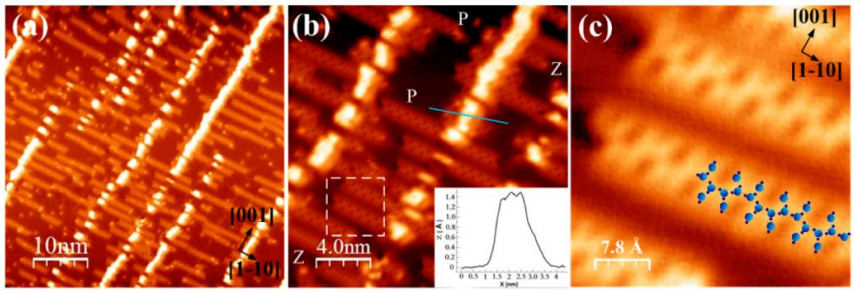

Figure 2. STM images of water on an oxygen pre-covered Cu(110) surface that has been annealed to 180 K. Adapted from.[2]

Heating the surface to 180 K resulted in conversion of the hexagonal chains/c(2x2) network, leaving behind linear ordered water-OH chains that aligned down the [110] direction (fig. 2). These chains are composed of a molecular water backbone that have branched hydroxyl pointing out alternate sides in the [001] direction with a two unit repeat. The alternating arrangement of hydroxyl on either side of the water backbone created two types of chains, P and Z (fig. 2b) with a stoichiometric amount of water and hydroxyl (1:1), further description of the chains can be found in chapter 4. This was supported by the DFT calculations, which also showed that the presence of OH stabilised the structure, pinning the water along the centre of the chain.[9]

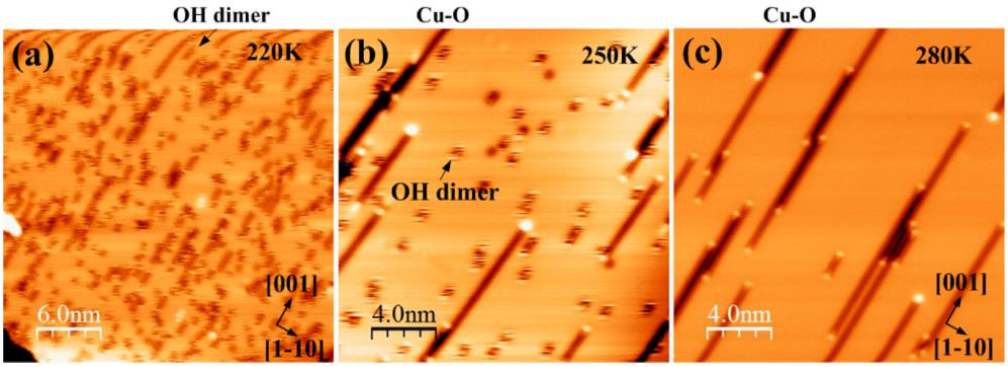

Figure 3. STM images of showing the gradual change in surface structure as water is heated on the oxygen pre-covered Cu(110) surface. a) 220 K. b) 250 K. c) 280 K. Adapted from. [2]

Annealing the surface to 220 K resulted in the decomposition of the previous phase, revealing many dark surface rows with sharp bright dashed features, caused by OH groups with the oxygen switching orientation along the [100] direction, a process trigged by the STM tip (fig. 3a and b). The dark rows that run along the [001] direction can be attributed to Cu-O chains, caused by a disproportionation reaction i.e. $2OH_{(ads)} \rightarrow O_{(ads)} + H_2O_{(g)}$. This was supported by the Cu-O chains increasing in size in the [001] direction as the temperature increased to 250 K (fig. 3b), converting more of the OH into Cu-O chains (fig. 3c). Having established the interactions between oxygen and water on a planar Cu(110) surface, we will now discuss the adsorption of water on a stepped Cu(511) surface to understand water's structure before the influence of oxygen co-adsorbate.

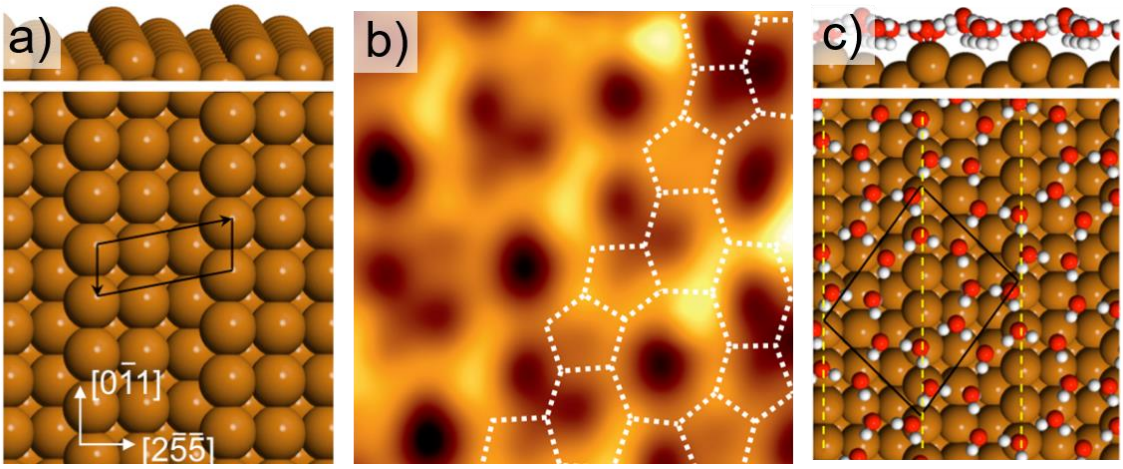

Figure 4. a) Simulation of the Cu(511) surface with the unit cell highlighted in black. b) An STM image illustrating the 2D network of ring structures of water on the Cu(511) surface at 0.83 ML. c) A model of the 2D network for the low coverage structures. Adapted from.[1]

The corrugated Cu(511) surface provides an ideal environment to mimic a typical rough surface, consisting of ordered terraces that are three atoms (6.6 Å) wide, which creates a whole array of hydrophobic and hydrophilic sites, similar to that of a rough surface that might be found on Cu catalysts (fig. 4a). The first wetting layer binds water tightly to the low coordinate step sites and more weakly to the terraces, forming an intact water network with an array of octamer, hexamer and pentamer rings. Each of the water molecules in this network forms three hydrogen bonds, with half of the water molecules orientated planar to the surface and donating two protons to the neighbour, and the other half orientated H-down and donating a single proton (fig. 4c). Theoretical calculations for this arrangement show that this structure is stabilised by having four water molecules bound flat on the Cu step sites, pointing out over the step and

perpendicular to the step dipole, which allows for H-bonds to form below the step to the three waters that have their free OH groups aligned H-down next to the Cu step (fig. 4c).[1]

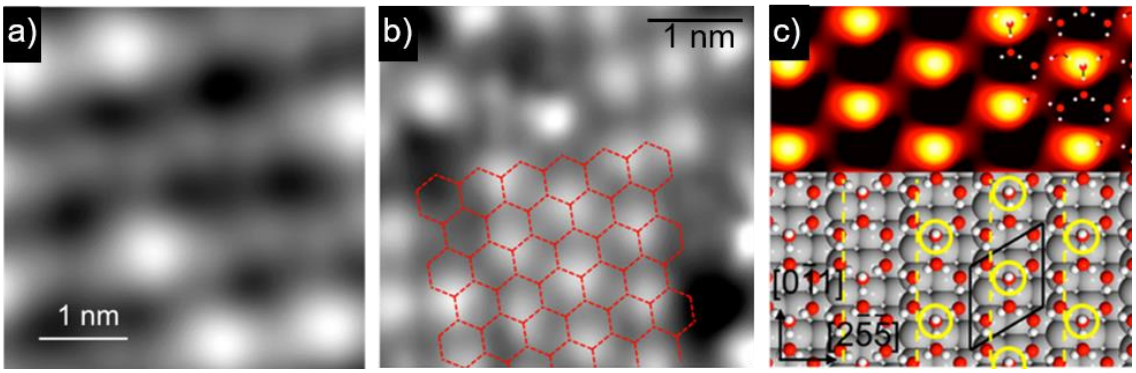

Figure. 5. An STM image of a single layer of water on the Cu(511) surface, showing the formation of a hexagonal network. a) close up. b) with a hexagonal overlayer. c) DFT simulated of the formation of the hexagonal arrangement of water with an STM image above that was achieved by increasing the tunnelling current to bring the tip close to the surface. The yellow circles highlight the positions of the H-up water in the hexagonal arrangement that cause the bright features in STM. Adapted from.[1]

Further increasing the coverage close to saturation resulted in the layer relaxing into a hexagonal 'ice-like' arrangement. To release any strain caused by the compression induced by the additional water molecules, the structure buckles to form a hexagonal network that is ideal for commensurate growth.[10] This buckled hexagonal layer consists of two waters molecules that are bond flat in a double donor arrangement on the atop Cu sites and are separated by a vacant Cu site along the step, with the final four water molecules on the terrace completing the network by bonding as double donor and three single donors. There is only a single uncoordinated hydrogen in this arrangement that points away from the surface (highlighted in yellow), which results in the STM images and the simulation image above (fig. 5).

These intact water structures on Cu(511) are much different to the intact water structures found on other on Cu surfaces, particularly Cu(110), which forms intact water pentamer chains that run along the [110] direction. This suggest that if water were to react with oxygen to form water/OH structures on Cu(511), the structures formed may also be different to those found previously on Cu(110). In addition, as the surface is heated, water dissociation does not spontaneously occur on a clean Cu(511) surface, further suggesting that the surface is more similar to the behaviour of water on a terrace which does not dissociate water. This, therefore, questions our understanding of steps, and whether an ordered stepped surface interacts differently to a disordered stepped surface with more kink and defect sites. Since little is known about how water interacts on an ordered stepped surface, and the activation energy for water

dissociation on Cu(511) has been found to be high, we have chosen to investigate whether the dissociation process can be activated using oxygen. This will provide a better understanding for how water on ordered regions on stepped Cu surface may behave, which further serves as a direct comparison to the structures formed on disordered regions of a stepped Cu(110) surface (chapter 5), and on the flat Cu(110) surface mentioned above. Low temperature STM, TPD, LEED and DFT was used to explore the structure and interactions of water on an oxygen pre-covered Cu(511) surface, with results providing evidence that the dissociation process can be activated by oxygen.

7.2. Experimental

The Cu(511) surface was prepared by repeat cycles of cleaning, which involved sputtering the surface with Ar^+ ions for a period of 10 minutes, followed by the surface being annealed to 500 K. An oxygen pre-covered surface was achieved by increasing the ambient pressure of oxygen at 300 K until various coverages of oxygen were adsorbed to the surface. All LEED experiments used low current channel plates to prevent dissociation caused by electrons fired at the surface. All of the water and oxygen exposures were quantified by STM, which defined a single layer of water/oxygen completely covering the surface. All of the water films grown in the neighbouring chamber were quantified using molecular beam calibrations that were based on the water absorption on the Cu(511) surface, which is discuissed in chapter 2. This enabled a single layer dose (1 layer of water) to be defined as 0.67 water/oxygen per Cu surface atom, which was based on the wetting of the first layer hexagonal structure on Cu(511). The sticking probability of oxygen was considered in these calibrations, which enabled us to dose equal quantities of oxygen and water down on the Cu(511) surface. However, we note that this was only used to estimate the coverage of water and oxygen on the Cu(511) surface, which allowed us to form comparisons with a known 2D wetting layer.

7.3. Results and discussion

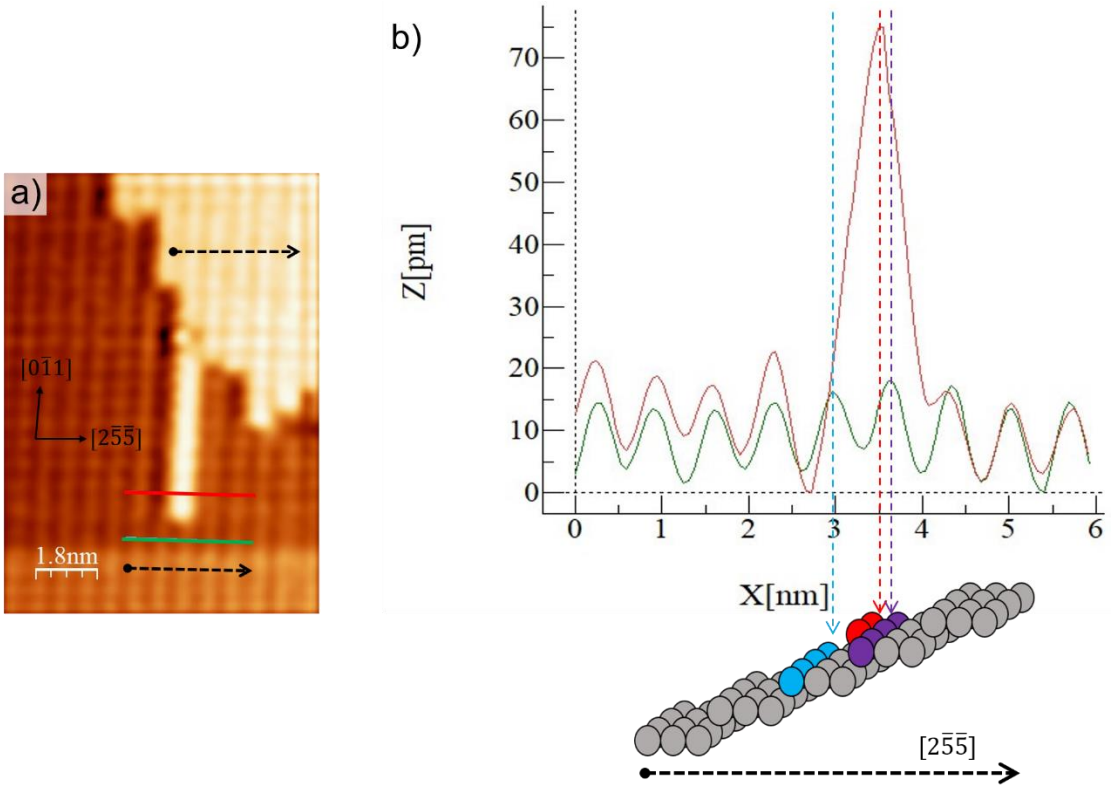

Figure 6. a) STM image showing regularly spaced rows of Cu atoms filling each of the terraces, with the step direction highlighted in a black dash, and two line profiles highlighted in green and red. b) Shows two merged line profiles that were taken from figure a), illustrating the position of the addition Pt row on the Cu(511) surface.

Investigating the position of additional bright rows of Cu protruding from the edge of terraces on the Cu(511) surface enabled us to determine the step direction of the surface. This is because any additional Cu rows will always choose to sit in the highest coordination sites, for example, chain sites below the Cu step edges will have a coordination number of seven, compared to six atop the step edge, resulting in the additional row sitting below the step with the higher coordination stabilising the additional Cu rows. This can be observed in STM images (fig. 6a), by placing line profiles across terraces with an additional row (highlighted in red), and comparing it with the line profile of the neighbouring rows without the additional Pt row (highlighted in red). The merging of both line profiles shows that the additional row sits closer to the first step, highlighted in purple, than the second step, highlighted in blue (fig. 6b). This therefore shows that the topmost layer decreases with each step edge, facing along the line in the $[2\bar{5}\bar{5}]$ direction highlighted by a black dashed arrow (fig. 6)

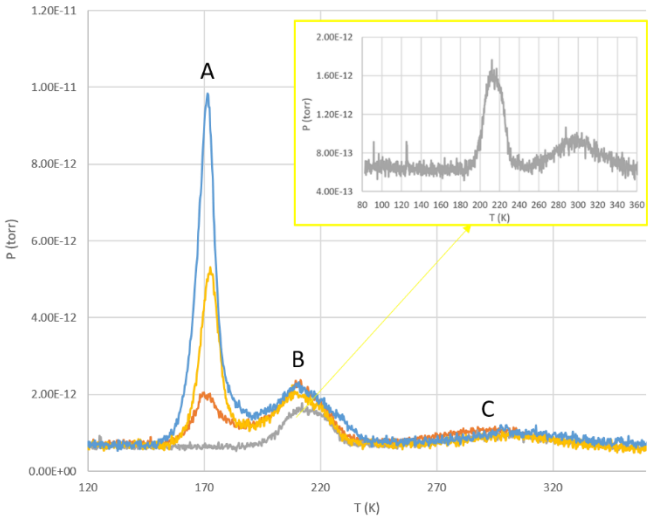

colour	Water (H_2O)	Oxygen (O)	ratio
	0.4 layers	0.1 layers	4:1
	0.3 layers	0.1 layers	3:1
	0.2 layers	0.1 layers	2:1
	0.1 layers	0.1 layers	1:1

Figure 7. TPD spectra showing a gradual increase of water dose with a fixed coverage of oxygen on the oxygen pre-covered Cu(511) surface, with the smallest TPD peak highlighted in yellow to show the relative size of peak C compared to peak B. The table shows the O coverage estimated by extrapolating the O_2 dose from the pressure of the gas, compensating for the relative effusion rate of O_2 compared to water and assuming all the O_2 adsorbs and dissociates.

The coverage of water was increased in 0.1 layer increments on the oxygen pre-covered Cu(511) surface until there was approximately four times as much water to oxygen on the surface. This allowed us to understand the oxygen dependence of the structures that formed and the relative ratio of O:H_2O that would be present on the surface, assuming water does not dissociate when heated on a clean Cu(511) surface,[10] as seen in chapter 2, but all the O reacts. Heating various coverages of water on an oxygen pre-treated Cu(511) surface lead to the formation of three characteristic peaks, A (ca. 170 K), B (ca. 200 K) and C (ca. 300 K), as seen in figure 7. The three TPD profiles show the binding energies of different structures as they are heated on the surface, before water is desorbs intact in peak A. Moreover, it is clear that the reaction of water and oxygen has formed OH, as the peak at 300 K is too high in temperature for water to be present. This peak is assigned to the recombination of OH ($OH_{(ads)} + OH_{(ads)} \leftrightarrow H_2O_{(g)} + O_{(ads)}$) at high temperature, which is also observed on Ni(110) and Cu(110).[2, 11] These TPD peaks on Cu(511) lie in a similar temperature regime as those found on flat Cu(110), with studies reporting a (2:1) water/OH c(2x2) hexagonal network at ca. 160 K, (1:1) water/OH 1D chains at ca. 200 K and pure OH phase at ca. 260 K.[9, 12, 13] The latter phase on Cu(110) is 40 K lower than the corresponding peak found on Cu(511), which suggest that OH must bind more strongly Cu(511). This would indicate that the structures formed in each of the phases on Cu(110) may be similar to that on Cu(511), since a comparable amount of thermal energy is required to remove each phase on Cu(110),

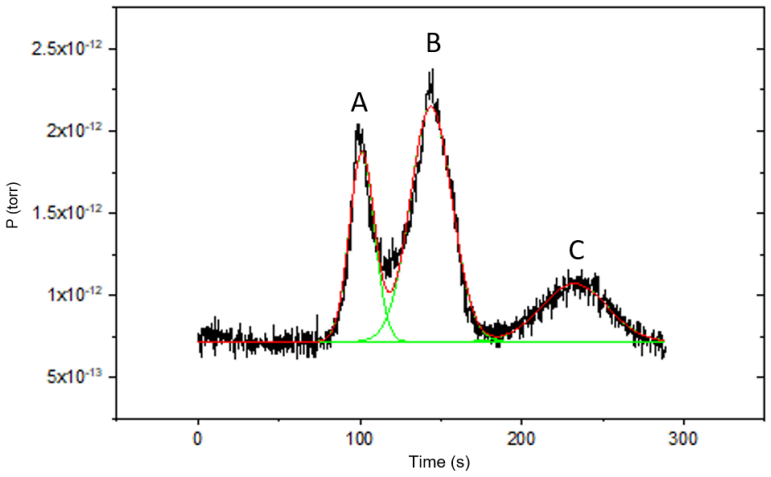

Peak	Integrated area	Integrated percentage (%)
A	2.33E-11	24.4 ± 1.2
B	4.93E-11	49.7 ± 1.8
C	2.47E-11	24.5 ± 2.0

Figure 8. An integrated TPD profile of 0.3 layers of water on 0.1 layers of oxygen on an oxygen pre-treated Cu(511) surface. The table below each TPD spectra shows the total integrated area and percentage, with the percentage errors taken from subtracting different baselines off the spectra. This analysis indicates that the actual ratio of water to O on the surface is 4:1, suggesting an O_2 adsorption and dissociation probability slightly less than the unity assumed to estimate the O coverage in Fig 7.

To further understand whether the composition of the water/OH structures on Cu(511) were similar to the those observed on flat Cu(110), we integrated each of the TPD profiles to calculate the approximate ratio of water desorbed in the latter two phases. These two phases were key, as if the structure at B is the same to the 1:1 water/OH structure on Cu(110) at 200 K, then we would expect the size of peak C (OH phase disproportionation) to be half that of B. This hypothesis is based on the assumption that reaction with O is complete and no water dissociation is occurring during the course of heating the surface from B to C, otherwise, the size of peak C will be much greater as the continued dissociation of water would create a larger OH phase. We note that there is some variability in the values calculated in figure 8 due to the error associated with subtracting the baseline to obtain the integrated areas, however, we took an average of multiple values to create the most accurate results.

We choose the TPD profile highlighted in orange in figure 7, as we wanted to make sure the structure at both phase B and C had formed, excluding any errors associated with there not being enough OH/water for both phases to form. This is one of the reasons why we did not include the grey TPD profile, as the area for peak B is slightly less compared to the other TPD profiles in figure 7. Moreover, this TPD profile in orange was just as peak A started to form, thus peak A will have less influence in the size of peak B compared to the other TPD profiles, which contain greater quantity of water in peak A that causes the peaks to overlap slightly.

The results in figure 8 revealed an approximate 2:1 ratio between the size of peaks B and C, suggesting that for each water that desorbs from phase B, half as much water desorbs from phase C, which is associated with OH disproportionation. These finding supports the idea that the B phase is composed of a structure that is approximately 1:1 water/OH, from which water desorbs as the surface is annealed past the B phase to leave just OH on the surface from the decomposition of the 1:1 water/OH structure. An identical 1:1 water/OH composition is observed on Cu(110) after the reaction of O and water, thus supporting our hypothesis that a similar structure is formed in the B phase on both Cu(511) and Cu(110). Moreover, this behaviour is also very similar to that found on Ni(110), with results in chapter 4 showing a 2:1 ratio between the latter two TPD peaks, and STM analysis concluding that the structure was in fact 1:1 water/OH chains. In contrast, the ratio of A and B is much harder to predict as there is a significant amount of overlap, and the size of peak A continues to increase with coverage, whereas peak C and B do not. This suggest that the structures formed in peak A are more complex, and must be composed of a wetting layer that holds far more water than the other two phases.

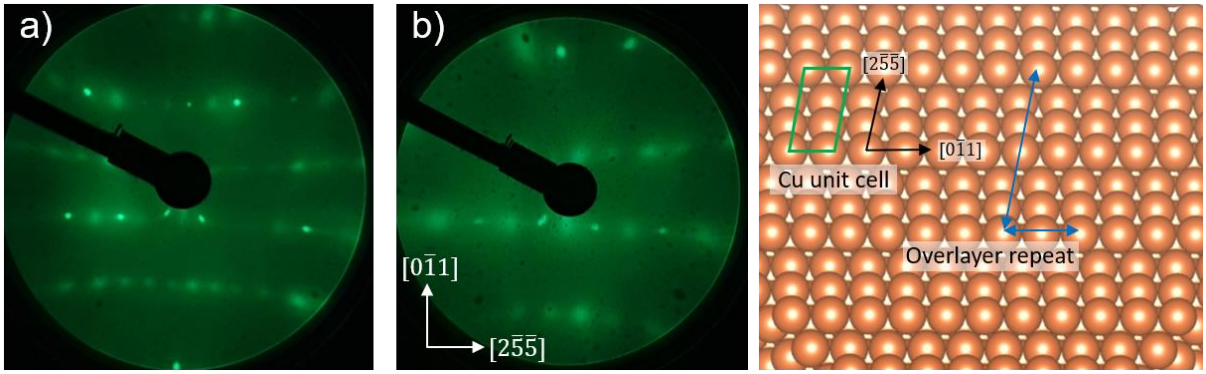

Figure 9. LEED pattern taken after one layer of water was deposited at 100 K on top of a single layer of oxygen on a Cu(511) surface and annealed to 170 K, revealing a (2x2) diffraction pattern. a) 80 eV. b) 63 eV. c) simulated image of the Cu(511) surface showing the unit cell Cu unit cell in green and the overlayer repeat found in image a) and b) in blue.

LEED was then used to observe the lateral order of any structures that may be present in the temperature regime of each of the TPD profiles in figure 7. The LEED images revealed a (2x2) diffraction pattern that was stable up to 200 K, prior to the desorption of peak B. The images in figure 9 show half order spots in between the integer order Cu spots in both the $[2\bar{5}\bar{5}]$ and $[0\bar{1}1]$ directions, showing a two unit repeat in both directions, as shown in figure 9c. However, since both images in figure 9 show some diffraction spots for the surface overlayer that are a little diffuse, there may also be some other structure or disordered regions at 170 K. LEED

patterns below 170 K did not produce a clear diffraction pattern, which suggests that there is a lack of order in the surface structure, only forming an ordered arrangement when enough thermal energy is provided at 170 K. Above 200 K, we find that the (2x2) LEED pattern becomes streaked in both directions until there is no clear diffraction pattern, prior to the pure OH phase at 300 K. Previous literature also observes the absence of any diffraction pattern for the pure OH phase on both Ni(110) and Cu(110), which suggested that the pure OH phase on Cu(511) is also disordered.

Further analysis of the coverage dependence of the LEED pattern showed that the diffraction spots in the $[2\bar{5}\bar{5}]$ direction was diffuse below a coverage of 0.6 layers (O + H_2O), which continued to get weaker until the coverage of both oxygen and water fell below 0.3 layers. In contrast, streaking was only apparent in the $[0\bar{1}1]$ direction as the coverage of oxygen and water fell below 0.3 layers, which suggest that the two times repeat in the $[2\bar{5}\bar{5}]$ direction is more coverage dependant compared to the $[0\bar{1}1]$ direction. This is similar to the corresponding phase on Ni(110), with 1:1 water/OH linear structures showing a regular repeat at higher coverage as the structures are forced closer together, and not at low coverage due to the structures preferring to maximise their separation distance.

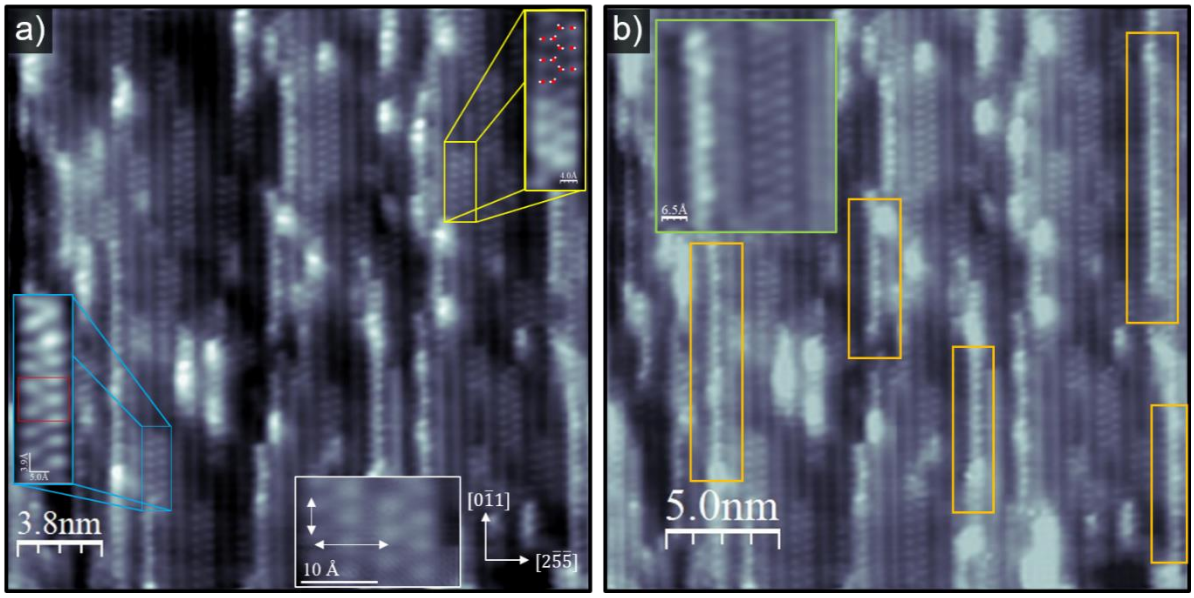

Figure 10 a) An STM image of partially dissociated water structures formed on the Cu(511) surface after annealing to 160 K, showing 1D branched chain structures. The region highlighted in yellow is a close up section of an ordered 1D chain on the Cu(511) surface, with a model of the water/OH overlayer. The section highlighted in blue shows the same 1D structure to that highlighted in yellow, but with defect features, showing an irregular repeat highlighted in red, forming a slight larger spacing in the [0$\bar{1}$1] direction at one point along the chain. The section highlighted in white shows chains with a two unit repeat in both the [0$\bar{1}$1] and [2$\bar{5}\bar{5}$] direction. b) shows the same image as a), but highlights an additional structure that is narrower than the 1D chains highlighted in a), with a comparison between the two chains highlighted in green.

As water desorption proceeds slowly in peak B at 160 K, we observe the appearance of 1D linear zig-zag chains that run along the close packed [0$\bar{1}$1] direction with a two-unit repeat (fig. 10). Each of the chains that run along the [0$\bar{1}$1] direction show a preference to leave at least one Cu terrace in between each of the chains, which suggest that there is some form of chain-chain repulsion, with the chains maximining their separation distance. However, as the coverage increases and the chains are forced close together, we find that these chains order up, forming a two unit repeat in both the close packed and [2$\bar{5}\bar{5}$] direction (figure 10a, highlighted in white), agreeing with the LEED images in figure 9. Close analysis of the high contrast features shows that the chains to have a ca. 5.1 Å, or two Cu unit spacing in the [0$\bar{1}$1] direction, and a chain width of ca 7.8 Å in the [2$\bar{5}\bar{5}$] direction which is just over the spacing of the terrace width (ca. 6.6 Å). It is noticeable that some of the chains contain an irregular spacing that is roughly three times the Cu spacing along the [0$\bar{1}$1] direction, highlighted in red (fig. 10), occasionally alternating between a two and three unit repeat along the lower step edge (on the left hand side of the chain). Furthermore, the centre of the chain has a lower contrast than either side of the chain, indicative of molecules that are orientated planar to the surface, having a

lower contrast those molecules either side of the chain. This is something that is observed in hexagonal water/OH structures and 1D chains water/OH chains on Ni(110) and Cu(110), with planar water molecules showing a lower contrast to the H-up OH/H_2O molecules.

There is an additional minority structure present on the surface, which is highlighted in orange (fig. 10b), showing a narrower (N)-zig-zag chains that are shorter than a single terrace spacing, measuring ca. 5.5 Å in the $[2\bar{5}\bar{5}]$ direction. This 'N' type zig-zag structure consists of higher contrast features along the right side of the chain with a two unit repeat (ca. 5.1 Å) in the $[0\bar{1}1]$ direction, forming a structure that alternates with high and low contrast features above and below the step. These contrast changes in the structure could possibly due to either the structure bridging above and below the step, or water/OH having a OH bond point up and away from the surface on the right hand side of the chain. This type of chain has not been experimentally observed on Ni(110) or Cu(110) before, and therefore it is less clear as to what is the composition and arrangement of the structure. However, it is likely that this structure is stabilised by the presence of OH molecules as a pure water chain would not be stable up to 200 K, since water desorbs on a clean Cu(511) surface at ca. 160 K. Although the chain in figure 10b has not been experimentally observed on other surfaces, similar narrow zig-zag chains have been predicted to be stable on flat Cu(110) using DFT, showing water/OH filling two Cu rows along the close packed direction with a two unit repeat.[9] Although this DFT structure was not observed in STM on flat Cu(110), they may be formed here, but with a different orientation and composition of water and OH.

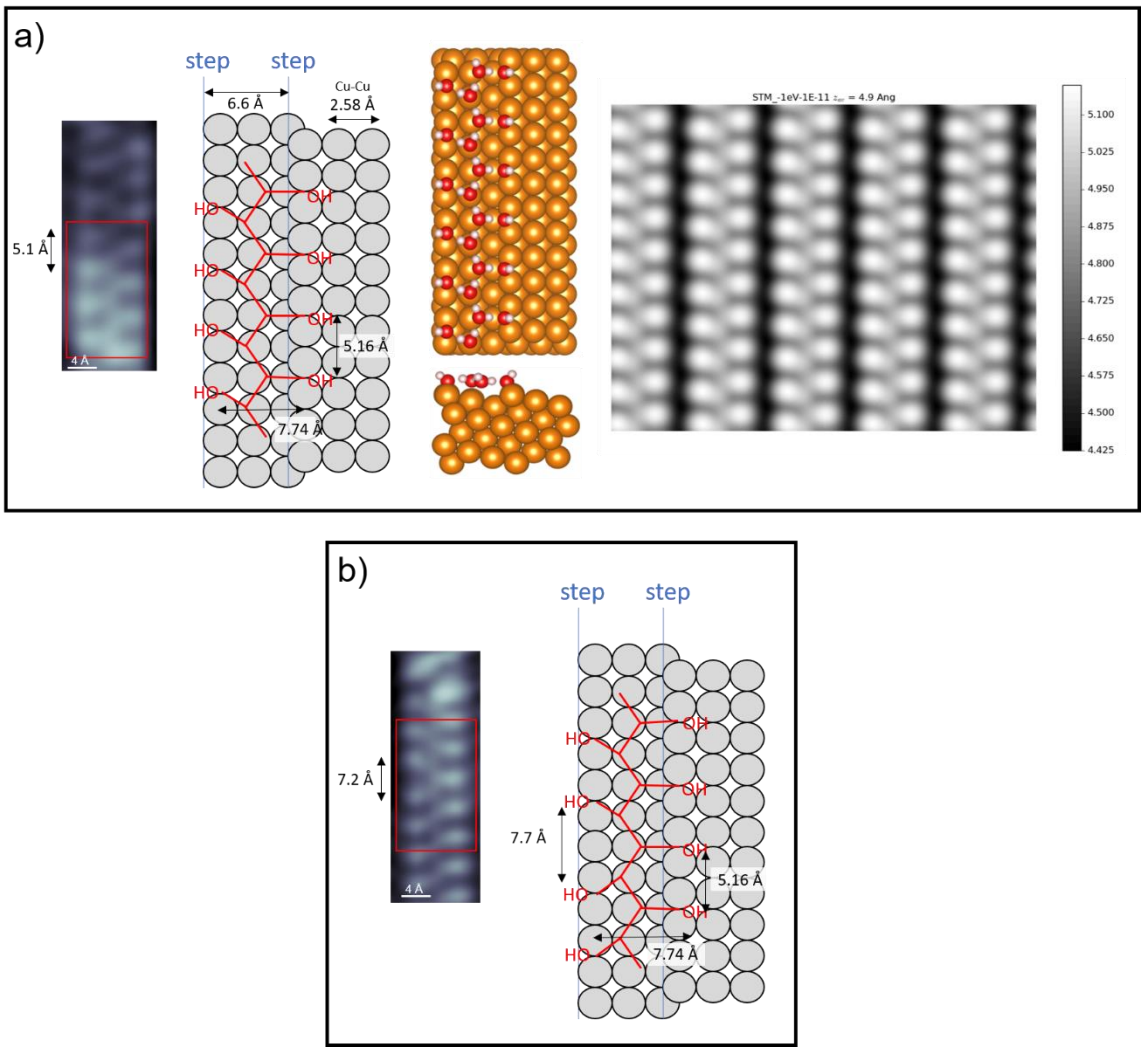

Figure 11. Shows an STM image with a schematic showing the position of the OH molecules either side of the zigzag chain, with the corresponding section taken from STM image highlighted in red. a) with an additional DFT simulation showing the position of water/OH on the Cu(511) surface and simulated STM image of the most stable structure.[14] b) the same zig-zag chain as a), but with a change in phase of OH on the lower step, causing a unit defect spacing, as seen in STM (fig. 10).

The structure imaged in figure 10a was investigated by Snowden[14] using DFT to find the most stable surface arrangement and test our hypothesis of the structure mentioned above. This resulted in the structure and simulations shown in figure 11a, which consisted of an intact water backbone with OH filling alternate Cu bridge sites along two Cu step edges in the close packed direction. The OH molecules sit in the Cu bridge sites, orientated slightly H up away from the surface compared to the intact water chain and have a two unit repeat, which was apparent in STM, causing the brighter features along either side of the chain (fig. 11a). Furthermore, the calculation shown in figure 11a uses the same two unit repeat in the $[0\bar{1}1]$ direction and produces a similar simulated STM image as the experimental image observed in STM (fig 11a). DFT stability calculations for the binding energy of the structure in figure 11a reveals a binding

energy of -0.86 eV/molecule, which is 0.1 eV/molecule more stable compared to all other structures calculated. It is clear that the structure highlighted in figure 11a matches very closely with those 1:1 water/OH 1D structures found on Cu(110) and Ni(110).[9, 11] Therefore, this shows that although the surface conditions have changed from flat on Cu(110) to stepped on Cu(511) surface, the 1:1 water/OH chains are able to accommodate the change in surface conditions so as to form a similar, stable hydrogen bonded structure.

The schematic structure shown in figure 11b matches closely with the STM image, showing an alternating 1:1 water/OH chain with an occasional ca. 3 unit repeat that is caused by the displacement of OH one unit along in the $[0\bar{1}1]$ direction. This displacement results in OH being positioned in the out of phase Cu bridge site compared to the top of the chain, which creates a slight change in the angle of the water H-bonds along the water chain. Since this behaviour occurs occasionally in STM images, it is plausible to assume that both arrangements have very similar stabilities, creating an occasional defect spacing as the chain alters the phase of OH along the lower step edge. DFT calculations find that this latter arrangement is just 20 meV/O_x less stable that OH having the original phase shown in figure 11a. This behaviour is similar to that shown by the 1D chains on Ni(110) and Cu(110), where the water chain can form either a 2 times or a 4 times zigzag period down a close packed Cu row, with the OH groups decorating either side of the water chains. In the case on the stepped Cu(511) surface, the OH groups along the upper step show a very regular period, but the H-bonding network to water allows some variability in the repeat along the lower step edge, with both of the possible phases observed in the same chain. Future DFT calculations will assess the arrangement and stability of these chains in more detail to provide evidence for the most appropriate structure, further clarifying the behaviour and position of water/OH along the Cu(511) steps sites.

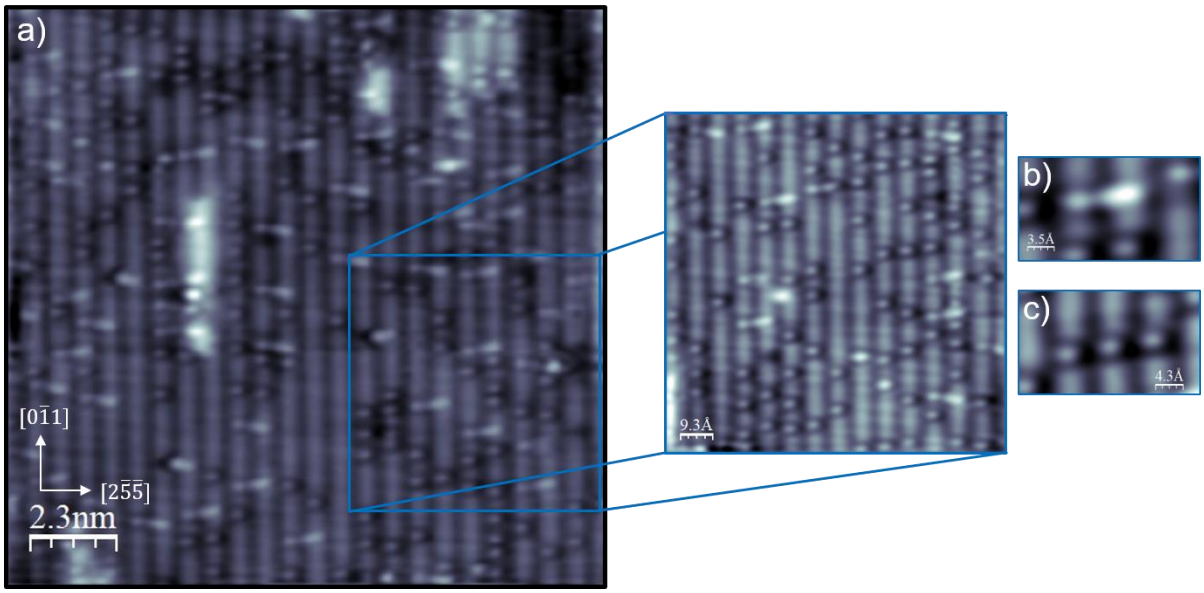

Figure 12. STM image obtained by heating water on an oxygen pre-covered surface to 270 K.

Further heating the surface above 200 K lead to the disappearance of the 1H_2O:1OH 1D chains (fig. 12a), leaving behind a hydroxyl phase that is associated with peak C (fig. 7). The images in figure 12b and c show a bright feature on one step with an adjacent high contrast streak on the next step and single features for a species that occupies a single Cu step site. Since we only observe the bright step features seen in figure 12c when oxygen is present on the surface, it reasonable to assume that these features represent oxygen atoms formed from either the OH disproportionation process, or by an excess un-reacted oxygen that did not form OH ($O_{(ads)}$ +$H_2O_{(ads)}$ → 2$OH_{(ads)}$). The latter is possible as it is hard to quantify an equal amount of water to react with the surface oxygen in this chamber, resulting in an excess of O being observed in STM images with the presence of OH molecules, something that is not observed on Ni(110), but is on Cu(110).[9, 11] Many of the lone oxygen atoms align in ordered arrangement on neighbouring steps along the [2$\bar{5}\bar{5}$] direction, or the close packed direction with at least a two Cu spacing in between each oxygen atom.

In contrast, the other structure in figure 12b is composed of an individual bright feature on one step with an adjacent high contrast streak in the next step in an 'up step' direction. These features seem most likely caused by a single oxygen that is hydrogen bonded to an OH dimer. This is supported by the fact that a high contrast streak is also present on both Ni(110) and Cu(110), with DFT suggesting that this high contrast streak is caused by the presence of OH molecules that have their hydrogen pointing away from the surface normal. Further analysis of this feature in figure 12b shows that the structure occupies approximately three Cu units (ca. 7.7 Å) in the [2$\bar{5}\bar{5}$] direction, with the high contrast streak occupying an equivalent two Cu

atoms, which supports the presence of a dimer. This also suggest that the dimer must bridge the Cu step, with one OH below the step and the second above the step edge in its favoured Cu bridge site, as mentioned previously. Moreover, since we do not observe a streaked feature on its own, our findings suggest that the OH dimer has a high affinity to be next to an oxygen atom, with oxygen potentially stabilising the dimer.

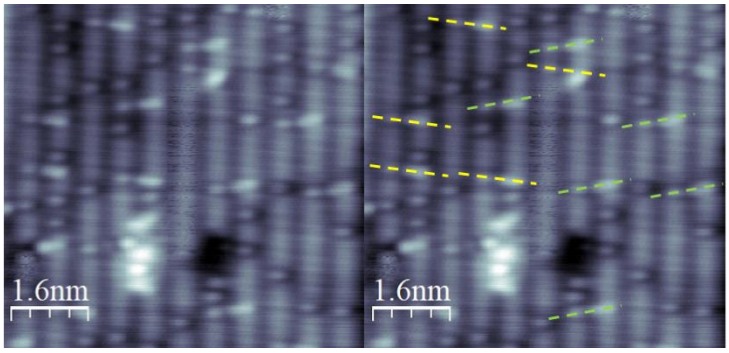

Figure 13. STM image obtained by heating a thin layer of water on an oxygen pre-covered surface at 270 K with copy of the same image showing the two different directions of the structure in yellow and green.

Calculations having established that O and OH adsorbates both prefer to sit in the Cu bridge sites, the image in figure 13 suggests that the OH dimer forms two orientations, with a lone oxygen sitting on an adjacent Cu site parallel to the OH on the neighbouring Cu row. The fact that we do not see these high contrast streaked features on their own, but always next to an oxygen, suggests that the OH dimer is probably hydrogen bonded to the oxygen, providing stability to the dimer. This is supported by TPD for this phase, with the corresponding phase on flat Cu(110) being ca. 50 K lower than that on Cu(511), with OH dimers for this corresponding phase on Cu(110) not being stabilised by O. These questions about the stability and structure will be addressed in further DFT calculations to explore the structure associated with the STM images above (fig. 12 and 13).

It is perhaps surprising that we saw no evidence water/OH forms a hexagonal structure associated with peak A, as otherwise the surface structures formed are similar to those structures reported on Cu(110) and Ni(110).[9, 11] Since the surface does form a hexagonal network with intact water, but does not when water is partially dissociated, this may suggest that the lack of hydrogen bond donation by OH may hinder the formation of a well-ordered hexagonal network that can bridge the steps. Instead, we observed disordered clusters of high contrast features with the occasional branched structures. These high contrast features are

typically caused by disordered clusters of water that adsorb on top of one another, which perhaps explains why we observe no clear structure.

Finally, this chapter has shown that the stepped Cu(511) surface, which consists of an ordered array of steps, behaves rather like a flat metal Cu terrace, as opposed to a disordered stepped surface, as dissociation is only activated in the presence of oxygen and the steps are not able to induce the dissociation process. This is evident in chapter 5, whereby the dissociation process is induced without the presence of oxygen on a disordered stepped Cu(110) surface, which contains many kink and defect sites to lower the barrier for dissociation, something that is absent on Cu(511). This, therefore, suggest that the type of step, whether it is ordered or disordered, plays an integral role in the reactivity of a surface, with our findings further indicating that a catalyst particle with a rough and disordered surface will be more reactive to water than an ordered catalyst face.

7.4. Conclusion

In conclusion, TPD analysis showed three characteristic peaks, labelled peak A (170 K), peak B (200 K) and peak C (300 K) for coverages of a single layer of both oxygen and water, with evidence to support the characterisation of 1:1 water/OH structures at peak B and O/OH phase at peak C. LEED analysis of each of these phases revealed only one clear diffraction pattern at 170 K, showing LEED pattern with half order spots in the both the $[0\bar{1}1]$ and $[2\bar{5}\bar{5}]$ positions. Further analysis using STM of each of these phases found 1:1 water/OH 1D zig-zag chains in the temperature regime of peak B, containing a two unit repeat along the close packed direction. This structure mimics the 1:1 water/OH chains observed on both Ni(110) and Cu(110) by accommodating the binding sites to adsorb OH on adjacent steps. This results in a more variable repeat along the lower step edge with OH able to adsorb at either bridge site on the lower Cu step, a conclusion which is supported by DFT calculations which find similar binding energies for the two different structures. Further annealing the surface to 270 K, resulted the formation of an oxygen and OH phase, which is composed of individual O molecules that have an affinity to bind along the step edge, with some O decorated by OH, probably as dimers that bind to the bridge sites below and above the neighbouring steps.

Despite the wetting of intact water being different to any other metal-water system reported previous, overall this study has found that the structures formed from the reaction of oxygen and water on the Cu(511) surface are close analogues to those found on Cu(110) and Ni(110), showing these 1D linear structures can adapt depending on the surface conditions, in this case

a particular step spacing. We hope that future DFT calculations will provide more of an insight into the structure and stability of the arrangement of O and OH in peak C and further information about the 1D chains in peak B.

7.5. References

1. C. Lin, G. Corem, O. Godsi, G. Alexandrowicz, G. R. Darling and A. Hodgson, *Journal of the American Chemical Society*, 2018, **140**, 15804-15811.
2. Z. Pang, S. Duerrbeck, C. Kha, E. Bertel, G. A. Somorjai and M. Salmeron, *The Journal of Physical Chemistry C*, 2016, **120**, 9218-9222.
3. S. Standop, M. Morgenstern, T. Michely and C. Busse, *Journal of physics*, 2012, **24**, 124103.
4. J. Carrasco, A. Michaelides, M. Forster, S. Haq, R. Raval and A. Hodgson, *Nature Materials*, 2009, **8**, 427-431.
5. A. Hodgson and S. Haq, *Surface Science Reports*, 2009, **64**, 381-451.
6. J. L. C. Fajín, M. N. D. S. Cordeiro, F. Illas and J. R. B. Gomes, *Journal of Catalysis*, 2009, **268**, 131-141.
7. C. Badan, M. T. M. Koper and L. B. F. Juurlink, *The Journal of Physical Chemistry C*, 2015, **119**, 13551-13560.
8. Y. Huang, C. Ling, M. Jin, J. Du, T. Zhou and S. Wang, *Physical Chemistry Chemical Physics*, 2013, **15**, 17804-17817.
9. M. Forster, R. Raval, J. Carrasco, A. Michaelides and A. Hodgson, *Chemical Science*, 2011, **3**, 93-102.
10. C. Lin, G. Corem, O. Godsi, G. Alexandrowicz, G. Darling and A. Hodgson, *Journal of the American Chemical Society*, 2018, **140**.
11. N. Gerrard, K. Mistry, G. R. Darling and A. Hodgson, *The Journal of Physical Chemistry C*, 2020, **124**, 23815-23822.
12. T. Kumagai, M. Kaizu, H. Okuyama, S. Hatta, T. Aruga, I. Hamada and Y. Morikawa, *Physical Review B*, 2009, **79**, 035423.
13. A. Spitzer and H. Lüth, *Surface Science*, 1985, **160**, 353-361.
14. H. Snowden, University of Liverpool, Surface Science, *Year 4, MChem report*, 2023.